INFORMATION TO USERS

This manuscript has been reproduced from the microfilm master. UMI films the text directly from the original or copy submitted. Thus, some thesis and dissertation copies are in typewriter face, while others may be from any type of computer printer.

The quality of this reproduction is dependent upon the quality of the copy submitted. Broken or indistinct print, colored or poor quality illustrations and photographs, print bleedthrough, substandard margins, and improper alignment can adversely affect reproduction.

In the unlikely event that the author did not send UMI a complete manuscript and there are missing pages, these will be noted. Also, if unauthorized copyright material had to be removed, a note will indicate the deletion.

Oversize materials (e.g., maps, drawings, charts) are reproduced by sectioning the original, beginning at the upper left-hand corner and continuing from left to right in equal sections with small overlaps.

UMI®

THE DEVELOPMENT OF NOVEL REACTIVE SPUTTERING METHODS IN THE STUDY OF STRONTIUM BISMUTH TANTALATE

By

Donald Bennett Hilliard

A Dissertation Submitted to the Faculty of the

DEPARTMENT OF MATERIALS SCIENCE AND ENGINEERING

In Partial Fulfillment of the Requirements
For the Degree of

DOCTOR OF PHILOSOPHY

In the Graduate College of

THE UNIVERSITY OF ARIZONA

2 0 0 2

UMI Number: 3073232

Copyright 2002 by
Hilliard, Donald Bennett

All rights reserved.

UMI®

THE UNIVERSITY OF ARIZONA ®
GRADUATE COLLEGE

As members of the Final Examination Committee, we certify that we have

read the dissertation prepared by Donald Bennett Hilliard

entitled The Development of Novel Reactive Sputtering

Methods in the Study of Strontium Bismuth

Tantalate

and recommend that it be accepted as fulfilling the dissertation

requirement for the Degree of Doctor of Philosophy

Ken Jackson	2/1/02
	Date
Brian Zelinski	2/1/02
	Date
Dunbar Birnie	2/1/02
	Date
William Bickel	2/1/02
	Date
Angus Macleod	2/1/02
	Date

Final approval and acceptance of this dissertation is contingent upon
the candidate's submission of the final copy of the dissertation to the
Graduate College.

I hereby certify that I have read this dissertation prepared under my
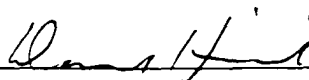direction and recommend that it be accepted as fulfilling the dissertation
requirement.

Dissertation Director Ken Jackson	2/1/02
	Date

STATEMENT BY THE AUTHOR

This dissertation has been submitted in partial fulfillment of requirements for an advanced degree at The University of Arizona and is deposited in the University Library to be made available to borrowers under rules of the Library.

Brief quotations from this dissertation are allowable without special permission, provided that accurate acknowledgement of source is made. Requests for permission for extended quotation from or reproduction of this manuscript in whole or in part may be granted by the copyright holder.

SIGNED: _____

ACKNOWLEDGEMENT

TABLE OF CONTENTS

TABLE OF CONTENTS – Continued

LIST OF FIGURES

LIST OF FIGURES -- Continued

LIST OF FIGURES -- Continued

LIST OF FIGURES - Continued

LIST OF TABLES

ABSTRACT

Contrary to the claims of numerous reports over the last two decades, there does not yet exist a viable plasma sputtering method for complex oxides such as the lead- and bismuth-containing perovskites. In fact, the lack of reproducibility in any vapor deposition means for such materials is the primary reason why the promise of nonvolatile ferroelectric RAM (FeRAM) has delivered so little over the last two decades, with only low-density devices being provided, instead, by solution and mist techniques (via both sol-gel and MOD).

In part, the present work provides the first comprehensive treatment of the challenges present in the plasma sputter deposition of ferroelectric strontium bismuth tantalate (SBT), with SBT thin films fabricated under a wide variety of deposition approaches. As such, ferroelectric SBT was successfully formed by the primary plasma sputtering methods used for ferroelectric materials in the past: namely, R.F. sputtering of ceramic targets and D.C. reactive sputtering of metal targets. Capacitors were fabricated to establish the ferroelectric properties of the SBT films. The approach allows for new insights into phase formation in the SBT system. The inadequacies of the previous sputtering approaches used for ferroelectrics (as well as High T_c superconductors) are highlighted in the context of their inherent run-to-run instability.

Subsequently, there is developed a new and rather fundamental vapor deposition technique, termed Electron-Assisted Deposition (EAD), which provides uniquely non-equilibrium growth conditions. This terminology is founded in the direct

contradistinction of the presently developed process with previously developed Ion-

Assisted Deposition (IAD) processes. The developed EAD process provides the first

means by which metallic-mode reactive sputtering, wherein the desired compound is

formed by surface reactions at the film's growth interface, can be implemented for a

ferroelectric or, in fact, the multicomponent perovskites, in general. In addition to other

benefits, such metallic-mode sputtering is found to be inherently more stable and

reproducible than the previously used ceramic-target and poisoned-target approaches.

1. INTRODUCTION

While this dissertation work is ostensibly based upon sputtered strontium bismuth tantalate (SBT) ferroelectrics. it actually reports a successful attempt to integrate three previously unrelated fields of research. namely (1) "Type II" UBM sputtering. (2) metallic-mode reactive sputtering. and. (3) perovskite ferroelectric deposition. To this end. some review required to understand the developed sputtering processes will be introduced in the explanation of the experimental setup. in Chapter 2. The SBT perovskite will then be further discussed primarily in the context of the specific materials processing results in Chapters 3 and 4. In Chapter 5. the results on SBT will then be related to a novel sputtering process developed. with conclusions in Chapter 6.

1.1 Ferroelectric Strontium Bismuth Tantalate

After several decades of development and speculation. integrated ferroelectric memories have nowadays become a reality. if only for a few niche markets. The majority of ferroelectric-based RAM (FeRAM) now available. and the vast majority of research performed for ferroelectric/piezoelectric applications. is based on the industry-standard ferroelectric ceramic. lead zirconate titanate (PZT).

However. the requirements of next generation ferroelectric devices have resulted

in broadly based speculation that a relatively uncharacterized member of the layered-

perovskite system. in particular. $SrBi_2Ta_2O_9$ (SBT). will replace PZT in future

nonvolatile memory devices. As in the case of all known layered-perovskite materials.

SBT comprises a superlattice structure of the Aurivillius homologous series. which is a

structure consisting of interleaved layers of $(Bi_2O_2)^{2+}$ and perovskite-like layers of

$\{(A_{m-1}B_mO_{3m-1})^{2-}\}_{m=1,2,3,...,\infty}$. Compounds of the Aurivillius series possess a resultant

chemical formula of $A_{m-1}Bi_2B_mO_{3m+3}$. where A is lead or an alkaline earth. and B is Ti.

Ta. or Nb. In this series. SBT is an m = 2 member. as shown in Figure 1.1.
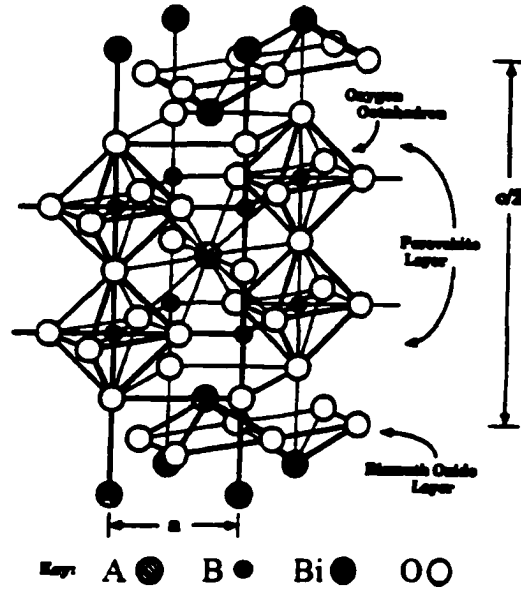
Figure 1.1: Schematic of half unit cell for m=2 layered perovskite.

Given the vast resources that have been expended to characterize the PZT system,

and the extensive know-how already successfully developed for utilizing this standard

material, one might justifiably ask whether embarking on the development of an entirely

new materials system is economically justified. However, the material properties of the

strontium bismuth tantalate (SBT) ceramic have been found to provide several crucial

advantages over the PZT family of ceramics in integrated ferroelectric applications.

Most prominent of these advantages is resistance to switching fatigue. While PZT is

generally found to lose considerable polarization above 10^8 switching cycles, in devices

utilizing the desired (platinum) metal electrodes, SBT is regularly witnessed to provide

fatigue-free switching above 10^{12} cycles. The orders of magnitude at issue distinguish

the low-cycle requirements of smart-card applications from those of ferroelectric RAM

(FeRAM).

Another important advantage of SBT is its low leakage current in the thin film

form, typically 100x less than that of PZT. This lower leakage current is of critical

importance if ferroelectric devices are to be scaled down to the projected densities. In

addition to providing lower power consumption, reduced leakage current also indicates a

commensurate drop in current-dependent breakdown mechanisms.

Yet another incentive for developing SBT-based ferroelectric devices is the

scaleability of both its dielectric and ferroelectric properties. Although PZT can provide

exceptionally high k values (dielectric constants in excess of 10,000 being reported), such

advantages are substantially diminished by the thickness-dependence, and the lack of

reproducibility of its dielectric properties at the reduced scale appropriate for competitive memory devices.

The lower coercive field. E_c. of the SBT ferroelectric also begets rather fundamental advantages in FeRAM fabrication. Since the attainable switching speed is a composite of the entire FeRAM circuit. and a significantly lower operating voltage reduces the effects of stray capacitance on the relevant RC constants. the lower E_c of SBT should translate into higher switching speeds. In a related manner. lower switching voltages also allow denser memory arrays. as cross-talk issues are scaled down accordingly. Also. amplifier performance requirements are considerably relaxed with the smaller operating voltages required. Another advantage of the lower E_c of SBT is a commensurately smaller applied field. which reduces both the current-induced and field-induced dielectric breakdown mechanisms.

However. in memory fabrication. significant barriers must be overcome before the previously mentioned advantages of SBT can provide an economic advantage. As continues to be the case in most ferroelectric applications. the primary bottleneck in technological progress lies in the material growth process. As the feature size in FeRAM is reduced further into the sub-micron range. process difficulties increase dramatically. Such difficulties include both achieving a uniform and repeatable composition in the multicomponent ferroelectric. as well as maintaining the integrity of the entire heterostructure through high temperature processing. In the end. issues that are infrequently addressed in published vapor deposition work on integrated ferroelectric research. such as reproducibly controlling composition. reproducibly maintaining smooth

surface morphologies. and reproducibly controlling grain size. would become "do-or-die"

issues in developing a production process for high density FeRAM. As feature sizes

approach the 0.13 um node the increased aspect ratios associated with such smaller

feature sizes can be expected to compound existing difficulties in composition control.

While there appears a consensus growing that MOCVD will prevail at these feature sizes.

the challenge of tightly controlling composition over such surface relief is daunting.

regardless of the deposition method.

Concerns over expending resources on exploring SBT as a new ferroelectric

system are compounded in light of these process issues. predominantly due to the higher

processing temperature of SBT. Whereas PZT may be formed at equilibrium

temperatures as low as 550C. SBT experiences full and reliable phase formation at

temperatures greater than 750C. Due to the reasons discussed above. this approximately

200C increase in processing temperature. combined with the high activity. low-

magnitude heat of oxidation. and high vapor pressure of bismuth. renders SBT a

significantly more difficult material to integrate into a capacitor. or field-effect transistor

(FET). heterostructure. The relative difficulty in forming the layered perovskite SBT

phase in a thin film device may be witnessed in the relative lack of progress in sputtered

SBT. despite the expertise already accrued in depositing earlier multicomponent oxides

such as PZT.

Another factor weighing heavily in favor of the PZT system is that SBT does not

appear to share the versatility of PZT. The PZT system enjoys widespread use due to its

possessing desirable figures of merit in a variety of ferroelectric. piezoelectric. and

pyroelectric applications. PZT is already actively employed in a myriad of commercially available imaging devices. transducers. sensors. and memory chips. As far as SBT is concerned. its piezoelectric and pyroelectric coefficients appear too low to ever warrant their exploitation. although. these low coefficients may allow some device applications. due to their high anisotropy in the SBT crystal structure. And while what little information is available on the electro-optic properties of SBT is somewhat promising. it is unlikely that they would warrant attempting bulk single crystal growth of this incongruently melting compound.

It thus seems likely that SBT. if it is to have significant economic impact. will be most likely limited to niche applications in the nonvolatile memory chip industry. Yet. even this potential impact must be viewed with the understanding that SBT is but a currently favored candidate amongst several possible materials systems in the ever-growing list of inorganic ferroelectric materials. This situation should. in turn. be viewed from the perspective that the nonvolatile RAM market may very well be eventually overtaken by fundamentally different technologies. such as either the currently favored magnetic RAM (MRAM). or novel ovonic unified memories (OUM).

Given this state of affairs. how does one perform research in the SBT system with any confidence of making a meaningful contribution to the evolution of general ferroelectric research? It is believed here that such confidence is difficult to come by in research efforts that perform device-oriented studies. This is especially true given the impracticability. at the university level. of performing reliable tests at the ULSI integration level for which SBT is intended.

1.2 Vapor deposition of Complex Oxide Phases

From the point of view of materials processing. however. SBT provides an opportunity to explore entirely more permanent and fundamental issues than can be offered by device-oriented studies. These issues pertain to the general challenges in vapor depositing thin films of multi-component. high-temperature oxide phases that contain a highly volatile species. In this set of materials. SBT is a rather extreme example of a multicomponent oxide that simultaneously possesses both high temperature processing requirements and a highly volatile component. From the perspective of vapor deposition processes. the SBT layered-perovskite system can then provide insights into the quite broad. and increasingly important. set of materials that comprise lead- or bismuth-containing complex oxides: a set of materials which includes. for instance. many of the most important ferroelectrics (the most functional subset of piezoelectrics. and. more generally. pyroelectrics). optically active garnets. and high-T_c superconductors. More specifically. the SBT system can also provide a template for exploring process approaches to the set of layered perovskites. This latter point is significant. since it presently appears that the high fatigue-resistance needed to satisfy future FeRAM requirements would most likely be achieved through use of a layered perovskite of some sort.

The primary obstacle in the fabrication of useful devices incorporating such complex. multicomponent oxides is the high processing temperatures required to produce the desired (frequently perovskite) phase. These high processing temperatures. as

suggested above. dramatically increase the difficulty in controlling the composition of the deposited film. and. also. may be incompatible with the underlying device structure. Efforts to reduce processing temperatures for such complex oxides are frequently based upon the utilization of energetic vapor deposition processes. wherein the various energetic particles existing in plasma-like or ion-beam deposition environments provide non-equilibrium. low-temperature. formation of the desired material phase. Practical vapor deposition methods that benefit from such energetic processing include various forms of plasma sputtering. pulsed-laser deposition (PLD). ion-assisted deposition (IAD). activated reactive evaporation (ARE). and plasma-enhanced chemical vapor deposition (PECVD). Of these methods. only the first two have a history of allowing adequate compositional control for Pb- or Bi-containing complex oxides. Of these two deposition methods. however. only plasma sputtering provides a proven energetic deposition technique that may be suitably incorporated into a manufacturing environment.

Accordingly. the present work explores the use of plasma sputtering. and in particular. magnetron sputtering. for low-temperature deposition of the SBT ferroelectric oxide. Rather than taking a device-oriented approach to SBT. despite its being perhaps a "flash-in-the-pan" integrated ferroelectric. the present work views the SBT system as an opportunity to develop new insights into the. now widely used. reactive magnetron sputter deposition process. Thus. the primary focus of this work is on both the SBT material and the development of new materials processing methods for. and insights into. depositing all such complex compounds.

2. EXPERIMENTAL BASIS & SETUP

2.1 Focus of Chapter

The vacuum deposition processes developed and used in the present work may be generically represented under the category of magnetron sputtering. Because well-engineered magnetron sputtering equipment has become readily available from commercial sources. materials scientists and electrical engineers now use this method to deposit a vast array of thin film materials. frequently under the assumption that there exists. somewhere. a solid understanding of the magnetron sputtering process. Unfortunately. this is an erroneous assumption and. oftentimes. the resultant thin film material or device under study is far less mysterious than the physical processes by which it came into being. This state of affairs becomes quite evident as the sputter process requirements become more stringent and/or complex. and reproducibility becomes an all-important issue. Even the very complex subject of ferroelectric thin film heterostructures. such as those fabricated in this work. can at least benefit from a fairly voluminous and. practically speaking. complete body of basic ferroelectric theory that has changed very little in the last thirty years. Conversely. the lack of a basic theory to predict magnetron deposition processes (except after a particular process is already developed) is integral to the. fortunately. continuing dynamic nature of the magnetron sputtering field. Accordingly. rather than rehash salient features of integrated ferroelectric theory. or recite engineering data on ferroelectric SBT. it is seen here as far

more constructive to address the real bottleneck in advancing ferroelectric technology, which is, in nearly all cases, the materials process at hand.

2.2 Review of the Magnetron Sputtering Process

The term "plasma" will be defined here, as elsewhere, in the general sense of a gaseous assembly of electrons and positive ions, characterized and maintained by its tendency to seek a state of space-charge neutrality. As such, plasma is a unique phase of matter, and is frequently referred to as the "fourth state" of matter. The use of plasma sputtering to vaporize and condense thin film materials, like all vapor deposition processes, is a fundamental process that occurs throughout nature. It is difficult to ascertain the first observation that a grounded or negatively biased surface could be sputtered by the positive ions residing in adjacent plasma. In general, the observation of plasma sputtering dates back to the late 19th century, and Edison acquired patents on its application early in the 20th century. Penning later disclosed the magnetic confinement of sputtering plasma in 1939. While the success of all vapor deposition methods was contingent upon the continual realization of improved vacuum technologies in the 1940's to the present, magnetron sputtering was not introduced as a successful deposition method until the late 60's to early 70's.

2.2.1 The Basic Glow Discharge

Most of the basic understanding of magnetron sputtering discharges can be directly correlated to our basic understanding of unmagnetized, low-pressure, weakly

ionized glow discharges. For this reason. it is instructive to periodically consult the classical parallel-plate geometry historically used to demonstrate this model. both as a reference for the various plasma regions. as well as to remind us of the rudimentary nature of this correlation. In figure 2.1 is a well-known schematic of a classical. inert gas. D.C. discharge in an evacuated glass tube as introduced in the seminal text by Cobine. The discharge structure of Figure 2.1 may be obtained. depending on the discharge gas. at pressures in the order of one torr (1 mm Hg) down to the neighborhood of 20-50 mtorr.

In these capacitive discharges. most power is deposited in the region near the cathode sheath. corresponding roughly to the Crookes dark space in Figure 2.1. It is thus in this region that most of the voltage drop. and the highest field. takes place. If one observes the current-voltage relationship of the power applied to the discharge tube of Figure 2.1. two fairly distinct regions are found. At low power levels. the discharge will have a characteristic operating voltage. which is virtually independent of current. This latter condition is referred to as the *normal glow* region of discharge operation. in Figure 2.2. and is characterized by the negative glow constricting or expanding over the area of the cathode in accordance with a decrease or increase in the applied power. so that. as in Figure 2.2(a). the power density. j_c. is constant. At higher power levels. there is a transition to a condition where an increase in the operating current will bring about a proportional increase in the operating voltage. where $I \propto V$. In this region of operation. the so-called *abnormal glow* region in Figure 2.2. the opportunity arises for the potential between the cathode surface and the adjacent "negative glow" region. which is classically
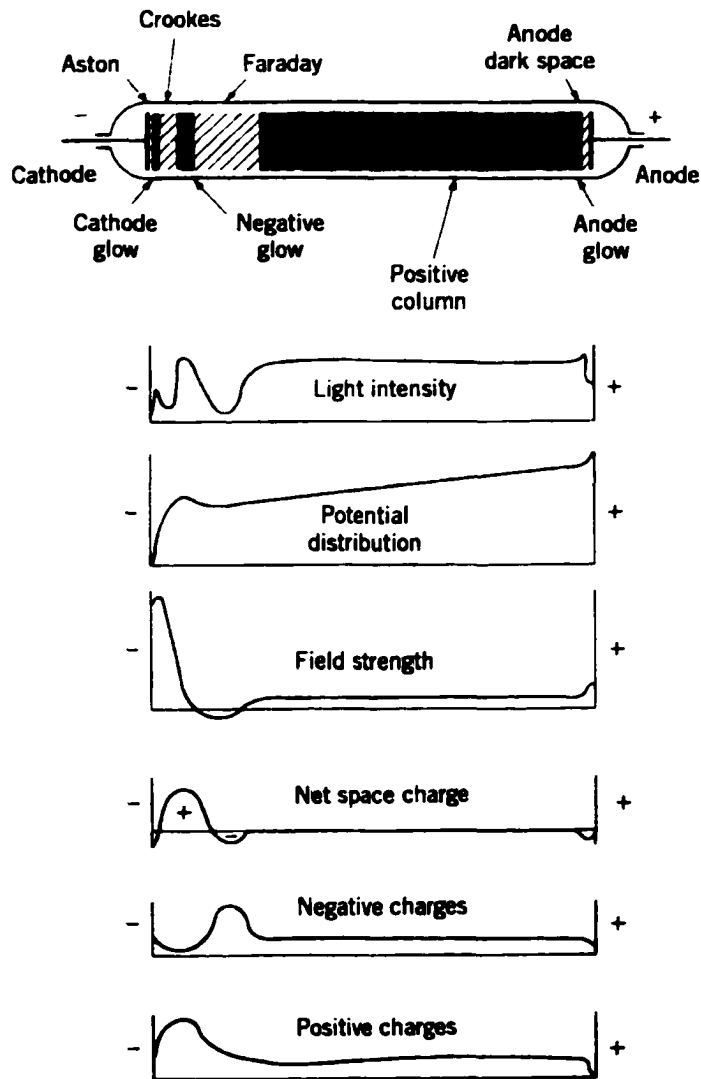
Figure 2.1: schematic and characteristic profiles of a classic, tubulated. D.C. glow discharge (Cobine. 1958)

of a slightly positive space-charge potential, to become suitably large to promote efficient

sputtering of the cathode surface. It is, thus, in this abnormal glow region that a

sputtering discharge may be efficiently operated.

(a)   (b)
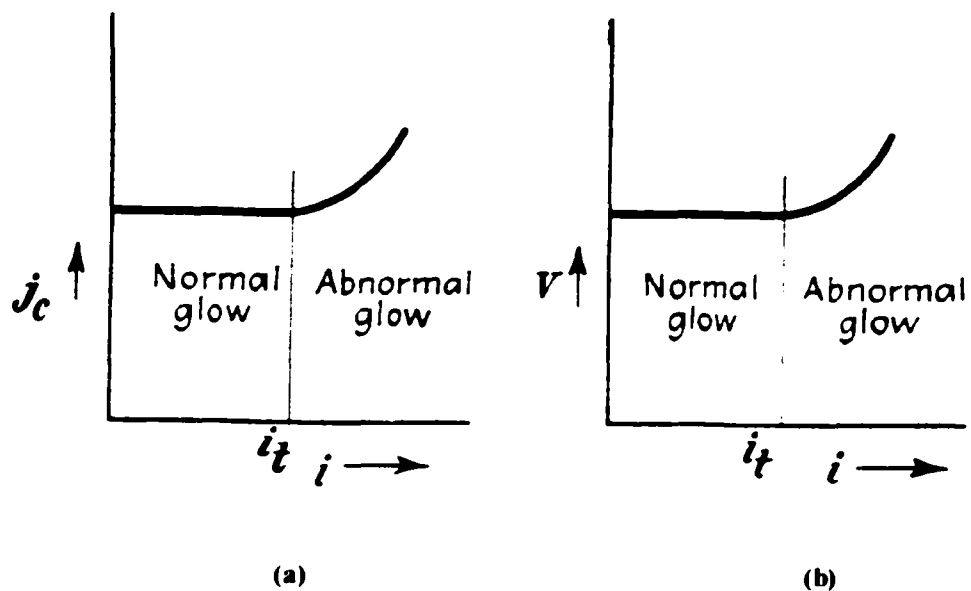
Figure 2.2: Current density vs. applied current (a), and voltage vs. current (b), for the negative glow region of a D.C. glow discharge.

It should be noted that, while the relatively simple low-pressure D.C. discharge of

Figure 2.1 provides the classic example of a weakly ionized plasma, there still exists no

analytical means by which to predict its general structure. Nevertheless, some very

valuable physical insights have been developed to describe its interrelationships and

those of plasma in general. These basic insights will be highlighted here. as they will find utility in later chapters.

2.2.2 Ambipolar Diffusion

The most fundamental set of assumptions relied upon in the treatment of collisional plasma are based upon ambipolar diffusion. Of primary importance to these assumptions is that. in a gaseous assembly of positive ions and electrons. fluctuations in local space charge will be compensated so as to maintain. in general. space charge neutrality. As such. population densities $n_{ion} = n_{elec}$. and both negative and positive charge. in accordance with their own mobility. will respond to local fields that exist on an order larger than their own shielding radius. The charge-to-mass ratio of electrons is >1800 times that of the ions. and. since mobility will scale inversely to the square root of this factor. electron mobility will be much greater. starting at about $(1800)^{1/2} \cong 42$. for hydrogen. Hence. electron mobility will perform most of this compensating function in an unmagnetized plasma. and the electron shielding radius becomes the characteristic Debye length. λ_D of the plasma. Such behavior dictates that these random fluctuations in collisional plasmas will account for most charge motion. so that net displacement of charged particles can be rightly viewed as a diffusive process.

As a diffusive process. various constituents of a collisional plasma region may be given a standard diffusion constant. which Lieberman has derived from basic force equations:

$$D = (\pi/8) \lambda^2 v_m \qquad (1)$$

where λ is the mean free path and v_m is the collision frequency. In accordance with the

Einstein relation. the mobility constant for the species under consideration would then be

$$\mu = (\,|q|\,/\,kT)\,D \qquad (2)$$

with q representing either positive or negative charge. Using the "congruence

assumption" that enables analysis of an electropositive plasma. namely. that the flux of

electrons and (positive) ions into or out of a plasma region can be equated. an ambipolar

diffusion constant can be derived from the force equations:

$$D_a = \frac{\mu_i\,D_e\,+\,\mu_e\,D_i}{\mu_i\,+\,\mu_e} \qquad (3)$$

where the subscripts. i and e. signify coefficients for ions and electrons. The ambipolar

diffusion constant reflects that the separate electron diffusion and ion diffusion rates will

be replaced by that of their coupled motion. Using the observation that. in unmagnetized

plasma. $\mu_i \ll \mu_e$. one can further simplify (3) by dropping μ_i. so that

$$D_a \cong (\mu_i\,/\,\mu_e)\,D_e\,+\,D_i \qquad (4)$$

and. utilizing the Einstein relation. this again simplifies to

$$D_a \cong D_i\,(1 + T_e/T_i). \qquad (5)$$

In the non-magnetized. weakly ionized plasmas considered in this section. $T_e \gg T_i$. so

that electrons and ions will both diffuse at an ambipolar rate that lies between their

respective free-particle diffusion rates.

2.2.3 The Sheath Region

The creation of a positive ion sheath is another essential consequence of ambipolar diffusion. If a plasma is initially placed in a volume contained by electrically floating walls. it will expand to fill that volume. and. due to the much higher mobility of the electrons. most collisions with the walls of the container will initially be those of the electrons. resulting in a net negative surface charge on the container walls. Subsequently. ions will be accelerated to a container wall in response to the created field. resulting in the equilibration of wall charging. and hence. of ion and electron arrival rates at the container wall. At equilibrium. the wall will retain a net negative surface charge. so that a positive ion sheath. on the order of a few Debye lengths. will form in the region immediately adjacent to the wall. effectively shielding the neutral plasma from the negatively charged wall. An observation that is implicit. but rarely discussed. in the formation of a stable positive ion sheath is that the floating material-gas interfaces are usually far more prone to retain negative. rather than positive. surface charge.

While the much higher mobility of the electrons. alone. indicates that the wall will retain a net negative charge. the common use of electric or electromagnetic energy to power plasmas will also result in a much higher average electron temperature (velocity) relative to that of the ions. further increasing the resultant negative surface charge at an electrically floating container wall. The negatively biased surface that deposits power into the plasma will develop an increased sheath potential corresponding to the voltage difference between the cathode surface potential. V_c. and the adjacent plasma potential. V_p. Because V_p in the adjacent negative glow is close to neutral. and classically. slightly

positive. with $n_e \cong n_i$, the sheath region provides the most accessible means of analyzing

the plasma. since it will generally contain the full potential. and current. applied to the

cathode. and may generally be assumed to be dominated by a positive ion space-charge.

2.2.4 The Bohm Criterion

If a low-pressure. weakly ionized plasma. where $T_e >> T_i$. is incident upon a

floating or negatively biased wall. positive ions accelerated through the resulting sheath

region may be assumed to be in free fall. rather than mobility limited. In addition. the

electron density. with a Boltzmann distribution. may be assumed to decrease primarily

within the sheath. such that space charge neutrality is maintained up to the sheath edge.

These assumptions are the basis of the Bohm criterion. through which Bohm postulated

the existence of a small field. and a minimum resultant ion velocity – the Bohm velocity

– to be required in the plasma region immediately adjoining the sheath region. The

standard derivation will not be recited here. except for the result that a minimum

"presheath" ion kinetic energy. $K_{ion} \geq T_e / 2$. is required. which provides the Bohm

velocity. v_B. as the lower limit of ion velocity entering the sheath region:

$$v_{ion,s} \geq v_B = (eT_e / M)^{1/2} \qquad (6)$$

This result is obtained for a single Maxwellian T_e. An important result of the Bohm

criterion is that it provides a straightforward means for estimating the potential drop

between the plasma and a floating wall. $V_p - V_f = V_w$. Once equilibrated. electron flux

and ion flux to the wall can be equated. and an estimate for the floating potential may be derived:

$$V_f = - T_e \ln(M/2\pi m)^{1/2} \tag{7}$$

where M is the ion mass and m is electron mass. A multi-mode electron temperature is common in sputtering plasmas. and a multi-mode version of this result will find use later in this work.

2.2.5 Child's Law

The Child's law. also known as the space-charge equation. is of importance. since it is frequently cited as a valid description of voltage-current relations in the sort of low-pressure (< 10 mtorr) sputtering environments used here. As in the case of the Bohm criterion. the Child's law is the consequence of the Poisson equation. given a Maxwell-Boltzmann energy distribution. While the Bohm criterion benefits from the convenient boundary conditions allowed for charge and mass conservation in electropositive plasma near the sheath region, the use of Child's law to describe plasma behavior assumes space-charge to be effectively dominated by one type of charge carrier in the sheath region. The Child's law was originally derived for the general case of an electron diode. where J is electron current. V is the voltage. and x is the distance between the electrodes:

$$J = \frac{(2e/m)^{1/2} \, V^{2/3}}{9\pi x^2} \tag{8}$$

However. it is valid for space-charge-limited current flow of a single carrier. whether of a positive or a negative sign. With its relatively high voltage (compared to the electron temperature) the cathode sheath may be approximated as being occupied by only positive ions. so that positive space-charge dominates. The sheath thickness may then be treated as the characteristic distance. x. between the ion-emitting sheath-presheath boundary and the boundary of the cathode surface. The voltage. V. is then the sheath potential. which may be approximated as the applied voltage. Since the secondary electron coefficient at the cathode. γ_{se}. will normally be quite small. ion current to the cathode will dominate. and so the current of the discharge is approximated as the ion current. J. in the Child's law.

Other sheath laws. which are used to describe higher-pressure. more collisional discharges than used here. also assume an ion-dominated space-charge within the sheath region. with a mobility-limited ion current. These latter sheath laws frequently contain a factor $(1 + \gamma_{se})$. where γ_{se} is the secondary electron coefficient at the cathode surface. so that the contribution of electron current will be $j_{elect} = \gamma_{se} j_{ion}$. It is common. in this context. to cite a value of $\gamma_{se} = 0.1$. for a pure argon sputtering gas. It should be noted that the Child's law does not accommodate such a contribution of secondary electrons. The resultant difficulties that then arise in using such a sheath law for magnetron sputtering environments will become clear in the results of this work.

(a)

(b)
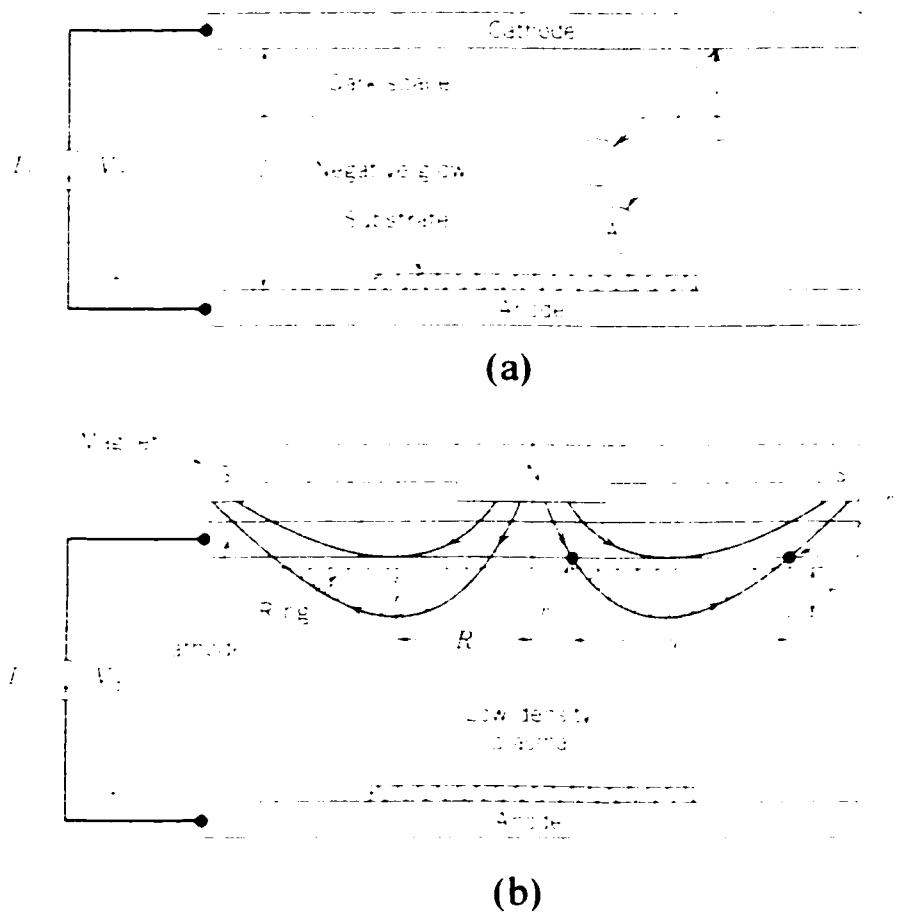
Figure 2.3: Standard configurations for (a) a classic. unmagnetized. parallel-plate. diode sputtering. and (b) magnetron sputtering.

2.3 Magnetron Sputtering

The situation described in Figures 2.1-2.2 is qualitatively quite similar to the original. unmagnetized. glow discharge sputtering geometry shown in Figure 2.3a. except that the distance between the parallel plates is considerably reduced. which is found to

eliminate the positive column. as well as to foreshorten the Faraday dark space. Due to the lower pressure limit of the original diode sputtering process being in the 20-50 mtorr range. this foreshortening of the discharge space is required if sputtered material is to effectively migrate from the eroded cathode. or target. to a substrate at the anode plane. This limitation on the "throw distance". as well as limitations in the directionality. power density. energy. and general versatility.of the simple diode sputtering environment. has been greatly alleviated by the introduction of a self-closing magnetic field. B. to confine the sputtering plasma to the space adjacent the cathode. as indicated by the hatched region in Figure 2.3b. The resultant sputter source is termed a magnetron. though its operation and purpose are obviously quite different from the microwave source of the same name. There has been a vast and diverse array of magnetron designs described in the literature. with cathode geometries comprising various disks. cones. cylinders. hemispheres. and segmented combinations of the same. However. the principles of operation that are common to these various designs are discernible in Figure 2.3b.

An essential characteristic of the magnetron source is the formation of a magnetic trap. This is accomplished through the use of either permanent magnets or electromagnets placed within the cathode assembly. so that the magnetic field terminates at the cathode surface. Normally. permanent magnets are placed at the back of the cathode target. as in Figure 2.3b. The effect of the magnetic trap on the discharge behavior may be first appreciated through the consideration of the gyration of charged particles in a uniform magnetic field resulting from the Lorentz force:

$$F = q(E + v \times B)$$ (9)

where the particle velocity. v. having a component. $v_\perp$. perpendicular to **B**. results in gyration about a guiding center coincident with the direction of **B** = B_0 z. The inward Lorentz force may be equated with the particle's centrifugal force to obtain the radius of gyration:

$$|qv_\perp B_0| = mv_\perp^2 / r_{gyr}$$ (10)

$$r_{gyr} = v_\perp m / qB_0$$ (11)

In terms of energy. $mv^2/2 = qV$. we obtain for electrons:

$$r_{gyr,e} \approx \frac{3.37(V)^{1/2}}{B_0} \text{ cm} \quad (\text{V in volts}).$$ (12)

and for singly ionized ions:

$$r_{gyr,i} \approx \frac{144(V \cdot M)^{1/2}}{B_0} \text{ cm} \quad (\text{V in volts. M in a.m.u.}).$$ (13)

For a typical magnetic field. B_0=100 Gauss, a relatively hot. 4 eV, electron results in $r_{gyr,e} \approx 0.07$ cm. The confinement of charged particles to gyrating paths along relatively strong magnetic field lines will then tend to reduce mobility of the particles across field lines to exit the magnetic trap. On the other hand. for a the typical argon ion at near-room-temperature. $r_{gyr,i}$ will be much greater than one centimeter. The energies chosen are somewhat anecdotal. since secondary electron energies will scale to the full sheath

potential (hundreds of volts) and the high energy tail of ion energy distributions will vary. However. the generally much smaller radius. relative to trap dimensions. of the electron gyration – or. conversely. the ratio of the Lorentz force to particle inertia – indicates that the confinement of the sputtering discharge in a magnetron is primarily due to the efficient confinement of electrons. The mobility of ions across magnetic field lines will then be decreased. as well. insofar as ambipolar conditions persist.

2.3.1 Diffusion in Magnetron Sources

Because. in a magnetron sputter source. plasma will be lost only across the magnetic field lines of the trap region. diffusion processes may be described only in terms of a perpendicular ambipolar diffusion constant:

$$D_{\perp a} = \frac{\mu_{\perp i} D_{\perp e} + \mu_{\perp e} D_{\perp i}}{\mu_{\perp i} + \mu_{\perp e}} \qquad (14)$$

which is similar to the previous isotropic ambipolar diffusion constant. However. in the case of a closed and strong magnetic field (around $B > 150$ Gauss). the situation is reversed. in that the perpendicular electron mobility is now much lower than that of the ions. which are relatively unaffected. Therefore. $\mu_i >> \mu_e$. and the electron mobility term may be dropped from the demominator. so that a very different ambipolar diffusion constant may then be obtained in the same way as in the non-magnetized case:

$$D_a = D_{\perp a} \cong D_{\perp e} (1 + T_i/T_e). \qquad (15)$$

Again. $T_e \gg T_i$ in the weakly ionized plasmas used in any materials process. so that ambipolar diffusion from the magnetron trap is essentially determined by its ability to trap electrons.

2.3.2 Drift Currents in Magnetron Sources

The self-closing nature of the erosion "track" in magnetron sputter sources. which results from a toroidal magnetic field in Figure2.3b. is also essential for desirable operation. The self-closing aspect of all magnetron sputter sources is necessary to efficiently contain the various drift currents that will possess substantial velocity components tangentially to the erosion track. The concept of drift current will be important in later chapters. Drift currents generally refer to mechanisms by which the guiding center. which may be any line of the magnetic field. of electron (or any charged particle) gyration can be displaced. While there is a common notion. frequently published. that such drift is due to the familiar $E \times B$ force. this perception is not physically justified. In fact. the well-established condition that most of the voltage drop takes place over the very narrow – less than one millimeter – ion sheath at the cathode (target) surface would generally indicate no basis for any substantial field to exist in the required orientation. However. other drift mechanisms result from various forms of nonuniformity in the magnetic and electric field. Such nonuniformity is amply provided in the. spatially. quite inhomogenous magnetron sputtering plasma. Lieberman has summarized some of the main drift currents in processing plasmas. which are listed in Table 2.1.

Guiding Center Drifts

General force drift	$v_F = \dfrac{(F/q) \times B}{B^2}$
Electric field drift	$v_E = \dfrac{E \times B}{B^2}$
Curvature drift	$v_R = \dfrac{2 K_\parallel}{q} \dfrac{R_c \times B}{R_c^2 B^2}$
Grad-B drift	$v_{\nabla B} = \dfrac{K_\perp}{q} \dfrac{B \times \nabla B}{B^3}$
Polarization drift	$v_p = \dfrac{m}{qB^2} \dfrac{\partial E}{\partial t}$

Table 2.1: Various drift currents that occur for charged particles in both electric and magnetic fields (after Lieberman, 1994).

Penfold has suggested that drift currents in magnetron plasmas may be primarily attributed to (a) B-field curvature drift, (b) reflection from the ion sheath (effectively, the cathode), and (c) drifts due to B-field gradients. The resulting net drift current is apparently not small. Measurements of the drift current in a sputtering magnetron,

through observation of inductive effects, have produced magnitudes 4 to 10 times that of the actual current provided to the cathode.

While it is still a matter of conjecture what the actual distribution of electron energies, and associated gyration radii, is within the magnetron's negative glow region, a number of electrical probe studies appear to comfortably establish that, similar to simple diode sputtering, there exists a bimodal electron temperature distribution in the magnetron sputtering environment. This bimodal distribution is typically divided between a large low-temperature component, typically in the area of $T_e = 0.2$ eV, and a smaller high temperature component in the neighborhood of 4 – 8 eV. In magnetrons that possess efficient trapping, with a well-matched magnetic field, the electron energy distribution between the edge of the negative glow region and the substrate will typically be overwhelmingly composed of the low-temperature component, while the high-temperature electrons are found to reside only in the negative glow region. This observation is consistent with the understanding that the high-temperature electrons are actually the secondary electrons emitted from the cathode and, after being accelerated through the sheath region, thermalized by a succession of ionizing collisions. The low-temperature electrons are thought to be the result of the creation of electron-ion pairs in negative glow and elsewhere. It has also been reasoned, recently, that the low-temperature electrons may receive energy due to their Landau damping of plasma oscillations driven by the secondary electrons.

2.4 Magnetron Design

As is the case with any physical phenomenon that works exceptionally well without human input, the poorly understood complexities of the magnetron sputtering environment can be largely ignored for many of the less demanding deposition requirements. Most magnetron deposition processes for unreacted electropositive material, such as metals, alloys, and semiconductors, fall into this category. However, the art of plasma sputtering represents a vast and diverse array of both equipment and physical phenomena. A lack of appreciation for this diversity frequently leads to the tacit, if not explicit, assumption that the findings of work performed in one limited region of process space, with a single tool set, may be generically applied to the field of plasma sputtering as a whole. Studies are performed using commercially available sputtering systems, or, systems that are an assembly of modular components, e.g., magnetrons sources, substrate fixtures, chamber, etc. available from well-established vendors. While this is a natural economic development, such an approach frequently leads to a false sense that the modular sputtering technologies utilized are representative of the breadth of sputter processing characteristics. That this is not the case will be demonstrated in the research reported here, which is largely the result of "homemade" components that the author designed and machined to provide specific characteristics that have not been enabled in previous equipment designs.

Moreover, in the published literature reporting sputter deposition, there is very infrequently any reference to the actual design or characteristics of the magnetron sputter source. Presumably, the source, as a " planar magnetron" for instance, is thought to be

sufficiently specified to provide a meaningful relationship between the deposition process used and the reported results. In fact, until the last decade, even the most exhaustive texts available could only report the few plasma diagnostic studies performed on these highly non-equilibrium plasmas. In the few sputtering texts where the topic was raised, it was reported that substrate self-biasing would typically be in the neighborhood of a few volts negative. Substrate current studies revealed that, of the flux of particles reaching the substrate, only as much as a few percent were ionized. Overviews of sputtering would typically report that less than 1% of the sputtered flux would be ionized. While these experimental results were not reported as an exhaustive study of charge transfer in magnetron plasmas, they have often been interpreted as such.

In the late 1980's, research was conducted which greatly increased understanding in the area of practical magnetron design. Window and Savvides performed a series of studies elucidating the effect of the magnetron's magnetic field upon its delivery of charged particles to the substrate(Window and Savvides 1986) (Window and Savvides 1986) (Savvides and Window 1986). For the sake of convention, they designated three basic types of magnetron fields: "balanced magnetrons" were magnetron sputter sources in which the oppositely poled magnet assemblies were effectively matched, and provided nearly equal magnetic flux. On the other hand, "unbalanced magnetrons" were sputtering sources in which the two magnetic fluxes were clearly not equally matched. "Type I" unbalanced magnetrons were designated as the variety in which the magnetic flux provided on the inside of a typical magnetron's closed discharge track was much greater. "Type II" unbalanced magnetrons were of the variety in which the magnetic flux
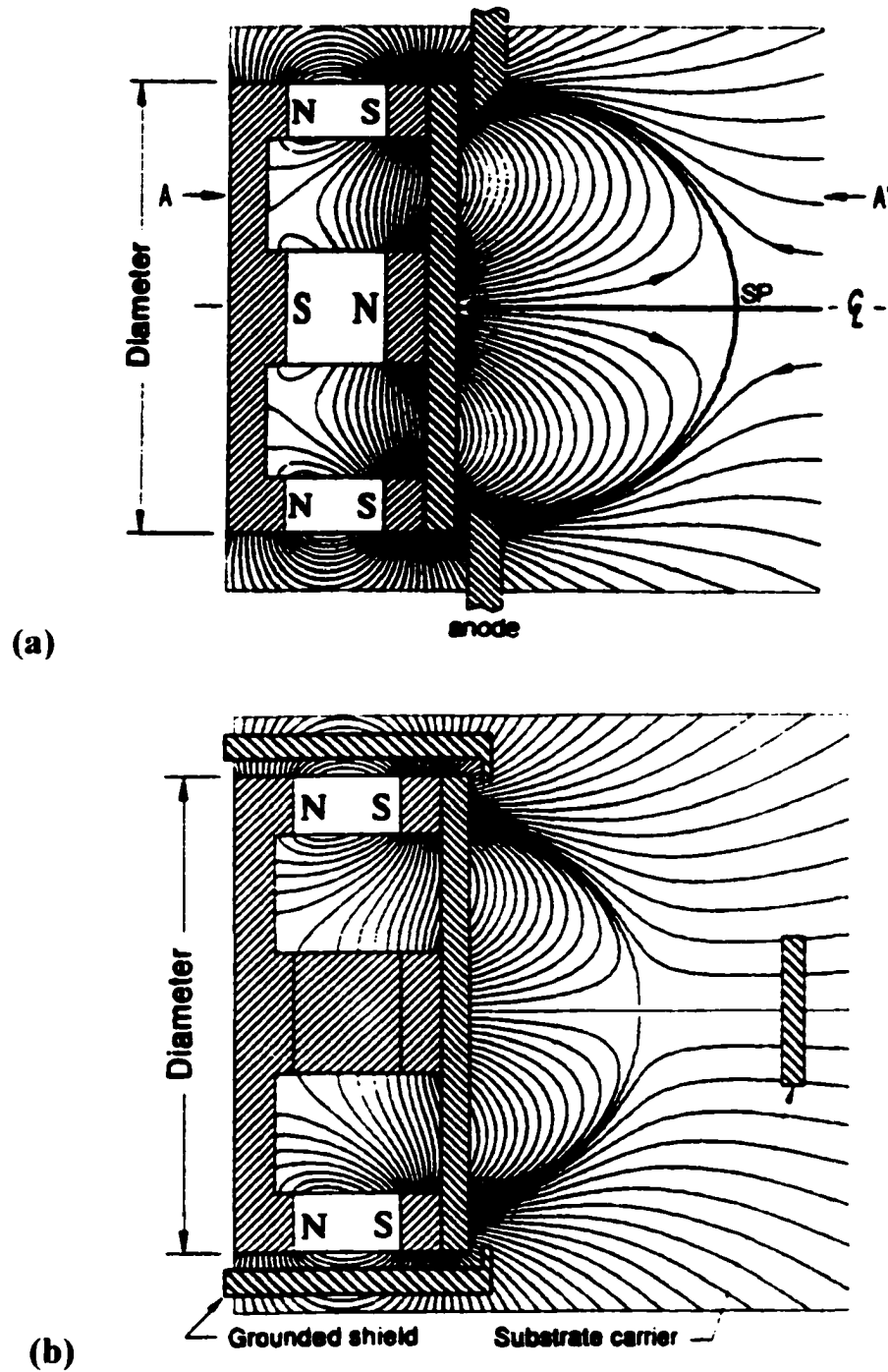
Figure 2.4: Generic magnetic field mapping for (a) a circular magnetron possessing an essentially balanced magnet set. and (b) a circular magnetron possessing a magnet set that is unbalanced in the manner of a "Type II" unbalanced magnetron (UBM).

provided by the magnet assembly on the periphery of the track was much greater. These designations are depicted in Figure 2.4. where a generic magnetic field map for both a "balanced magnetron" and a "Type II" unbalanced magnetron are shown.

In observing the plasma probe I-V characteristics of these three magnetron designs. it then became apparent that two different magnetron sputter source designs might easily produce completely different growth environments at the substrate. The on-axis "Type I" unbalanced magnetrons were found to generally produce an even less energetic environment than was previously noted for magnetron sources. However. the "Type II" sources were found to provide a highly energetic environment. This energetic environment results from the excess magnetic flux of the outside magnetic field forming a magnetic trap. As is evident in Figure 2.4(b) the "Type II" design can result in termination of the excess field lines at the substrate. or probe. The charged plasma species of the magnetron plasma will thus be guided toward the substrate in Figure 2.4(b). resulting in what is frequently described as a secondary plasma forming in the adjacent space.

As a result of such "Type II" behavior. an immense amount of interaction between the charged plasma species – electrons. positive ions. and negative ions – and the substrate is seen to take place. In Figure 2.5 are typical probe I-V characteristics for on-axis behavior of a "Type II" unbalanced magnetron.
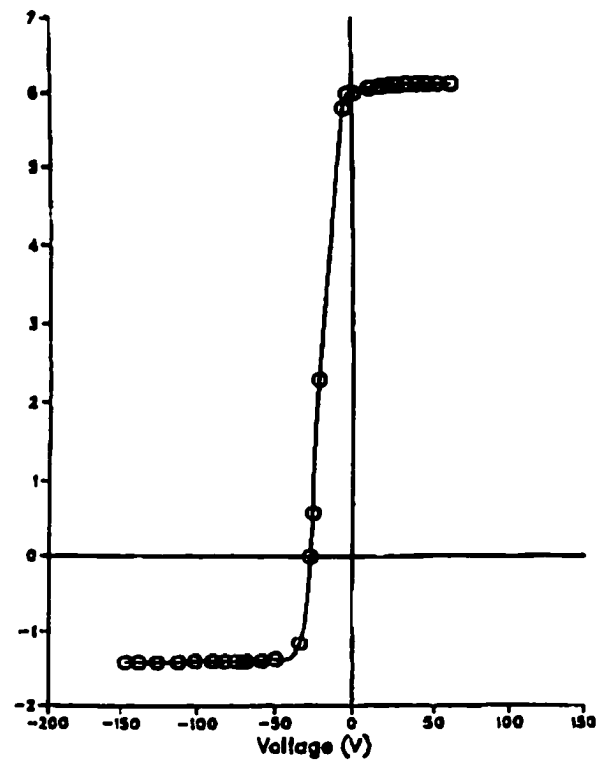
Figure 2.5: Substrate I-V characteristics for "Type II"
Magnetron with Ar sputtering gas.

One basic parameter that characterizes the operational behavior of these different

magnetron designs is their ability to trap electronic charge within the magnetic field

produced. The ability to trap electronic charge within the magnetic field of a magnetron

sputtering system indicates the degree to which the magnetic field, at its various locations

in the vacuum, are "closed" or "open." Open magnetic fields are defined, in this context,

as fields that allow electrons to escape to a grounded surface during operation, whereas, closed fields do not. Of course, the distinction is only a question of degree. It should also be pointed out that the electron-trapping characteristics of a particular magnetron design depend very much on the precise design of the chamber as a whole, as well as on the specifics of the particular process developed.

An important feature that differentiates the two field patterns of Fig. 2.4 is the location of the outer magnetic field cusp that is symmetric about the central axis of symmetry. One may note that the outer cusp region of the UBM does not intersect the grounded sputter shield as it does in the case of the "balanced" magnetron in 2.4(a). One may also note that this difference in placement of the cusp region in the two depicted sources of Figure 2.4, a substantially "closed" field is set up over the UBMII, whereas much of the balanced magnetron field intersects a grounded surface and is thereby, "open." In other words, the precise geometry, as well as the magnetic properties – such as the magnetic permeability, susceptibility, etc. – of the chamber components and sputtering target, will effect how electrons behave in the operating magnetron source.

Previous studies have attempted to assess the energy distributions and densities for various ions present in unbalanced magnetron sputtering environments. The results of these studies vary considerably, as do the respective experimental set-ups used. (Kadlec a 1997) (Howson 1997) (Hubler and Sprague 1995) (Window and Savvides 1986). In addition, the dependency of ion fluxes on various parameters of UBM environment have been studies, including the effects of sputter shield design (Telling and al 1998), Penning ionization (Miyazaki 1999), and sputtering gas pressure (Howson and J'Afer 1990).

This substantial increase in the understanding of magnetron design and the breadth of deposition environments possible has lead to a variety of subsequent modifications of the basic magnetron types of FIG. 2.4. many of which utilize additional magnets or an array of magnetron sources to enhance the ion flux of a "Type II" magnetron (Sproul 1993) (Zlatanovic 1997).

Given the tenuous nature of the processes revealed in the studies cited. it should hopefully be widely apparent in the UBM field that the general deposition characteristics of a magnetron sputter source are also contingent upon the precise process under study. However. the tenuous nature of magnetron behavior can frequently be overlooked in non-reactive processes. or in forgiving reactive sputtering processes that are not well inspected. In high-tolerance reactive sputtering processes. however. the many potential mechanisms that can govern film properties come to full bear. The exploration of true reactive sputtering (not supplemented RF processes) is fairly limited in the UBM field. comprising mostly tribological nitride coatings for machine tooling. which are known to benefit generally from energetic ion bombardment during formation.

2.5 Experimental Setup

In this research. magnetron sputter sources with greater magnetic flux density at the periphery of the target (Type II) were often utilized. This choice would seem antithetical to the commonly perceived requirements of sputtering multi-component
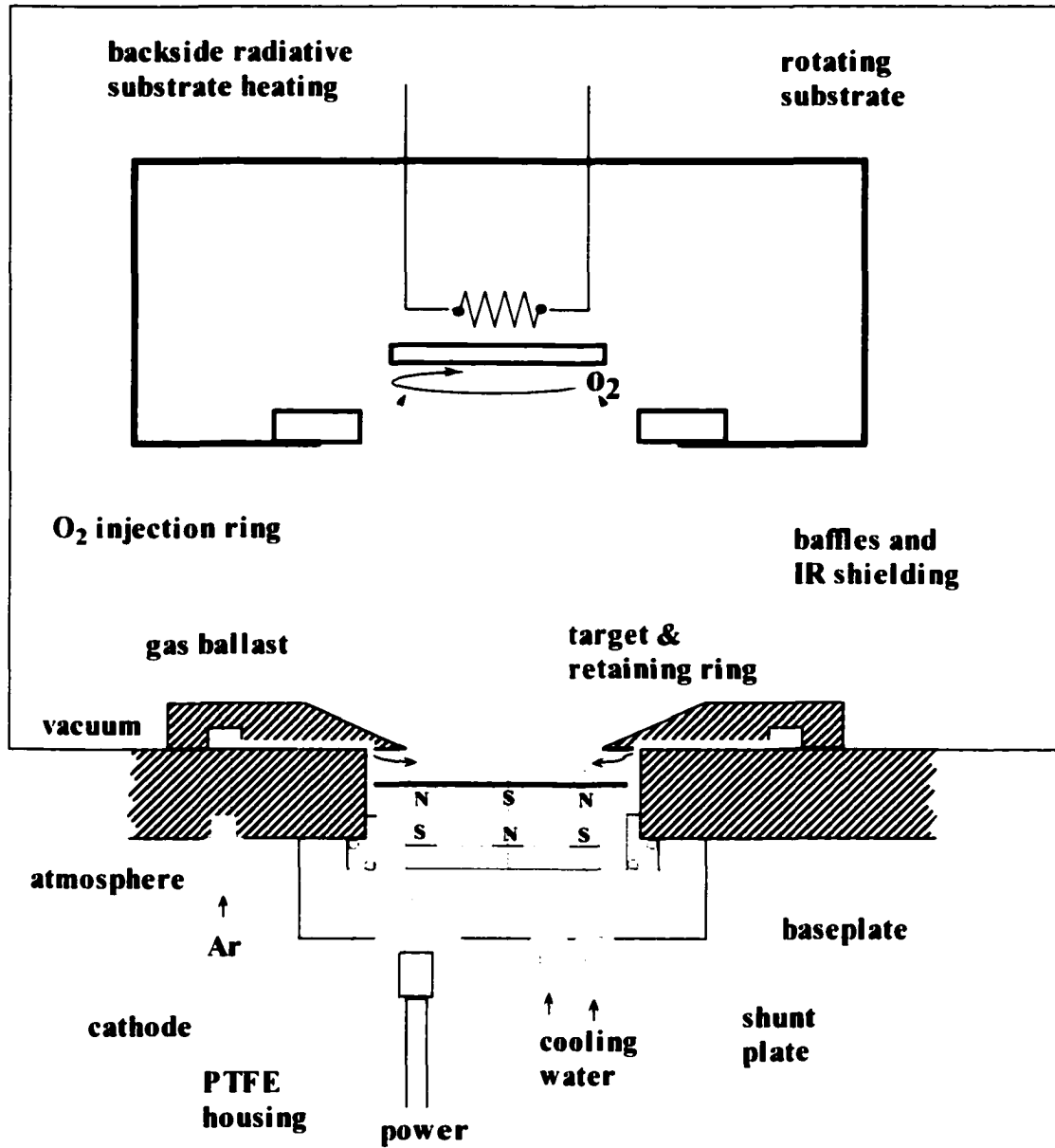
Figure2.6: Typical magnetron design used in sputtering experiments.

oxides. First and foremost is the well-documented tendency for energetic negative

oxygen ions to bombard and re-sputter the substrate. thereby preventing stoichiometric

transfer of the multi-component target phase; a tendency of plasma sputtering of oxides in general. Second, there are the problems perceived to arise as a result of energetic ion bombardment in general; namely, a general increase in defects as well as preferential resputtering of volatile components in the growing film. However, Type II UBM's may be used to avoid ion bombardment in an off-axis deposition geometry, wherein substrates are placed largely outside of the region of heaviest ion bombardment. Also, there are possible modes of magnetron operation, with unbalanced magnetic fields, that have not yet been revealed. These possibilities are explored in the following chapters

The magnetron sputter sources used in the present work were designed and fabricated solely by the author. Several sources were produced and used to satisfy the various experimental configurations used in these studies. The design of one of the sources is shown in FIG 2.6. While the source depicted was designed for external mounting, which somewhat simplifies the design and manufacture, another design utilized provides for internal mounting by a bellows connection, thereby allowing variable placement of the magnetron sputter source for further enabling co-sputtering experiments. A design aspect of all sources constructed, however, is that they allow for interchangeable magnet sets, thereby allowing for a wide selection of different operational characteristics.

The configuration of Figure 2.6 is for on-axis sputtering, as indicated by the shared axis of rotational symmetry. This allows basic features of the substrate heating assembly to also be shown. The heater assembly used backside radiative heating of a zirconium substrate backing plate, which allowed for rotation of the substrate without the

difficulties associated with implementing a rotating heating element in vacuum. The IR

shielding and ceramic hardware that were supported within the substrate heating

assembly are eliminated in the figure for clarity. The IR shielding implemented was

sufficient to allow >600C substrate temperatures. which turned out to be more than

adequate for the non-equilibrium growth studies performed.

Figure 2.7 is a schematic highlighting essential features of the deposition

chamber. The general configuration is that of a "sputter up" arrangement. wherein four

magnetron sputter sources are arranged symmetrically around a central pumping port (

(expanded 6" ASA). All guns utilize 2" targets and are mounted at a 15° incline toward

the chamber's center. A fifth gun was later constructed for placement over the central

vacuum port. so that a variety of co-sputtering arrangements could be achieved. An

assortment of shielding for placement between and around the guns was implemented to

perform such functions as prevention of cross-contamination between the sources.

allowing shielding of the substrate for presputtering. and allowing containment of the

sputtered flux and gases. Such shielding is omitted here for clarity.
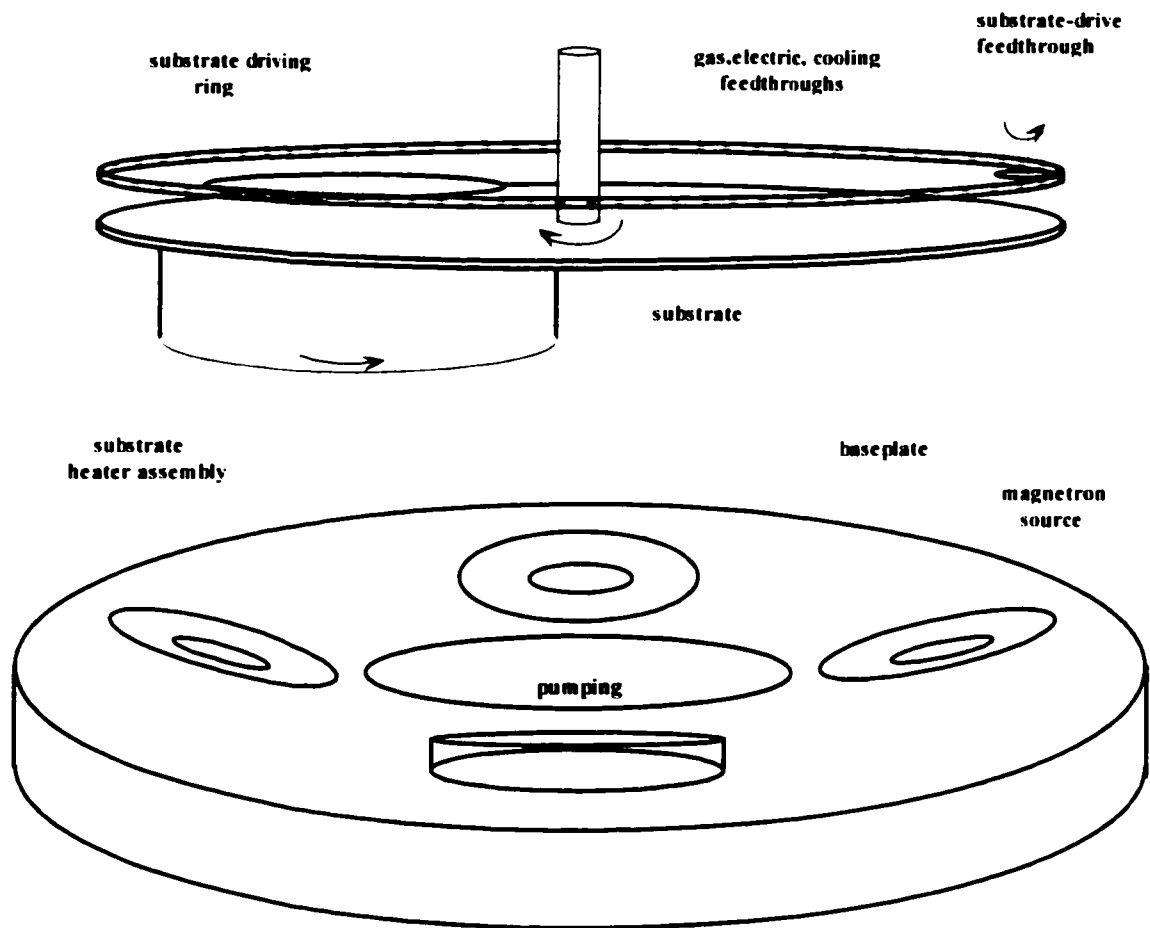
Figure 2.7: Deposition chamber geometry.

The basic form of the planetary used is also depicted in Figure 2.7. As indicated

in the figure. a substrate heating assembly was constructed. which can be translated

through 360^0 so as to allow placement of the assembly at various locations with respect to the magnetron sources. Utilities for the substrate heater assembly are provided through the central feedthrough, which includes power, water cooling, thermocouple signal, and a reactive gas line. The circular translation of the substrate heater assembly is indexed, so that its precise position may be determined and repeated. A second rotary motion feedthrough allows rotation of the heated substrate around it center of symmetry, during deposition.

The general layout of vacuum and gas-flow hardware used for much of the present research is depicted in Figure 2.8. The 6"ASA pumping stack utilized a chevron throttle valve below the liquid N_2 trap, rather than above it, for the purpose of maintaining the pumping speed of the LN trap for hydrocarbons and water, regardless of the throttle valve position. While diffusion pumps have fallen into disfavor for many applications, partly due to the contamination risks of improper maintenance, the diffusion pump was preferred for the present research. This preference is due to both the diffusion pump's high pumping speed for the sputtering gas, Ar, as well as its ability to pump lighter gas fractions that otherwise effect plasma characteristics.
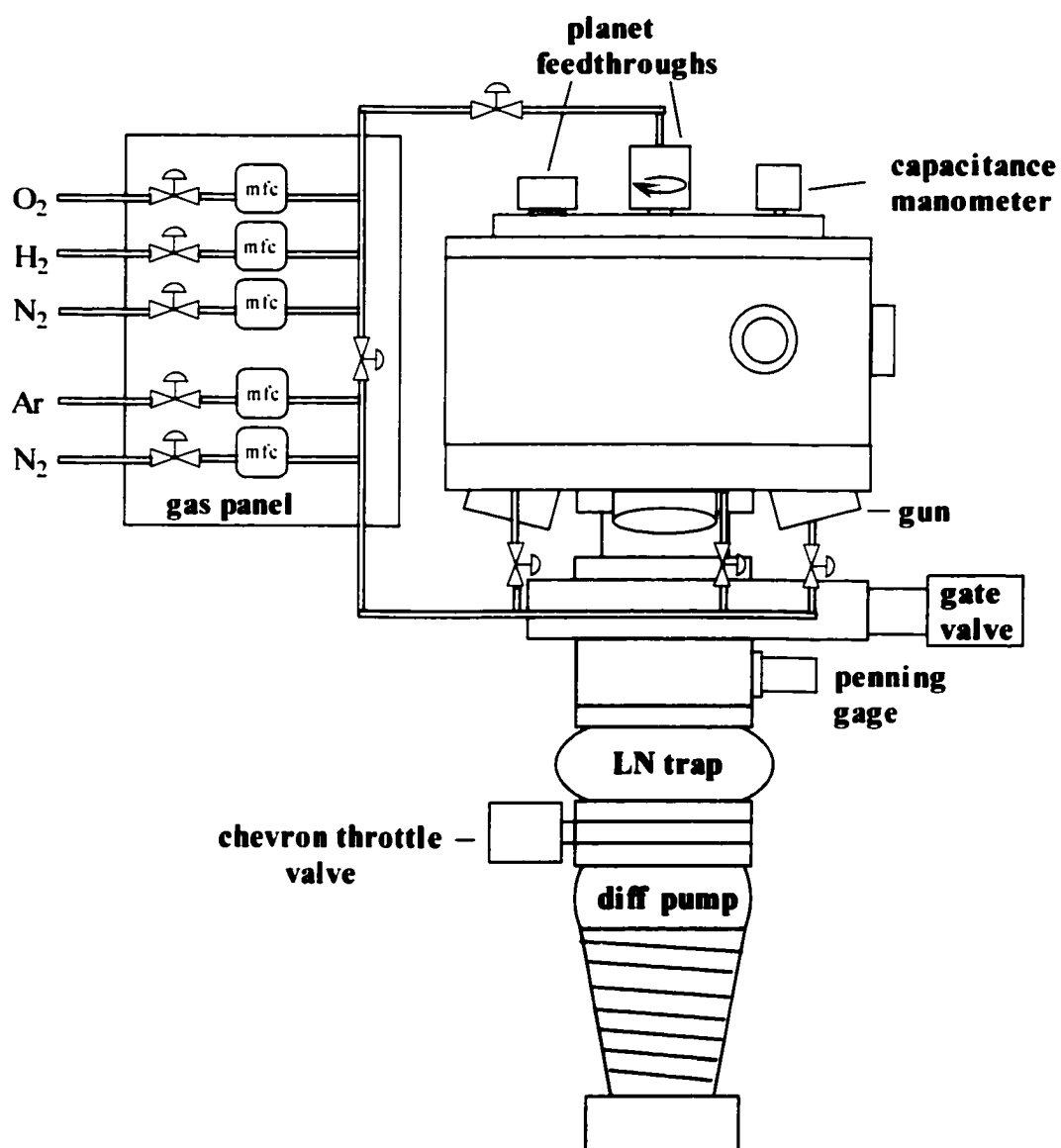
Figure 2.8: Essential plumbing of vacuum system used in the present work.

It may be noted from Figure 2.8 that the gas panel may provide gases to the chamber separately or mixed to either the planetary system or to any combination of magnetron sources. Additional valves and filters for maintaining panel cleanliness are not included for clarity. Redundant pressure gages. including a 1 Torr capacitance manometer. were utilized for attaining an accurate and repeatable reading of the sputtering pressures.

The sputtering power supplies used in this work included a 5kW ENI OEM-25 power supply for R.F. sputtering at the standard 13.58 Mhz. The D.C. sputtering experiments were conducted with both an Advanced Energy MDX 1kW power supply. and an older-style homemade D.C. power supply utilizing a high-reactance transformer. bridge. voltage multipliers. and LCR filtering. These two very different types of D.C. power sources allowed the ability to negate power conditioning factors in ascertaining some of the more novel plasma effects explored in this work.

2.5.1 Substrate Temperature Issues

The issue of substrate temperature in vacuum materials processes is one that is frequently dealt with in an overly casual manner. Frequently. substrate temperatures are reported which only describe the temperature of a thermocouple junction. the latter which may be far from thermodynamic equilibrium with the material growth interface. The use of pyrometric techniques which record a temperature from a relatively complex thin film stack must also be viewed with a healthy skepticism. The reason for uncertainty in both cases derives from the dominance of emissivity issues in high vacuum heat transfer. and

the fact that the growing thin film will normally represent only one extremity of the substrate heating apparatus. In the growth of dielectric thin films. the issue is further complicated by the relative transparency of typical oxides (non-conducting oxides) to infrared radiation. Add to this the fact that. in the case of ferroelectric films. the oxide film is frequently being grown on a highly specular metal electrode material with high. broadband. reflectivity in the infrared region (e.g.. platinum).

In processes that produce films in conditions of relative thermodynamic equilibrium. these issues produce only fairly minor corrections. In energetic processes. however. such problems may be substantially magnified. In fact. the question of substrate temperature in these energetic processes is. on closer inspection. a very nebulous one. Certainly. energetic processes have been shown to allow lower substrate temperatures with respect to thermodynamic equilibrium phase formation. This is achieved through the existence of energies. at the film growth interface. representing temperatures far exceeding that of the substrate bulk. The question remains. however. as to what sort of temperature gradient is best representative of the energy transferred the underlying substrate layers. Most frequently. low-temperature formation of a film is desirable by virtue of the temperature limitations of the immediate underlying structure. as is the case in the fabrication of high density FeRAM. It therefore follows that low-temperature processing. if it is to have any practical meaning. must be defined by its ability to avoid compromise of those substrate features that are incompatible with "conventional" process temperatures. This is by no means assured by the temperature that is seen by a thermocouple junction located elsewhere in the substrate heating apparatus.

3. RADIO FREQUENCY SPUTTERING IN ON-AXIS AND OFF-AXIS

DEPOSITION OF SBT

3.1 General Approach

The three "sputter-up" scenarios in Figure 3.1 indicate the three basic geometrical arrangements explored in the RF sputtering work performed in this dissertation. Figure 3.1a represents the on-axis sputtering geometry – with various incident angles – used most often in balanced magnetron sputtering. or for energetic ion bombardment in Type II unbalanced magnetrons. Figure 3.1b represents the 90^0 off-axis sputtering geometry used often for higher pressure epitaxial growth, and used here with the Type II unbalanced magnetron to avoid energetic ion bombardment of the growing oxide. Figure 3.1c represents the obliquely off-axis sputtering geometry, used here to explore growth effects due to the intermediate ion energies witnessed in this region of the sputtering environment.

Up until the present writing, all previous work reported on the plasma sputtering of SBT has been conducted through RF sputtering of a pressed ceramic target. In fact, the vast majority of work conducted in the plasma sputtering of such complex oxides is performed by this method. The reason for this is operational simplicity. In sputtering processes for complex oxides, transferring the composition of a ceramic oxide target to the substrate is a relatively straightforward task at suitably high (>20mTorr) pressures.

While the development of film properties will still rely very heavily on the skills of the operator, the problems associated with compositional control and reproducibility

are greatly reduced. Compositional control problems are all but eliminated if one

conducts sputter deposition of a ceramic target in high oxygen partial pressures in the 90^0

off-axis mode.
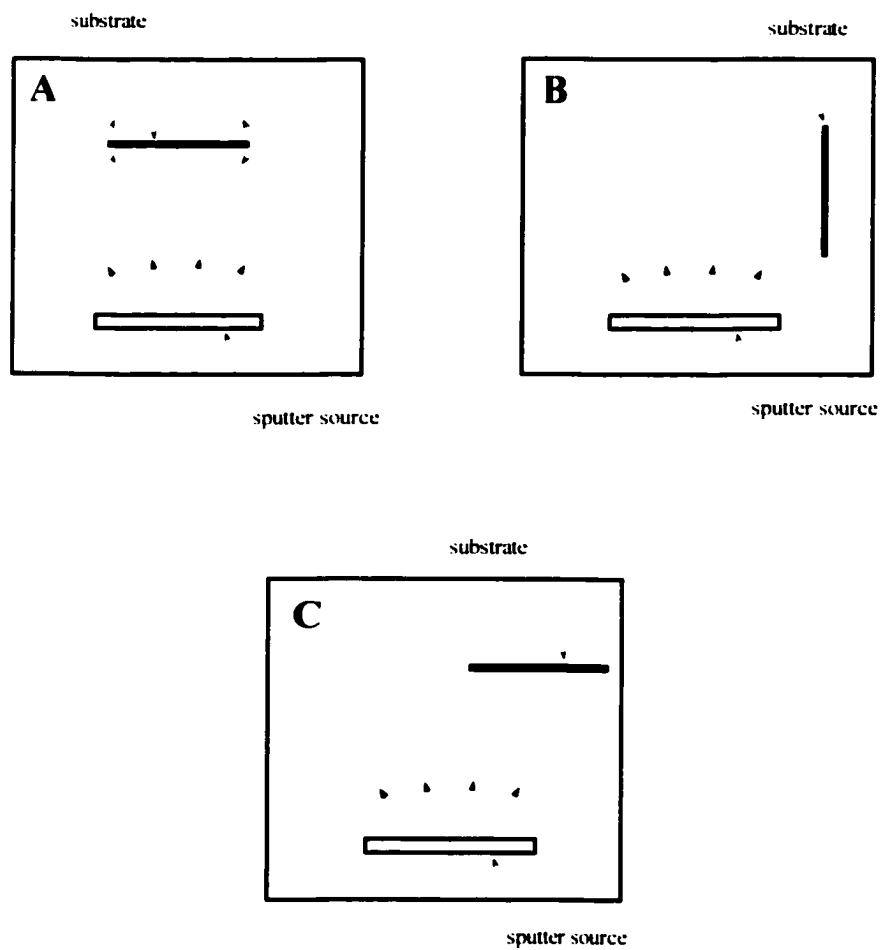
Figure 3.1: The three basic chamber geometries used for
R.F. sputter deposition from ceramic SBT targets.

In such processes, the oxygen is provided in sufficient abundance to ensure the surface of the target remains completely oxidized. At the same time. the 90° off-axis mode removes the substrate from damaging and resputtering interactions due to on-axis bombardment by fast neutrals and negative ions accelerated through the cathode potential. Also. in these high oxygen partial pressures. the sputtering rates of the metals are equalized to the consistently low sputtering yields of their respective oxides; and in fact. to the sputtering rate of the resulting oxide phase (e.g.. perovskite). Even in the event that phase separation occurs at an originally. say perovskite. target surface. while the sputter yields of these metal oxides will differ somewhat. the variation is orders of magnitude less than that of metals. This is especially important when sputtering multi-component materials containing metals of dramatically different vapor pressures. such as in the case of PZT or SBT.

However. sputtering of multi-component oxides at these high oxygen pressures presents severe limitations on the less obvious issues of thin film formation. One such limitation pertains directly to one of the primary goal of this work: that is. lowering the deposition temperature of the SBT deposition process. While high pressure sputtering holds promise for processes in which a high substrate temperature is not an issue (for instance. sputter epitaxy has achieved notable success at near equilibrium growth temperatures). the non-equilibrium mechanisms that allow low-temperature phase formation can generally be seen to vanish as the sputtering pressure reaches several tens of millitorr. A sense of this transition may be acquired through consultation of the well-

accepted Thornton model of pressure-temperature-film structure relationships for a diode

sputtered metallic film.

Another limitation of sputtering at these high pressures (>50 mtorr) is the

difficulties in achieving dense microstructures and smooth surface morphologies. These

two issues are mentioned simultaneously because their causes are frequently intertwined.

This is particularly true in the case of SBT. where films deposited in an amorphous

phase. or the low-temperature fluorite phase. must be post annealed at temperatures

approaching 800 °C. This post-annealing inevitably results in grain-coarsening. resulting

in increased surface roughness. as well as the inevitable occurrence of voids. Even as-

deposited films will show substantial increases in film porosity as the sputtering pressure

is increased. This latter tendency becomes quite marked at lower substrate temperatures.

while films deposited above the epitaxial temperature may tend to surface-roughen in

accordance. essentially. with the crystal growth anisotropy. As a result of these issues

associated with higher pressure sputtering. the deposition of SBT. throughout the present

work. has been conducted in the lower end of the magnetron sputtering pressure range.

between 1-10 mTorr.

3.2 Target Development

In the preliminary stages of the work described in this chapter. experiments were

conducted in RF sputtering of SBT through the use of powder targets. An advantage of

using the "sputter-up" configuration is that one is allowed to perform initial experiments

efficiently and economically by using powders of the intended target material. before

taking on the expense of custom target manufacturing and being delayed by lead-times. Instead. easily obtained. high-purity oxide powders of the required mole fraction are ball-milled and placed in an aluminum dish of the required target dimensions. Long pre-sputtering periods. at low RF powers. are utilized to sufficiently clean and stabilize the powder target before actual deposition begins. Lightly packing the powder into the dish will normally expedite thermal transfer to the water-cooled cathode. without resulting in fracture or rupture of the powder target. Although power densities are quite limited. powder targets allow preliminary results to be obtained without the costs associated with attempting various stoichiometries in ceramic targets.

The first runs conducted with powder targets were performed using powders of the SBT composition. While the author has found this method useful for depositing ferroelectrics and other multi-component oxides. studies performed on sputtered SBT using powder targets were unusually troublesome. As a result. however. insights were obtained into the failure mechanisms and limitations of sintered ceramic SBT targets.

It was found that these targets were prone to catastrophic failure during sputter deposition. in which case. local hot spots on the sputtered target surface would initiate an exothermic transformation throughout the powder. This transformation manifested in a "Roman candle" appearance at the sputtering target surface. It was determined that such catastrophic failure occurred only when bismuth was present in the target powder mixture. This determination proved useful later. as power scaling tests on (unwanted) ceramic SBT targets would ultimately result in similar catastrophic behavior. resulting in glowing spots in the target. and ultimately in "sparks" and spalling. Such behavior

became likely at target powers exceeding 200 watts R.F., for a two inch target. Reasons for this behavior may likely be attributed to the plasma/vacuum reduction of the bismuth oxide, in addition to the mutual affinity between Sr and Bi at elevated temperatures.

The desired phase development for RF sputter deposition from ceramic targets is obtained most reproducibly by maintaining the RF power at a considerably lower level than what would be desired for a high throughput system. Attempts to increase the RF power supplied to the SBT target resulted in one of several undesirable outcomes. The more predictable of these outcomes is target cracking and spalling, due to thermal shock. These difficulties have been reported elsewhere in the literature of sputtered SBT ceramic targets(Lee 1997). While thinner targets and more efficient thermal sinking will improve thermal shock resistance and reduce the extent to which the composition at the target surface is modified, such issues appear to be permanent in the sputtering of complex oxide targets that contain disparately volatile components.

The first ceramic targets used were commercially supplied uniaxially hot-pressed targets supplied by the Praxair Corporation. Two such targets were obtained, with nominal compositions of $SrBi_2Ta_2O_9$ and $SrBi_{2.1}Ta_2O_9$. Depositions were performed with the heated substrate assembly located at various on-axis and off-axis positions. The substrate temperature was varied within a range of 300-600 °C. Also, the total pressure was varied between 2 to 7 mtorr, so that quite a large number of deposition experiments were performed to adequately sample the resultant process space. It was thus adequately determined that these target compositions tended to produce Bi-deficient films in the low total chamber pressures (<10 mtorr) used here for non-equilibrium growth. The X-ray

diffraction data from these films indicated a variety of Bi-deficient phases. varying from the Bi-deficient pyrochlore phase to even various forms of strontium tantalate.

With the observation in initial thin film studies that the target compositions obtained from Praxair frequently resulted in bismuth-deficient films. in-house capabilities were developed for producing several ceramic SBT targets with different Bi-rich stoichiometries. This effort was undertaken to determine whether SBT ferroelectric thin films could be obtained more readily with an appropriately compensated target composition. Various targets were prepared through mixing oxide powders of the appropriate molar quantities. These mixed powders were uniaxially pressed in a stainless steel die. and subsequently annealed at 1100 °C in oxygen. Bismuth loss was accounted for by weighing the targets after the annealing cycle.

3.3 Non-Equilibrium Growth Studies

One of the primary goals of this work. and for much of the thin film work in SBT. is to lower the processing temperature of SBT so as to meet the thermal budgets allowable for device manufacture. Because of this latter requirement. most of the thin film deposition performed in this work was aimed at attaining as-deposited. low-temperature formation of the perovskite phase on heated substrates.

It has become recognized that. while ferroelectric SBT provides fatigue-free operation on standard platinum electrodes. the high temperatures required for processing SBT. as well as the reactivity of bismuth. present additional problems in using metal electrodes with this material. The probability of encountering hillock formation. which

plagued earlier work in PZT. increases with the greater processing temperatures of SBT. Aside from hillock formation. an even greater difficulty encountered in using platinum metal as the electrode material in SBT devices is the propensity of bismuth to react with the underlying electrode structure. The diffusion of bismuth from the SBT film into the underlying platinum electrode is a problem that has been well documented (Matsuki) (Tsai 1998) (Park 1997). However. the activity of Bi in the underlying electrode metal is found to present unique. frequently heteroepitaxial. issues when SBT is deposited by vapor deposition methods. as will be discussed in the following sections. Such issues greatly complicate the process of unambiguously identifying both the phases/orientations present in the completed heterostructure. as well as the mechanisms by which the resultant structure is achieved. These difficulties become greater still when the process is as highly non-equilibrium as the reactive sputtering processes developed here. wherein various metastable phases may form.

Due to the complexity introduced by using metal electrodes. studies were frequently performed using amorphous fused silica as the substrate. The use of fused silica eliminated problems associated with bismuth diffusing into the alternative metallic substrate materials. and provided an amorphous standard on which to observe crystal growth orientation. The x-ray amorphous nature of fused silica also enabled unambiguous identification of the diffraction data in establishing new phase development information.

3.4 On-axis and Obliquely-Off-Axis Sputtering

Some simple yet informative studies were performed using stationary, fused

silica, substrates to determine the effects of plasma bombardment on SBT phase-

development at the substrate, with the "Type II" unbalanced-magnetron source. Large

(6"X6") fused silica plates were positioned over the magnetron, so as to determine the

range of "off-axis" positions one might expect to obtain successful formation of the SBT

phase at the reduced operating pressures desired. These deposition runs were conducted

at room temperature. The fused silica plates were subsequently scribed and diced into

smaller sections for annealing. Performing XRD analysis on these pieces then allowed a

construction of the relative adsorption of the sputtered Sr, Bi, and Ta components as a

function of off-axis positioning for room temperature deposition. One may note that

these process conditions do not provide a promising means for depositing materials that

are sensitive to re-sputtering of a volatile component from the growing film, at least in

any on-axis position.
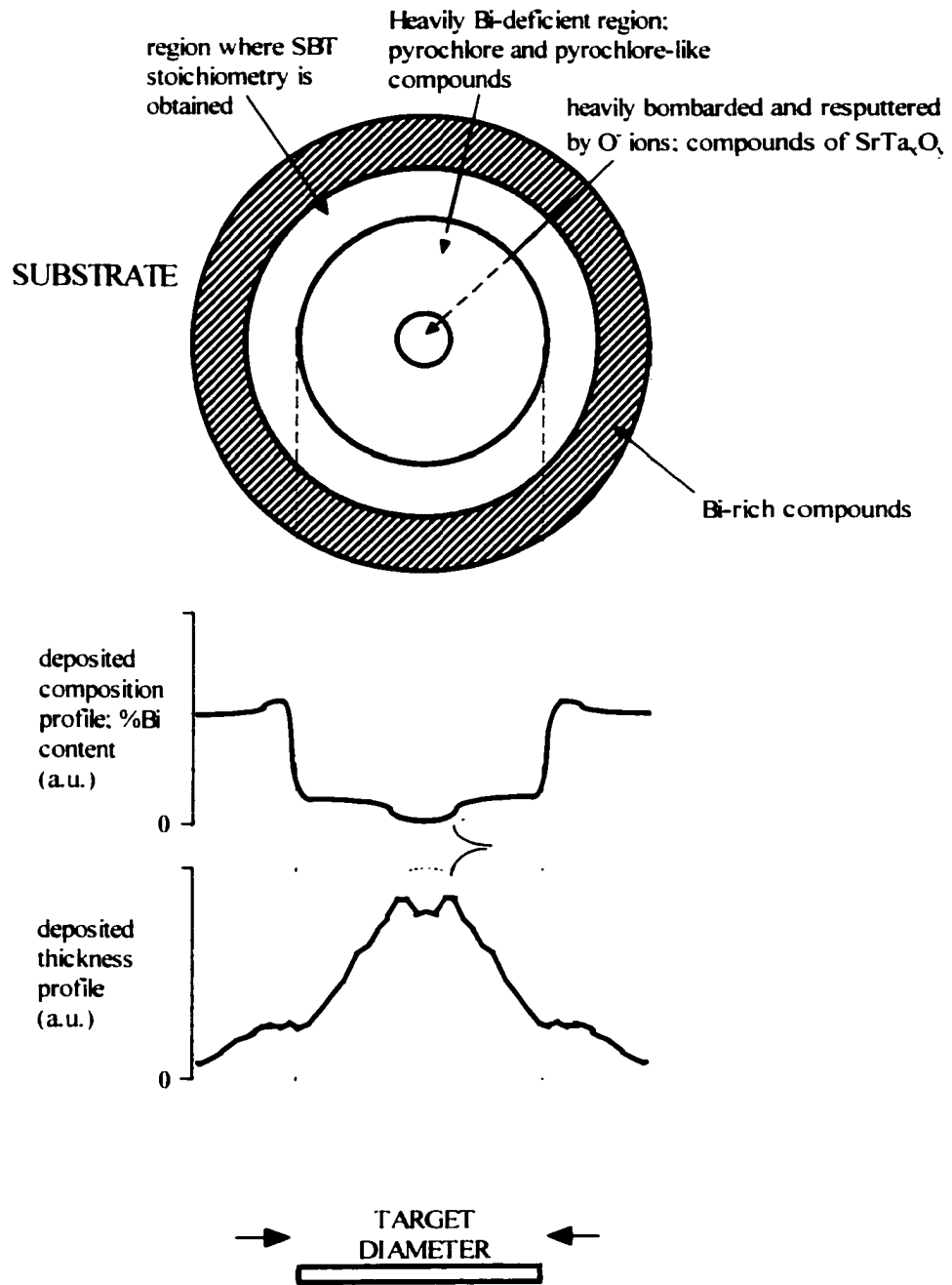
Figure 3.2: Spatial composition and thickness profile
produced by on-axis. RF. unbalanced magnetron
sputtering of SBT target.

The spatial composition and thickness profiles are shown in Figure 3.2. which is

characteristic for the typically applied "Type II" UBM sputter source. Though it as such.

the inhomogenous thickness profile is not a "cosine distribution", as typically witnessed

for metal sputtering at short target-substrate distances (Vossen. Kern 1978). Target-to-

substrate distances in this geometry, roughly a 3:1 aspect ratio to the target diameter.

tended to cancel these effects. which was evident in the roughly $\pm5\%$ distribution in the

sputtering of low volatility metals. Instead. the inhomogenous deposition profile of

Figure 3.2 is obtained primarily as a result of the interplay of the "Type II" unbalanced

magnetron source and the oxygen-containing environment. The energetic nature of this

unbalanced magnetron environment was manifested differently. depending upon the

precise process conditions. However. the effect of heavy re-sputtering at the substrate in

the on-axis region. as depicted in the resultant Bi-deficient film in Figure 3.2. was

common to all RF-unbalanced magnetron sputtering experiments. The heavily re-

sputtered central region of the substrate indicates the formation of a negative ion "beam"

at the sputtering axis. The formation of such negative ion beams. by electronegative

gases such as oxygen. in sputtering sources has been discussed by other researchers

(Penfold 1995). It may be expected that this effect is significantly enhanced for

unbalanced magnetron "Type II" sources.

In the present work. this negative ion beam has been found. under some

conditions. to prevent *any* deposition at the central on-axis position. In some instances.

when depositing on a Pt electrode stack. a central 1-2 cm diameter region of the Pt

electrode had actually been completely sputtered away. leaving only a bare ZrO_2

adhesion layer. While the deposition profile of Figure 3.2 does provide a rather unique depiction of the "Type II" unbalanced magnetron sputtering environment used here. its significance in developing new methods for depositing complex oxides will become more evident in the following chapters.

3.5 90^0-Off-Axis Sputtering of SBT onto Heated Substrates

While 90^0 off-axis sputtering is a technique that is unlikely to be incorporated into a production environment. it does allow a relatively straightforward means of transferring the target stoichiometry to the substrate. without the damaging effects and re-sputtering that tend to plague on-axis deposition. The use of 90^0 off-axis sputtering with a "Type II" unbalanced magnetron allowed for studies to be performed in a much less energetic deposition environment. though the precise placement of the substrate proved to largely effect film growth at lower pressures (P < 10 mTorr).

The fabrication of ferroelectric SBT capacitors. in 90^0-off-axis sputtering, on room temperature substrates with suitable electrode structures. proved to be relatively straightforward. As a result of these observations. a series of experiments in 90^0-off-axis sputtering of SBT onto heated fused silica substrates was performed to provide standards for subsequent on-axis sputtering on Pt electrodes. In these 90^0-off-axis studies. substrate
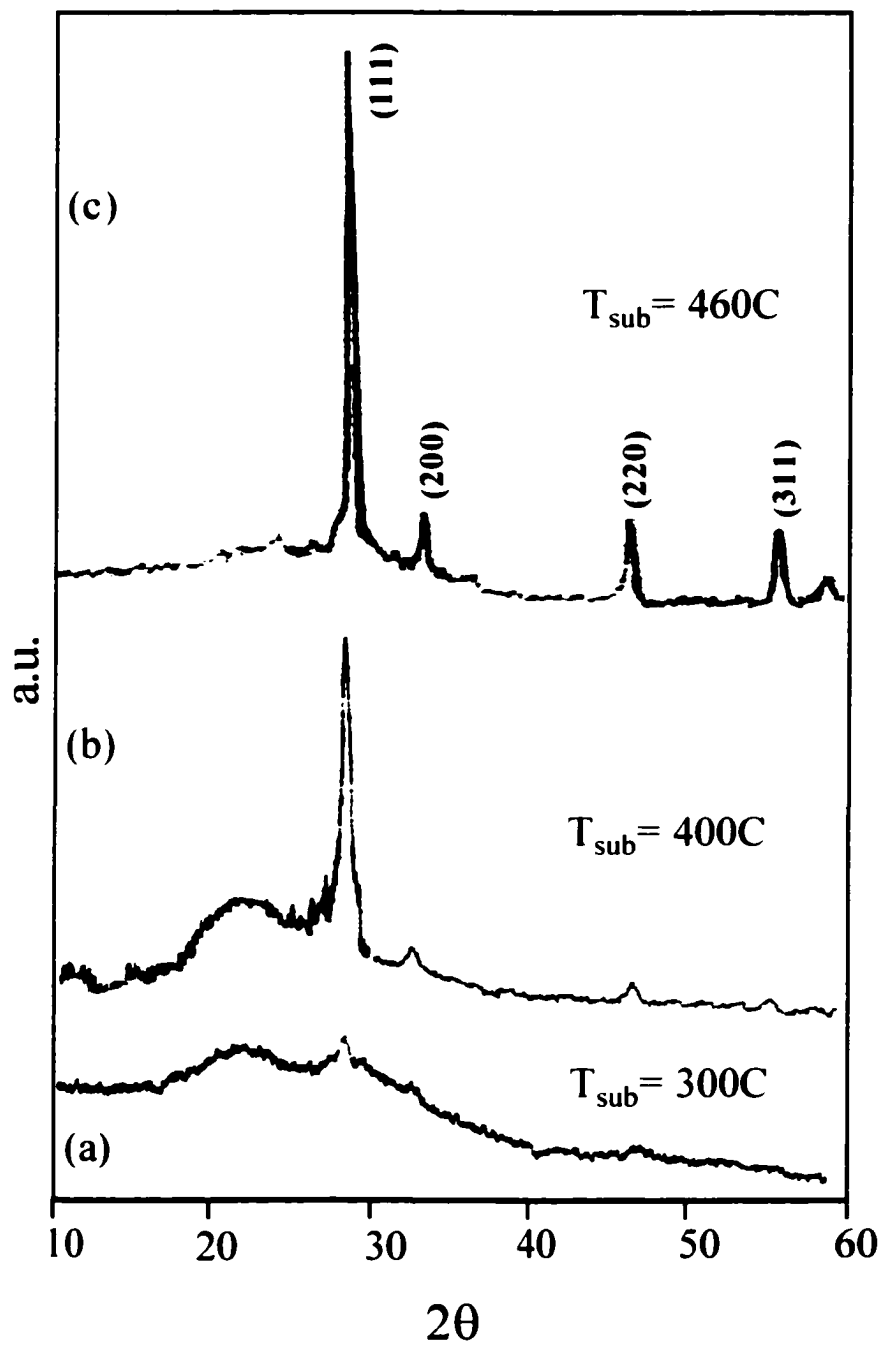
Figure 3.3: XRD 2-θ scans series of as-deposited 90°-off-axis.
RF-unbalanced magnetron sputtering; phase development
on SiO_2 for different T_{sub}.

temperatures were varied from room temperature to 600 °C, using a stationary, resistance-heated substrate fixture. Higher substrate temperatures were not used because it was soon determined that this configuration allowed a considerable reduction in the substrate temperature required for deposition of phases in the SBT phase space.

In Figure 3.3 is presented the phase development of SBT films deposited on heated fused silica substrates, from a ceramic $Sr_{0.8}Bi_{2.3}Ta_2O_x$ target using low pressure, 90°-off-axis, "Type II" unbalanced magnetron sputtering. The x-ray scans of Figure 3.3 would, at first, appear to be the development of ferroelectric SBT, and essentially identical phases are reported as ferroelectric SBT in the existing literature. Given the almost identical match of 3.3(c) with the ferroelectric SBT phase, as well as the degree of crystallinity observed, it was hoped that such low-temperature thin film development would provide the sought-after ferroelectric properties. Unfortunately, repeated capacitance testing of this phase in various fabricated devices has determined that it is not ferroelectric.

It is suggested here that Figure 3.3(c) is an alternative, apparently metastable, phase that has not been properly identified in the literature. It is submitted here that Figure 3.3(c) is the fully crystallized version of the frequently reported defective fluorite phase, which is normally observed in a poorly crystallized form, as may be seen ahead in Figure 3.5(b). The phase of 3.3(c) is believed, here, to be metastable because it is only obtained through such non-equilibrium methods as those used here. It is not witnessed in work using more equilibrium methods, such as sol-gel, MOD, or bulk ceramic studies.

Since this phase development has not yet been properly identified. this phase will herein be referred to as the Metastable Fluorite (MF) phase.

In Figure 3.4. it is demonstrated that the MF phase of 3.3(c) is indeed of the desired SBT composition. The polycrystalline SBT structure of Figure 3.4 was obtained by annealing the MF phase. as-deposited on fused silica. at 750 °C in oxygen. whereby the actual ferroelectric SBT peak locations are obtained. It was disappointing but instructive to note that. whereas the x-ray reflections of the ferroelectric SBT phase normally appear to emerge from the poorly crystallized fluorite phase at around 700 °C in previous. more equilibrium-based studies. the metastable fluorite phase of 3.3(c) required annealing at 725-750 °C before transformation to ferroelectric SBT would commence. This added phase transformation barrier to achieving the SBT phase provides further evidence that the fluorite phase is a competing. high-temperature. metastable phase. rather than a low-temperature precursor phase. To further support that the phase development of Figure 3.3 is that of a metastable fluorite phase. rather than the ferroelectric SBT phase. it may be noted that annealing the MF phase of Figure 3.3 produces a consequent crystalline structure from which significantly broader x-ray reflections are obtained. in Figure 3.4. This result does not suggest further development and grain coarsening of an existing phase. but rather. that there has been a phase transformation to a new phase.
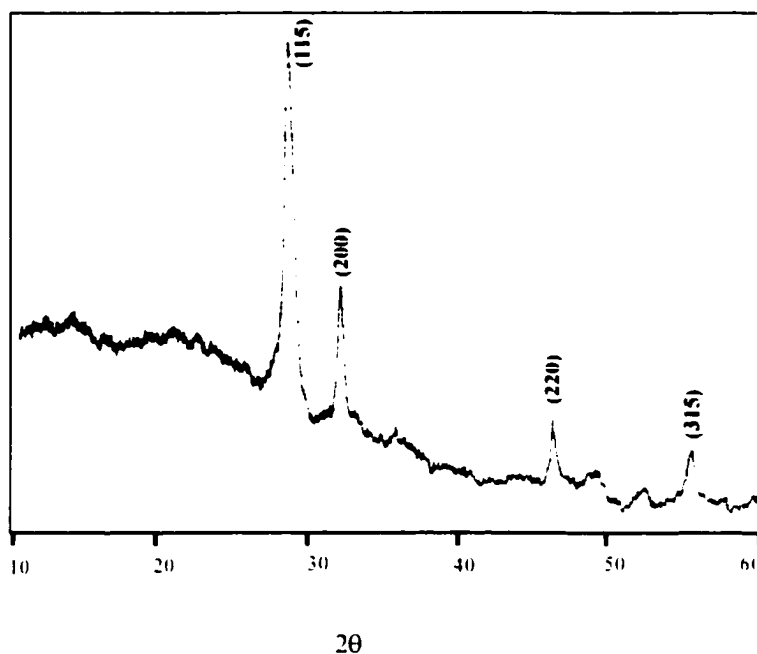
Figure 3.4: XRD 2θ-scan of an SBT film on fused silica, obtained by annealing the "MF" phase at 750 °C in O_2.

The XRD scan of a fully crystallized version of the as-grown MF phase is presented in Figure 3.5(a) for comparison to standard development of the fluorite phase, in Figure 3.5(b), obtained by annealing a powder, of the SBT composition ratio 1:2.2:2, at 630 °C in oxygen. As may be seen in the figure, the sputtering method developed here provides the development of a fully crystallized film at 460 °C, whereas the standard annealing process at 630 °C allows only a poorly crystallized version of the same composition.
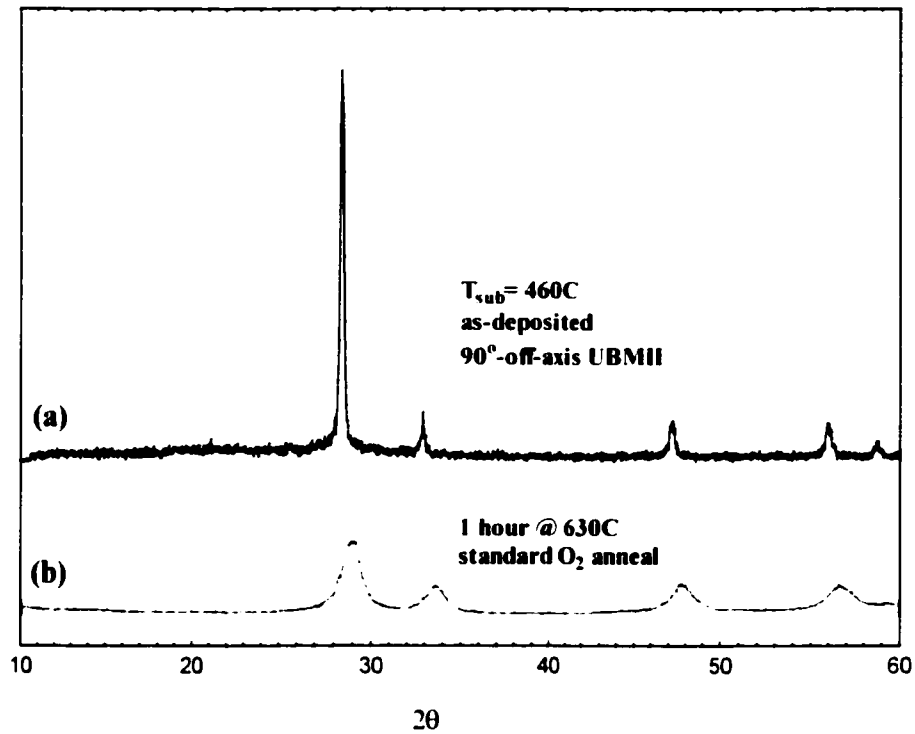
Figure 3.5(a) & (b): Comparison of MF phase developed with 90°-off-axis RF-unbalanced magnetron sputtering at T_{sub}=450 $^{\circ}$C. to standard development of same SBT composition powder at 630 $^{\circ}$C/1hr/O_2 anneal.

The development of the fully crystallized MF phase appears to be unique to

energetic. non-equilibrium growth processes. However. it appears the as-grown. fully

crystallized MF phase. suggested here. has been presented. in previous work. as the

ferroelectric SBT phase. with the strong reflection at about $2\theta = 28.4^{0}$ presented as the

(008) peak of c-oriented ferroelectric SBT (Li 1996) (Yang 1998). This work provides

the first recognition of this full phase development as corresponding to that of the

metastable fluorite phase, rather than to that of the SBT ferroelectric.

There is much evidence, found throughout the present work, that the development

of the MF phase is inherent in the more highly non-equilibrium growth processes. This

was evident in the present study by the repeated occurrence of the MF phase on a variety

of poly-crystalline and amorphous substrates, including fused silica, Pt and IrO. The MF

phase was also seen to occur for each of the very disparate, but all highly energetic,

growth environments developed in both this and the following chapter on reactive D.C.-

sputtered SBT. For example, the MF phase demonstrated here on Pt electrodes is

demonstrated again on a Ir/Ti/Si substrate, in Figure 3.8. SBTN (Tsai 1998).

Unfortunately, however, fabrication of thin films that possess a desired final SBT-type

composition requires quite different starting film compositions, depending on whether the

film requires a post-process anneal, due to the loss of Bi during the anneal. The loss of

Bi to both the electrodes and to the gas phase has been well documented (Dhote 1999)

(Kim 2000) (Im 1998) (Seong 1998). One major advantage of using the energetic,

highly non-equilibrium deposition methods explored in the present work is the ability to

create film compositions and phases without composition gradients incurred by out-

diffusion of a volatile component like Bi. Therefore, phase formation during the non-

equilibrium processing will reflect the initial composition of the formed film, whereas

high temperature post-process anneal will result in a phase formation dependent upon the

depletion of the volatile Bi to the surrounding electrodes and gaseous environment. As a

result, the desired composition of the film can be obtained only for the precise choice of

processing steps and electrode materials. For example, while the fully crystallized MF phase may be converted to phase-pure SBT on fused silica substrates, it is difficult to obtain the as-deposited MF phase on a metal electrode without it becoming Bi-deficient during the post-process anneal.

Figure 3.6(a) shows identical phase development, for as-deposited films at 500 °C, reported by Kim, et al. where it is assumed that the phase under consideration is the ferroelectric SBT phase (Kim 1999). They attributed the nonferroelectric properties of these films to excess Bi, where the existence of excess Bi was based upon XPS studies. However, such XPS data are not a clear indication of the overall film composition, since only surface states are interrogated. It should also be noted that other XPS studies have found that SBT films are inherently prone to surface termination with reduced Bi bonding states (Gutleben and al 1995).

A reported low-temperature MOCVD method was also found to exhibit the same MF phase, in Figure 3.6(b), where it is also misidentified as the SBT phase. As in the above report, the 28.4^0 peak is identified by Li et al. as the (008) reflection, though no other (001) reflections are present (Li 1996). The phase appears at 600 °C processing temperatures, but must be annealed at 800 °C to yield ferroelectric hysteresis.
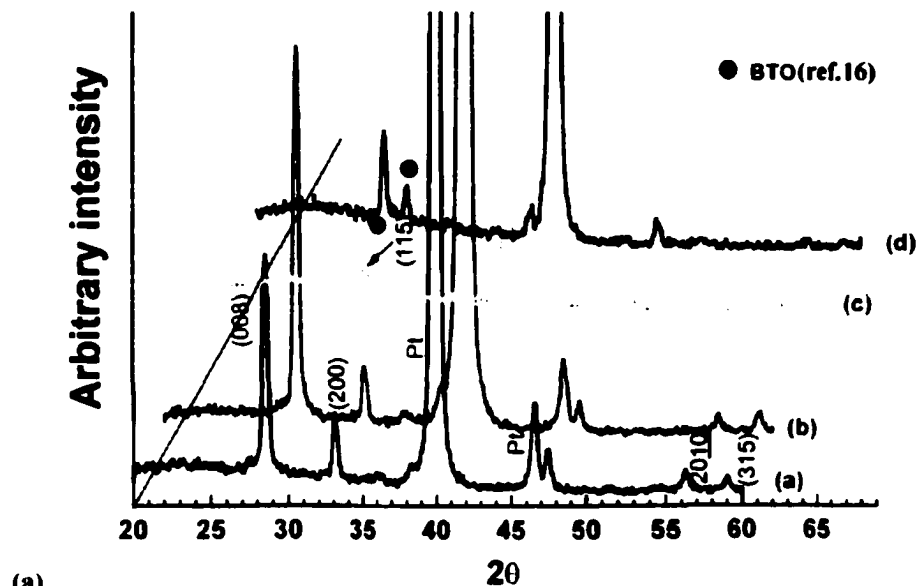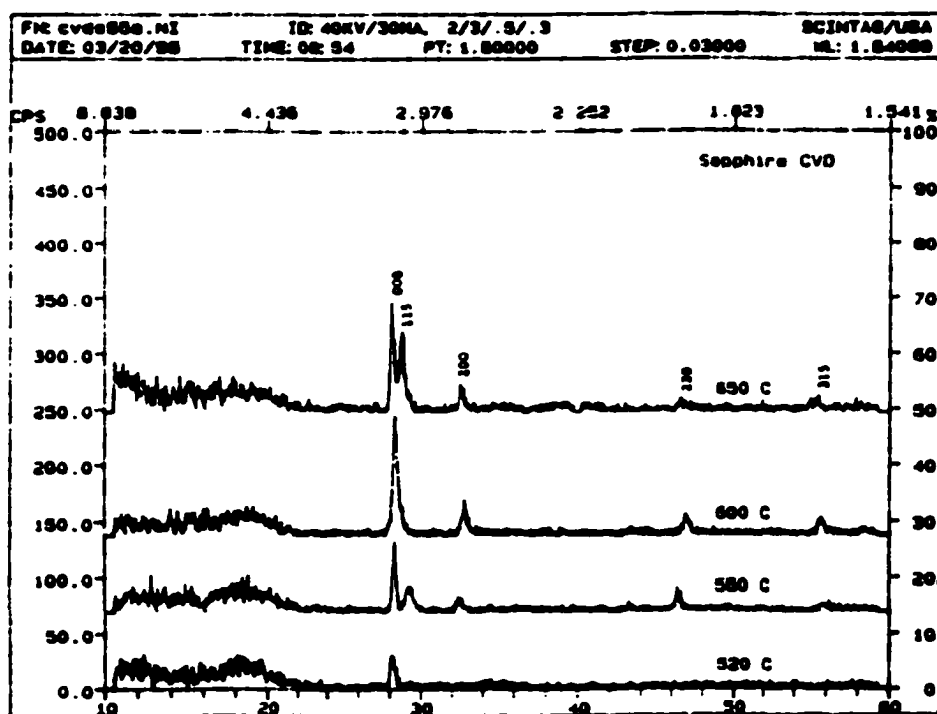
Figure 3.6: Example of previous (not identified) development of the "MF" phase by (a) a hybrid sputtering process (Kim 1999), and (b) a low-temperature MOCVD method (Li and al 1996).

Work on the Bi_2O_3 – Ta_2O_5 system. by Zhou. begins to illustrate the complex

phase space for these types of systems (Zhou 1992).   In this work. Bi:Ta ratios varying

between 1:1 to 60:1 were characterized through x-ray diffraction and TEM methods.

Zhou determined that the defect fluorite structure remained for solid solutions falling in

the range Bi_3TaO_7 to $Bi_{19}TaO_{31}$. The resulting XRD data for this composition region. in

Figure 3.7 revealed a fairly constant fluorite-like appearance. with peak positions quite

similar to the MF phase observed here. It was determined by Zhou that these structures

possessed various degrees of superstructure. thought to be based on cationic ordering.

While the development of this fully crystallized polycrystalline MF phase has not

been identified previously in the literature. it was reasoned that this fluorite phase might

be the same as a secondary phase witnessed frequently in the epitaxial growth of SBT. In

the epitaxial growth community there has been some confusion over identification of a

competing phase in the SBT system.   Lettieri. *et al.* have argued that this epitaxial phase

is an epitaxial impurity phase which may best be indexed to δ-Bi_2O_3. β-Bi_2O_3. or

$Bi_{7.80}Ta_{0.20}O_{12.20}$ (Lettieri 1998) (Lettieri. Weber et al. 1998). Other studies. such as

reported by Hyun. *et al.* have submitted that it is a fluorite-like phase. Lee. *et al.*

performed a TEM analysis of this secondary phase. grown epitaxially by PLD at 600 °C.

where it was indexed convincingly to fluorite structure (Lee 1999). This last study also

found that the as-deposited fluorite phase. as here. only slowly transformed to the
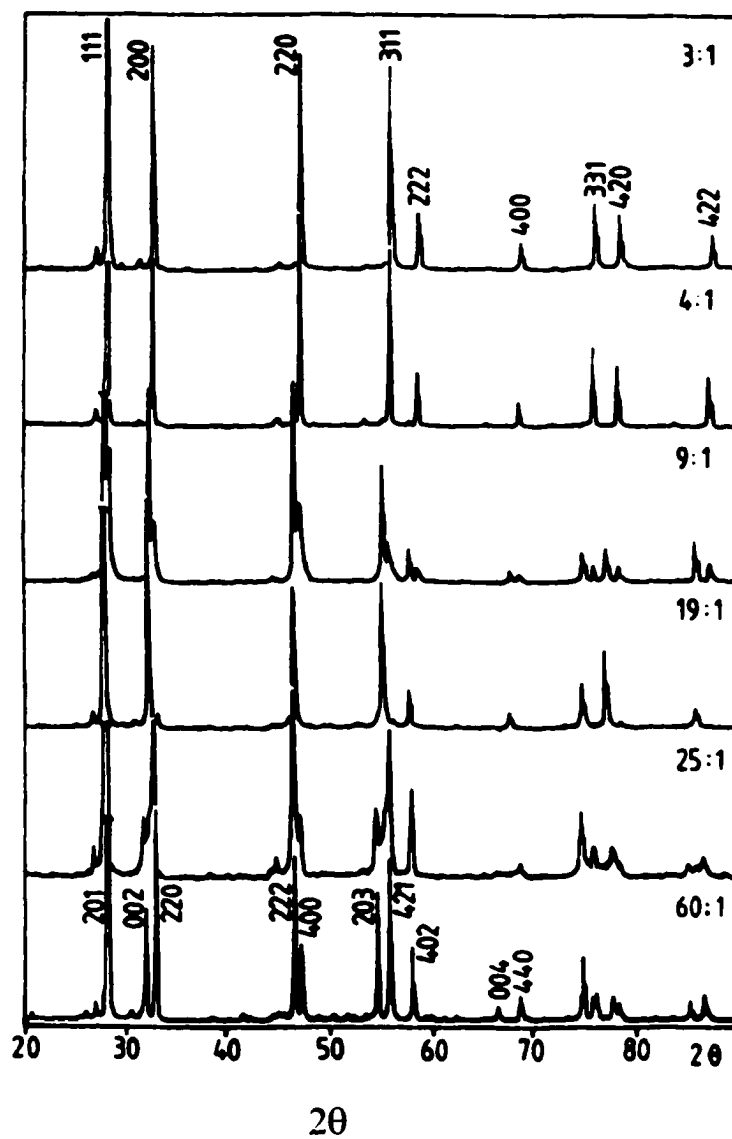
Figure 3.7: XRD scans of a series of
bismuth tantalate compositions (Zhou).

polycrystalline SBT after oxygen anneal at 750 °C for 1 hr. However, the lattice

constant for the secondary phase in these accounts was calculated to be 5.35 Å, whereas

the fluorite phase observed in this work indicates a lattice constant of 5.44 Å.
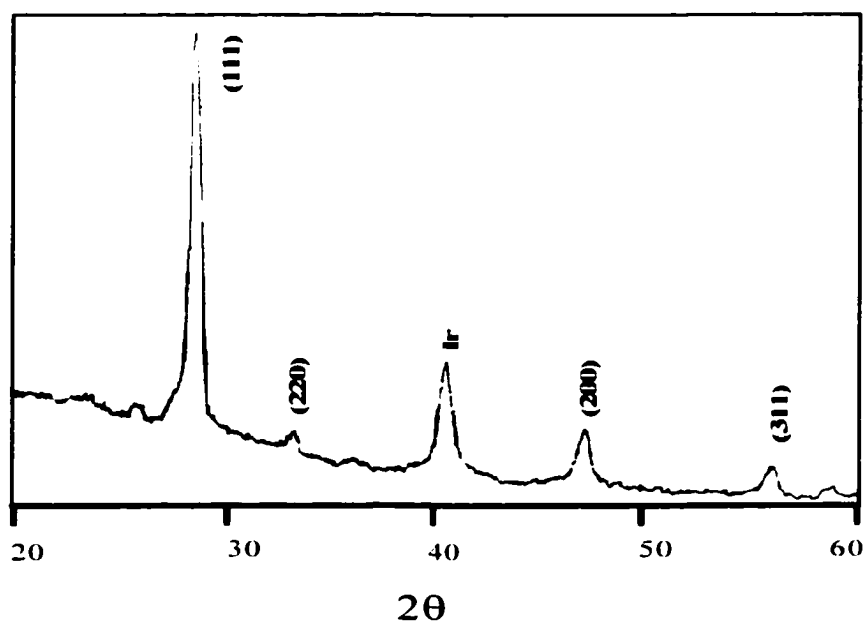
Figure 3.8:   XRD 2-θ scan of obliquely-off-axis, as-deposited SBT
on Ir/Ti/Si electrode at 430 °C.

The ability to use higher substrate temperatures during deposition, and therein

achieve fully crystallized, phase-pure, as-deposited ferroelectric SBT, was not realized in

these ceramic-target studies, due to some fairly permanent issues. One primary issue is

that it is not clear that a higher substrate temperature would ever result in a transition to

the ferroelectric phase. as it is not at all clear that the ferroelectric SBT phase is a higher

temperature phase than the MF phase. In some cases, the as-deposited film would

provide x-ray reflections that suggest a mixture of the MF and ferroelectric SBT phases.

as in Figure 3.8. These results occurred in the obliquely off-axis geometry of Figure 3.1.

which presumably provides greater plasma bombardment than in the 90^0-off-axis

geometry.

When the R.F. unbalanced magnetron process used in this chapter is conducted

with substrate temperatures approaching 500 °C or greater. the resultant films almost

invariably possess Bi-deficient phases. such as the pyrochlore phase in Figure 3.9.

obtained as-deposited at T_{sub}=500 °C. This trend would appear to establish that the

effective temperature at the growth front in the non-equilibrium sputter processes

developed is sufficient for growing the SBT phase. since the Bi-deficient pyrochlore

phase. observed here at T_{sub}=500 °C. generally requires a higher formation temperature in

equilibrium studies – 775 °C. as opposed to 725 °C – than that of the desired SBT phase.

That the effective growth temperature. provided in the sputtering environments used here.

is sufficient for SBT growth is further supported by the observation that the XRD scans

of these as-deposited Bi-deficient phases. such as the pyrochlore in Figure 3.9. are not

altered by the standard 800 °C anneal in oxygen. The main reflections of Figure 3.9 are

labeled according to Rodriguez. et al. (Rodriguez 1996).

It would thus appear that. in these highly non-equilibrium growth processes. the

ferroelectric SBT phase might be more readily obtained by suppression of the MF phase.

rather than by attempting to implement even higher effective growth temperatures. If

suppression of the MF phase is possible. the work presented here suggests that the

ferroelectric SBT phase could be achievable in the temperature range of 400-500 °C.

The second primary issue is the problematic adsorption characteristics of Bi in a

highly energetic plasma process. such as in the low-pressure unbalanced magnetron

process used for RF sputtering in this chapter. The difficulty arises in the propensity for

both Bi-poor and Bi-rich phases to develop under only very slight variations in the

process parameters. This process instability increases substantially as the chosen

substrate temperature is increased to the 500-550 °C range.
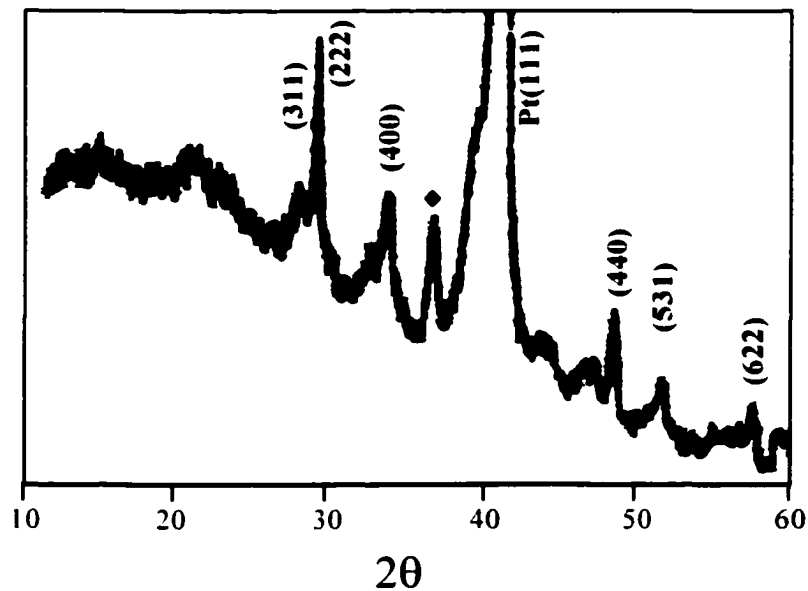
Figure 3.9: XRD 2-θ scan showing development
of pyrochlore at T_{sub}= 500 °C.

Fabricating ceramic SBT sputtering targets with even greater bismuth content than that utilized here would result in even greater instability in the composition at the target surface: hence, such measures were not considered to be a worthwhile course of action. Co-sputtering with a metal Bi target to augment the Bi content in the deposited films is a method that has been reported Yang, et al. and was also performed by the present author (Yang et al 1998) (Yang et al 1998). However, such a co-sputtering arrangement provides even less repeatability than in the case of sputtering a single Bi-rich, SBT target, due to the high sensitivity of the Bi sputter yield to target surface-oxidation. In such a co-sputtering arrangement, the presence of an adjacent ceramic-oxide target, co-sputtered with sufficient RF power, eliminates the ability to accurately monitor the environment of the metal Bi target, so that the actual sputter yield of Bi may fluctuate widely. While the SBT composition was deposited on room-temperature substrates with this configuration, the instability, especially in the unbalanced-magnetron plasma environment, proved this particular co-sputtering arrangement to be an unnecessarily awkward process to implement in either an R&D or a production environment.

Given the deposition profile provided by the unbalanced magnetron in Figure 3.2, it appears that one might reliably acquire the SBT phase by rotating the substrate at a slightly off-axis position. However, this was found to almost always result in either Bi-deficient films, or a prohibitively low deposition rate, in the RF sputtering of a ceramic target. It was concluded that, while on-axis and obliquely-off-axis RF-sputtering of SBT provided interesting and novel methods for exploring the behavior of Type II unbalanced

magnetrons, the lack of control, inherent in the sputtering of ceramic targets, combined with the energetic ion bombardment of the growing film, rendered such process geometries too unstable to enable a viable SBT process.

3.6 Electrical Characterization

Figure 3.10 is a schematic of the Sawyer-Tower circuit design used in the ferroelectric testing of the SBT capacitors. As can be seen, it is the simplest form of a capacitance voltage divider. The sensing capacitor is made relatively large, so as to provide almost no impedance for the current levels used. As a result, the primary voltage

Channel 1
(Applied Voltage)

Ferroelectric Film

AC Signal

Channel 2
(Polarization)
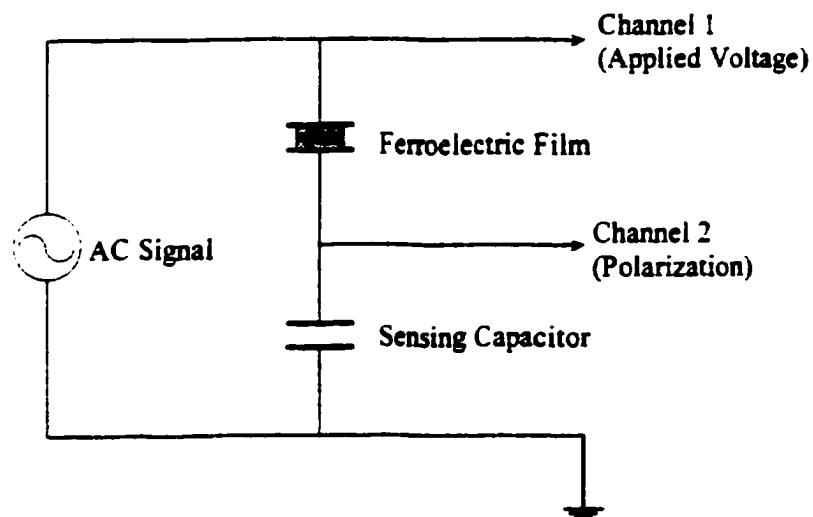
Sensing Capacitor

Figure 3.10: Schematic of Sawyer-Tower circuit
used for F.E. testing (after [4]).

drop will occur across the much smaller sample capacitor. which would be the SBT

capacitor. The value of the sensing capacitance must be accurately known. and the small

voltage drop across the sensing capacitor must be accurately read. if reliable readings are

to be obtained. Because of this latter reality. the sensing capacitance should also be small

enough to permit an adequate polarization signal for the oscilloscope. as well as to

provide adequately low (percentage) errors.

Pt (500Å)
SrBi$_2$Ta$_2$O$_9$ (2000Å)
Pt (1000Å)
Ti, TiO$_x$, or ZrO$_2$ (200Å)
SiO$_2$ (5000Å)
Si(100) wafer
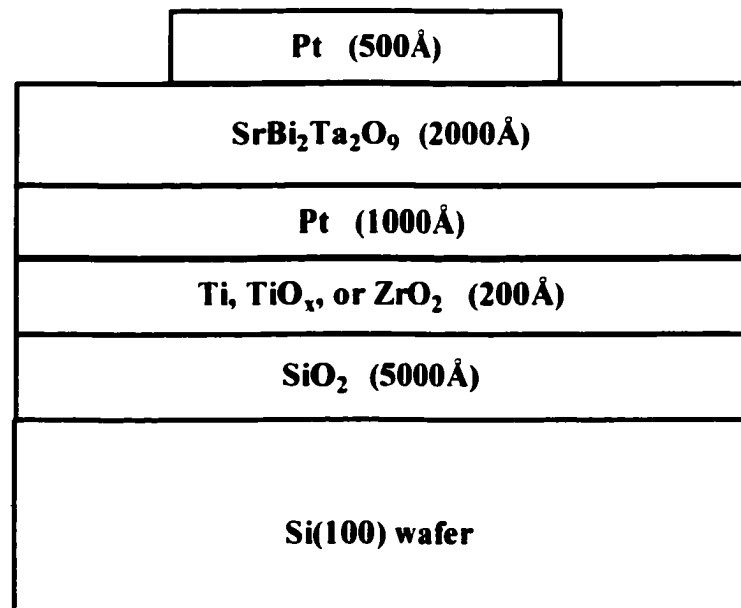
Figure 3.11: A thin film capacitor thin film
stack commonly used in this work.
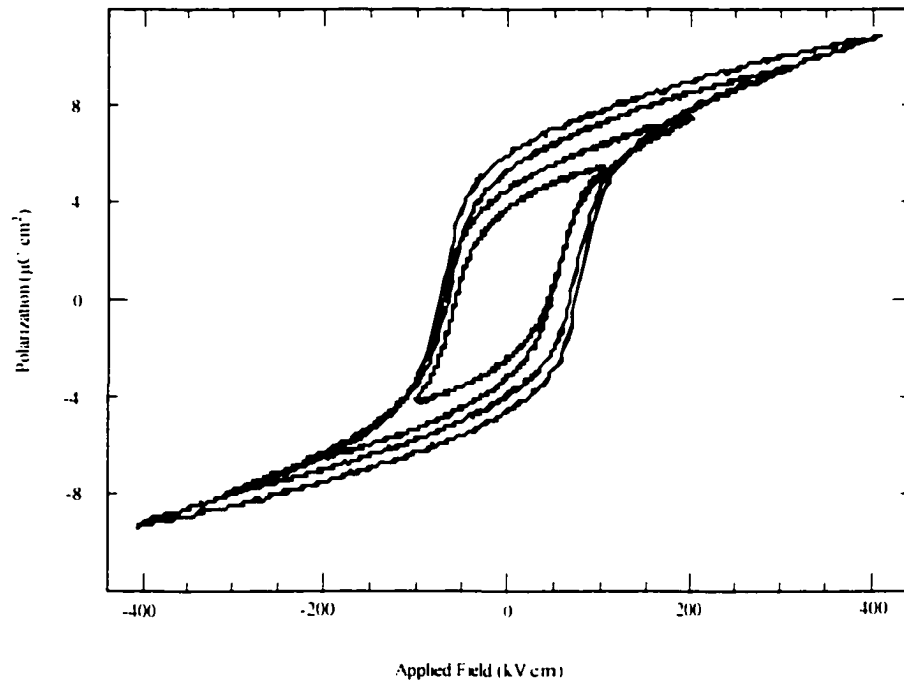
Figure 3.12: F.E. loop for RF sputtered film. deposited at room temperature. annealed at 750 °C in atmospheric O₂.

While various heterostructures were explored for fabricating the SBT capacitors. the standard stack fabricated is presented in Figure 3.11. Other approaches explored include various oxide adhesion layers – rather than Ti – for the interface of the electrode material to the underlying substrate. Experiments were also conducted with metal-oxide

electrode materials. IrO and Ru_2O_3. Various substrates other than Si(100) wafers were also used. These variations will be discussed later as they become relevant.

Figure 3.12 is representative of the ferroelectric hysteresis obtained for room-temperature-to-300 °C. 90° off-axis deposition of SBT films. after an atmospheric oxygen anneal at 750 °C for two hours. Such an annealing regimen is typical for the various deposition methods used for SBT. Ferroelectric properties were measured. yielding $2P_r=8.5$ $\mu C/cm^2$. and coercive field $2E_c=173$ kV/cm. under an applied field of 250kV/cm. While Figure 3.12 demonstrates well-saturated ferroelectric hysteresis. the coercive fields. E_c. required for the room-temperature/post-annealed SBT have been found to be relatively high in this work. The high E_c values recorded here are thought to result from a deficiency in Sr. in the deposited films. relative to Ta. The relationship of E_c to Sr-content in ferroelectric SBT has been well documented in solution chemistry studies. Various annealing regimes were utilized. though the slow diffusion of bismuth into the electrode metal limited the desirability of long annealing times. A typical ferroelectric hysteresis loop for a 700 °C-annealed SBT film is shown in Figure 3.13. which indicates a somewhat less saturated behavior. as well as a significantly lower P_r yielded ferroelectric properties of $2P_r=5.2$ $\mu C/cm^2$. and coercive field $2E_c=118$ kV/cm. under a 250kV/cm applied field.

Though ferroelectric SBT could be readily obtained by the room-temperature. 90°-off-axis method used in the preceding discussion. the use of post-process annealing to attain the SBT phase required unacceptably high temperatures. typical of SBT processing. Presumably. at relatively low target powers. and commensurately low

deposition rates. one could go on depositing and annealing SBT for an exhaustive

characterization of SBT capacitors. with a fairly long (by research standards) useful

target life. However. such an exercise would serve little practical purpose. as this high

temperature process is incompatible with the intended application: in addition. for the

characterization of intrinsic material properties. solution chemistry methods allow a far

more suitable. and economical approach.
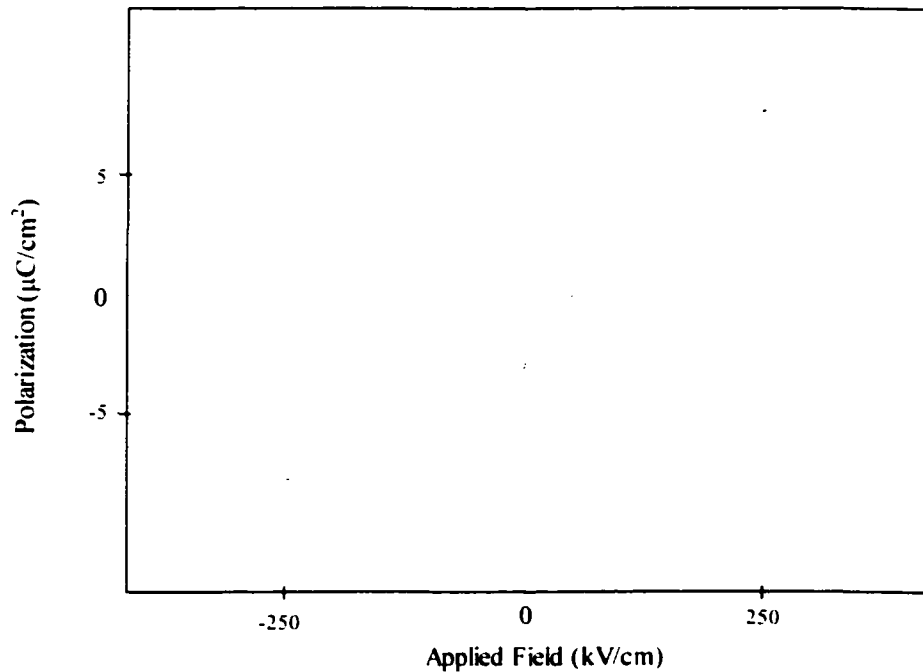
Figure 3.13: P-E loop showing ferroelectric behavior of
sputtered SBT. post-annealed at 700 °C/2hrs in O_2.

Applied Field (kV/cm)
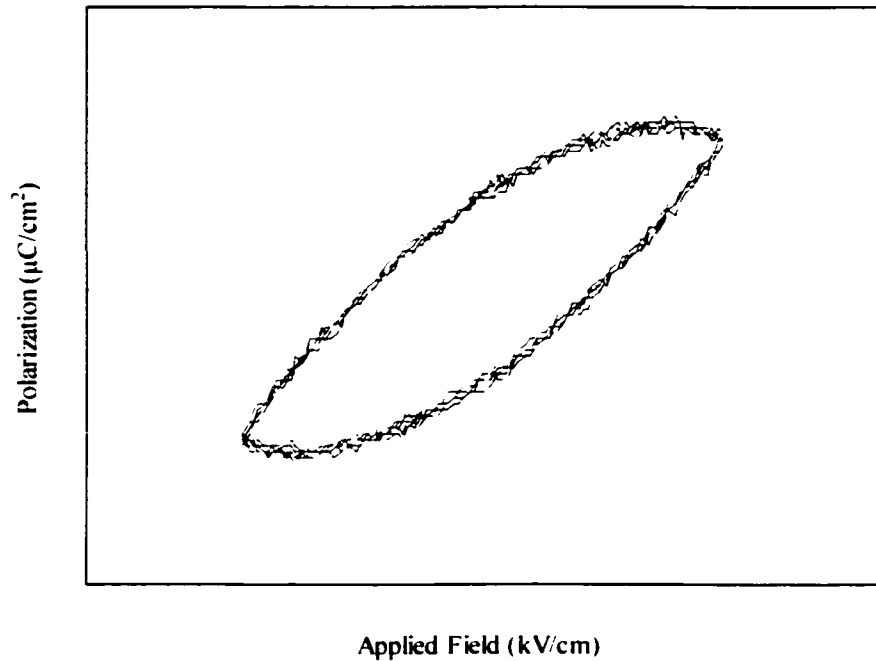
Figure 3.14: P-E loop indicating presence of ferroelectric phase in obliquely off-axis sputtered. as-deposited SBT. which corresponds to the as-deposited (430 ^{0}C) phase formation of Figure 3.8.

While the goal of forming phase-pure SBT. yielding adequate ferroelectric properties. in a low-temperature. *as-deposited* process was not realized in these studies. some ferroelectric behavior was observed in as-deposited films. possibly indicating a mixture of the MF and ferroelectric SBT phases. Another possibility. introduced in the thesis work of Dawley. for the inability to obtain satisfactory ferroelectric properties in the as-deposited SBT films of this work. is that the SBT phase possesses a lower limit in the grain size wherein it will display ferroelectric hysteresis (Dawley 1999). This lower

limit in grain size was placed somewhere in the neighborhood of 20 nm, as assessed by a

Scherrer-type analysis. It has been found throughout this thesis work that as-deposited

films do not display x-ray reflection peaks of half-width appreciably smaller than about

0.5^0, which corresponds to a grain size of about 18 nm, given relatively negligible

machine broadening. This suggests that there may be considerable development of the

ferroelectric SBT phase, albeit with the limited grain growth that may be expected, and is

observed here, for the highly non-equilibrium deposition methods explored here, wherein

adatom mobility and subsequent grain growth are limited by the relatively low

temperature of the solid phase.

The slightly ferroelectric behavior of as-deposited SBT thin films is indicated in

Figure 3.14, which corresponds to the phase development indicated by the XRD data of

Figure 3.8. The sort of behavior displayed in Figure 3.14 has often been presented, in

previous reports in ferroelectric work, as sufficient evidence of the desired ferroelectric

phase being obtained. However, the practice of taking measurements of the remnant

polarization or the coercive field is pointless in these circumstances, since such

measurements will be dominated by the dielectric properties of the deposited film.

3.7 Observation of a "Self-Healing" Process in F-E Devices

In testing for ferroelectric hysteresis, it was found that for capacitors originally

displaying shorted behavior, the capacitor structure could be "healed" through application

of a considerably higher test voltage. During application of the high voltage (typically

above 200 kV/cm) one could then observe the oscilloscope trace to return to a standard

hysteresis loop. as is shown in Figure3.15. In this way. fully shorted SBT capacitors would frequently convert to well-saturated ferroelectric traces that showed now evidence of lossy behavior. One could then test the same capacitor at voltages up to 400kV/cm. This observation would most often occur for SBT deposited at room temperature. The original basis for attempting such a procedure was the awareness of similar "burn-out" treatments given to discrete capacitors in industrial capacitor manufacturing (Lowe 1997). As shown in Figure 3.16. the latter burn-out stage creates a high current density through filamentary conduction paths – due to coating of the electrode metal through pin-holes and similar defects in the dielectric – so as to cause melt-back and de-wetting of the dielectric pathway.

Similar accounts in previous ferroelectric research are apparently limited to high voltage – rather than high current – treatment of already functioning devices. wherein the primary result is not in eliminating D.C. conduction. but increasing polarization (Scott and Pouligny 1988) (Amanuma and Kunio 1996). In these latter accounts. vaporization of filamentary paths are proposed by Scott as a mechanism for de-pinning domain walls (Scott and Pouligny 1988).
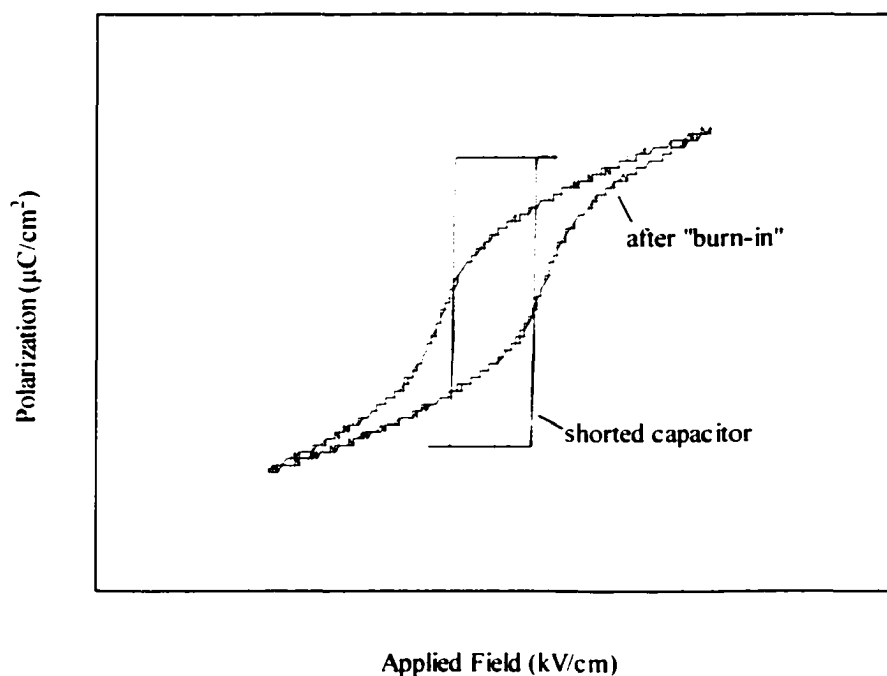
Figure 3.15: P-E loops showing initially electrically
shorted behavior. and non-lossy ferroelectric behavior
after high-current "burn-out" cycle.

3.8 Electrode Studies

It should be noted that. while the initial *room-temperature* deposition of the SBT

composition in the less energetic sputtering environments. presented earlier. was found

somewhat trivial. obtaining the underlying electrode heterostructures compatible with the

post-process anneal environment was not at all trivial.
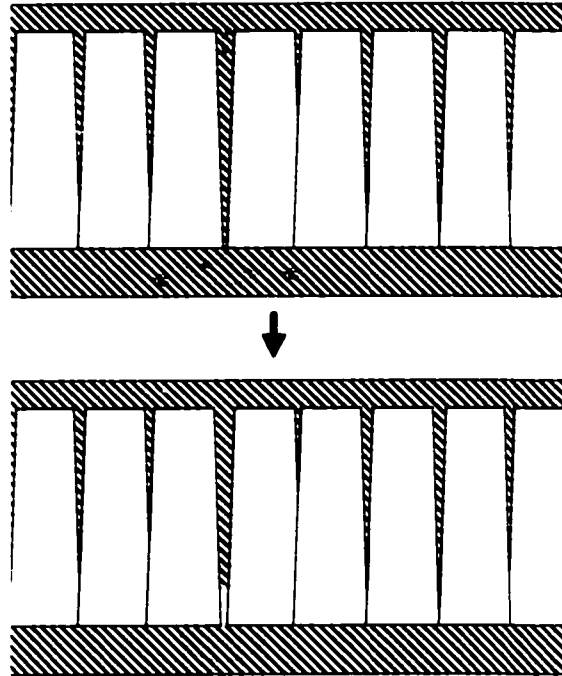
Figure 3.16: Schematic demonstrating
proposed filamentary capacitor burn-out.
with encircled area indicating high-current
density region before and after burn-out.

Studies have been performed here and elsewhere on the suitability of various

electrode heterostructures for SBT capacitors (Kim *et al* 2000). The issues surrounding

the relative merit of the various possible electrode heterostructures are inextricably tied to

the processing approach chosen for the entire heterostructure. The subject is vastly

complex, and will not be understood only by finding a practical electrode solution.

For example. Ir is a very promising electrode material for SBT. One reason is

that Bi has very low solubility in Ir. compared with Pt. for the relevant process

temperatures (<800 °C). In addition. the conducting oxide. IrO. may be expected to form at the SBT/Ir interface. providing an excellent electrically conducting diffusion barrier. Various experiments were performed here. using sputtered Ir electrodes and alternate adhesion layers. Successful phase development of the MF phase. the SBT phase. *and ferroelectric hysteresis* was achieved on Ir/Ti/Si electrode heterostructures. largely identical to that seen on Pt electrodes.

However. on annealing in O_2. the thickness of the intermediate IrO layer at the SBT/Ir interface was seen to be very dependent on the resistance of the overlying SBT layer to O_2-diffusion; whereas. such properties of the SBT layer are determined to great extent. by the underlying heterostructure. in addition to the SBT processing conditions. In addition. SBT or the fluorite phase. like δ-Bi_2O_3. may potentially act as an oxygen conductor at the annealing temperatures. which raises doubts about its use for blocking oxygen diffusion.

The tailoring of film stress. both in the underlying electrode. as well as in the SBT film. will also be central to the success of the particular electrode heterostructure used. Such stress control. while relatively straightforward for metal films. is a more formidable task for the complex chemistry of a metal oxide conductor. These various complications demonstrate the difficulties involved in electrode studies. and. in particular. as some of the inherent drawbacks of using Ir electrodes.

As such. material-based studies on electrode heterostructures can be. by and large. considered anecdotal. as precise process conditions. film thicknesses. and post-process treatments tend to completely determine the success or failure of a particular material

combination. All the materials studied here as electrode candidates proved successful for

specific process regimes. Each material was also noted to fail miserably. for unique

characteristics of that material. if the process conditions were not correct. Determining

the responsible mechanisms and correcting them with any confidence is well beyond the

scope of the present study. Needless to say. an empirical approach was found more

efficient.

3.9 Conclusions of Chapter

Energetic sputtering processes utilizing RF sputtering from a ceramic target have

been developed to perform low-temperature phase formation in the SBT composition.

Substrate temperatures for obtaining the fluorite phase were reduced by at least 200 °C.

whereas the degree of crystallinity obtained would indicate a yet even greater reduction

in effective growth temperature. A higher-temperature and fully crystallized version of

the. normally. poorly developed – at 600 °C – fluorite phase was obtained. which was

fully developed and phase-pure at a T_{sub} =450 °C. This fully crystallized fluorite phase

would transform slowly to the phase-pure ferroelectric SBT phase when annealled at 750

°C for 1 hour.

However. the fact that this phase-pure and well-crystallized fluorite structure

occurs only in non-equilibrium vapor deposition processes indicates that it is actually a

metastable high-temperature phase which. in more equilibrium fabrication methods. is

dominated by the SBT phase as processing temperatures are increased. Thus. it is

suggested here that the fluorite phase cannot be accurately viewed as a low-temperature

phase. as has commonly been perceived. but instead should be viewed as a competing

metastable phase that is thermodynamically favored only in highly non-equilibrium vapor

deposition processes. This view is also supported by the increased phase transformation

barrier to SBT. which arises in the occurrence of the fully crystallized MF phase. This

view is of practical import. as it would dictate that low-temperature formation of the

ferroelectric SBT phase should be approached not with the strategy of implementing

increasingly more energetic processes. but rather with the intent of suppressing

nucleation of the metastable fluorite phase.

The profile of Figure 3.2 provides a uniquely informative picture of the

ion bombardment in a unbalanced magnetron II oxide process. Due to the previously

discussed problems associated with negative oxygen ions and ion bombardment in

general. it was anticipated that sputter depositing in an on-axis configuration would

present insurmountable difficulties in controlling re-sputtering at the substrate. as well as

in implementing a reproducible process. As a result. most of the analysis done for the

research in this chapter was conducted for films deposited in the two modes of off-axis

deposition.

While all previous research in plasma sputtered SBT has relied upon RF

sputtering of ceramic SBT targets. the studies performed herein suggest that the use of

such targets in semiconductor manufacturing would be plagued by some persistent

drawbacks. Sophisticated target cooling strategies may significantly improve temperature

control at the surface of ceramic targets. but Bi- and Pb-containing ceramics will most

likely always be difficult target materials to accommodate. due to surface depletion of the volatile component.

At the time of this writing. there are three material phases associated with the processing and the general phase region of SBT: the ferroelectric "SBT" phase. a low-temperature. defective fluorite phase. and a Bi-deficient pyrochlore phase. The sputtering research performed in this dissertation has found that. in the non-equilibrium deposition methods required for low-temperature growth. there are quite a number of metastable phases. as well as off-stoichiometry phases that have not been commented on in the literature. The high volatility of Bi above 400 °C made as-deposited growth of the SBT phase progressively more unstable. and a single SBT phase. as opposed to the MF phase. could not be achieved by utilizing higher substrate temperatures.

Overall. there is a widespread tendency in the literature on SBT thin film processing. to identify almost any XRD data as the SBT perovskite. without evidence that it is ferroelectric. or additional structural characterization. Apparently. there is an assumption that the (unknown) phase space in the SBT compositional region is fairly simple. However. this appears to be an erroneous assumption. especially for non-equilibrium methods prone to forming metastable phases.

One could certainly go much further in investigating the properties of RF sputtered SBT produced in this chapter. Microstructure and electronic properties could be analyzed ad nauseum. However. such micro-engineering tends to put the cart before the horse. This may be witnessed in the fact that sputtering processes. in sputtered ferroelectrics to date. have fallen woefully short of their previously claimed success.

The intrinsic properties of SBT are better studied through more equilibrium means. such as through bulk studies, or through solution chemistry routes. Before such process-dependent properties are refined in the plasma sputtering of ferroelectrics. however, there first needs to be determined whether a more reproducible, and hence, actually tailorable process can be developed.

4. ALL-METAL TARGET. DIRECT CURRENT REACTIVE
SPUTTERING OF SBT

4.1 Focus of Chapter

The magnetron sputtering method introduced in this chapter constitutes the first time that metallic-mode sputtering has been reported for any of the important bismuth- or lead-containing perovskites. or. apparently. any perovskite oxide. As such. it is also seen to be the first time. as well. that a stable and reproducible method for reactive sputtering – from metal targets – of such complex oxides has been developed.

While the development of a method of depositing SBT from all-metal targets is itself a novel direction in SBT research. the goal of the work presented in this chapter was to develop an entirely different approach to the deposition of multicomponent insulators. Since phase formation for SBT occurs at a full 200 °C higher than PZT. and with an even slightly higher volatility of Bi over Pb. the SBT ferroelectric presents a much greater challenge in energetic sputtering processes than PZT. in terms of both controlling composition and avoiding damaging interactions at the electrode interface. It would then seem that. if previous D.C. reactive sputtering methods were not successful in developing a reproducible PZT process. then it is exceedingly unlikely that these processes would find success in the deposition of SBT. However. as described in the previous chapter on ceramic target sputtering of SBT. the R.F. sputtering of ceramic SBT targets is not an attractive alternative. either.

While the previous chapter dealt exclusively with the deposition and characterization of SBT films through the method of RF sputtering of a single ceramic target. this chapter describes subsequent efforts to develop a novel method for depositing SBT using D.C. reactive co-sputtering and an all-metal target configuration. This approach was purportedly developed successfully for the perovskite complex oxides. such as PZT-type ferroelectrics. over a decade ago (Adachi and al 1985) (Kim and al 1992). However. it is now generally acknowledged that sputtering such complex oxide insulators with all-metal target configurations is actually not nearly as "simple" as was previously claimed. This latter realization is readily apparent in the tooling choices of both industry and industry-sponsored research in such sputtered materials over the last ten years. which are dominated by a return to RF sputtering of a single ceramic target.

The vast majority of sputter-deposited complex oxides thin films – in both research and production – have been deposited from ceramic targets. With the impressive advantages of reactive sputtering. however. it once seemed that all multicomponent oxides would soon be deposited through the all-metal target approach. From the industry point of view. the advantages are primarily the following:

a.) a target life several times that of a ceramic target could be expected. due to a combination of factors: only the metal component of the film resided in the target: metal targets can be made thick due to good thermal conductivity. good thermal shock resistance. and the absence of the degrading effects of over-heating the sputtered surface.

b.) the deposition rates of reactive sputtering can easily be several times that of

ceramic targets. without excessive heating of the substrate or the risk of

catastrophic target failure.

c.) elimination of particulate problems associated with ceramic targets. and

d.) avoiding the high expense associated with ceramic target development and

manufacture.

To develop a genuine reactive sputtering process, one must sputter from metal

targets. In this. there have been essentially two basic geometries used for metal-target

reactive sputtering. The chamber may either be configured with separate magnetron

sources. or a single source may be used which incorporates a mosaic or composite target

formed of the separate metals of the desired multi-component oxide.

4.2 The Multiple Magnetron Approach

In reviews of the sputter deposition of ferroelectrics. it is standard to cite

examples of ferroelectrics deposited by DC reactive sputtering from separate elemental

targets. It is interesting to note that. aside from the benefits cited above. reactive

sputtering of multiple or mosaic elemental targets is frequently mentioned in reviews as a

technique that allows a high degree of control over film composition (Kim and al 1992)

(Adachi et al 1985) (Hayashi et al 1992) (Adachi et al 1990). Presumably. the control of

power to individual elemental targets is thought to allow control of the composition in the

resultant film. Historically. however. this optimistic scenario has not been realized.

Despite the numerous real benefits provided by such a scenario. industrial sputtering

processes for multicomponent oxides are, today, developed within the methodology of

RF sputtering from a single ceramic target.
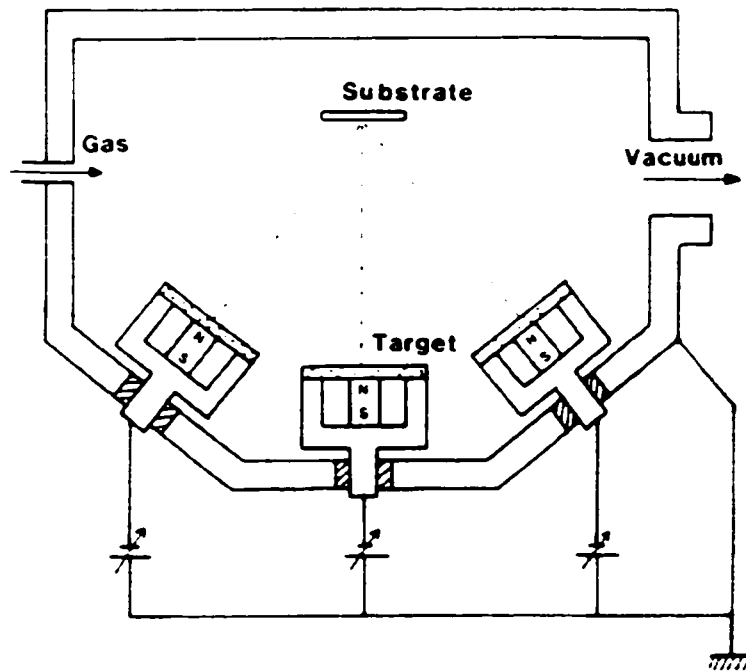
Figure 4.1: Essential geometry of previously reported multi-magnetron
systems used for sputter deposition of perovskites

Much of the "simplicity" associated with the multiple magnetron approach has

been assumed by virtue of the qualified success in depositing High-T_c superconducting

oxides (Wasa *et al* 1991). However, a crucial advantage that multiple magnetron

sputtering of High-T$_c$ materials has over ferroelectrics such as SBT is that there is a very large range of compositions that will yield a superconducting phase, whereas, the composition range for ferroelectric phases tends to be relatively quite narrow. As a result, the crucial issue of compositional control may be initially bypassed in multiple target sputtering of High-T$_c$ superconductors.

The process geometries reported in the previous work performed in sputtering ferroelectrics from multiple metal targets are essentially quite similar. All of these previous process geometries are represented uniformly by the schematic in Figure 4.1 (Adachi et al 1985). As may be noted from Figure 4.1, there is little attention devoted to the tailoring of gas flows for sputtering and reactive gases. It is a central premise of the present work that such process geometries. which do not actively tailor gas flows. preclude reproducible operation of the reactive sputtering process. It should further be noted that, despite the successful operation initially reported for these multiple magnetron processes, there has been little work subsequently conducted to support the optimistic outlook of such reports.

A simple and remarkable indication of this latter state of affairs is that, in none of the publications during the past fifteen years on reactive all-D.C., multiple magnetron sputtering of ferroelectrics. have there been any ferroelectric hysteresis curves included in the reports on this method (Maiwa et al 1992) (Kim et al 1997) (Adachi et al 1990) (Hayashi et al 1992) (Kim et al 1992) (Maiwa et al 1992) (Adachi et al 1985). Presumably, as the definitive indication of ferroelectric properties. as well as the most

significant application of ferroelectric films. such data would be published if it were

successfully obtained.

4.3 Reactive Sputtering of Ferroelectrics in General

In the past. notable research programs in D.C. reactive all-metal sputtering of

ferroelectric oxides were conducted primarily in reactive sputtering of PZT. as this highly

utilized material and its applications were seen as the greatest potential use of the metal

target approach. One may note that the most productive and sustained programs. where

source characterization was seriously treated. were carried out by the Sayer group at

Queens College and by a group at University of Texas in Austin. with both groups using

single mosaic targets(Croteau *et al* 1987) (Sayer 1986) (Sreenivas and Sayer 1988)

(Kumar *et al* 1992). It is very important to note that. in such previous work. operation of

a heavily oxidized target was accepted as the required mode for stable operation.

Other notable metal-target reactive sputtering work in PZT includes research

conducted at Siemens. where ferroelectric hysteresis was demonstrated with low-

temperature (450C) phase development. In this work. Bruchhaus *et al.* do not stress

target oxidation. but reported specific operating conditions – 5 mtorr oxygen and 10

mtorr total pressure in a diode system – for which poisoned target operation is implicit

(Bruchhaus *et al* 1992). These researchers also address the difficulties of working with

oxidized targets (Schrieter *et al* 1998). It should be noted that. while this work by

Bruchaus et al. was conducted using multiple diode sputtering cathodes. it is the only

account found here of actual ferroelectric loops reported for a multiple source. reactive

plasma sputtering of a ferroelectric. However. the diode sputtering method used can only be operated in an oxidized-target mode.

There is a report of so-called "quasi-metallic-mode" sputtering of PZT (Zhang *et al* 1996). However. further inspection revealed that this report misconstrued the original meaning of "metallic-mode sputtering" to mean only the use of a largely metal target. since no demonstration of any metallic-mode sputtering mechanism was given. In this latter case. there was no possibility of such a mechanism existing. given the use of PbO-ceramic in an R.F.-sputtered. mosaic target. Of the remaining reports on any type of metal-target sputtering of PZT. very few were able to demonstrate ferroelectric hysteresis. However. it is quite noteworthy that in all the reports of reactive metal-target sputtering of PZT – in fact. of any ferroelectric – that did not report specific operating conditions that correspond to the oxidized-target mode. none demonstrated ferroelectric hysteresis data.

The reasons for this omission can be attributed to the fact that. in metal-target reactive sputtering of any such multicomponent insulator. no report can begin to address the relevant issues of successfully establishing a reproducible process if it does not discuss the proper maintenance of the target surface: and hence. optimization of gas pressures and flow rates. Indiscriminately reporting only a wide range of operating pressures indicates that such optimization has not been performed. This latter situation. in turn. derives from the fact that both sputter yields and energetic ion populations are a tenuous function of the target surface state.

Sayer. *et al.* and others have concluded that unstable poisoning effects are best

avoided altogether by allowing the metal target(s) to become sufficiently oxidized.

thereby allowing a more repeatable surface state. albeit. with a considerably lowered

sputter yield. It appears. though. that the oxidized-mode reactive sputtering of multiple

metal surfaces has longer-term stability problems. deriving from differing responses of

the metals to extended oxygen exposure. as well as to the effect of continually changing

insulator coverage in the sputtering chamber. However. in the last fifteen years. there has

appeared no real alternative to this approach.

Given the rapid process development required and achieved in the semiconductor

industry. the reality that none of these metal target reactive sputtering configurations has

found commercial success in ferroelectric deposition underlines these unresolved issues.

If reactive sputtering of such compounds is to find its place in industry. a new approach is

required.

4.4 Metallic Mode Reactive Sputtering of Perovskites

The new approach developed here is to take a contrary position to the previous

work on sputtered ferroelectric perovskite materials. and to establish that a reproducible

and stable reactive sputtering process for these materials can only be attained. not by

completely oxidizing the target surfaces. but rather. by keeping them completely metallic.

Recently. one group *hypothesized* on the possibility that a metallic-mode. or at least.

quasi-metallic mode. sputtering process could be developed for PZT. based upon an

optical emission spectroscopy (OES) study of metallic target emission lines in an

ostensibly conventional sputtering system (Ayguavives *et al* 1998). However, this

conclusion was incorrectly based on the premise that one could implement metallic mode

sputtering of these materials only by controlling relative flow rates of the sputtering and

reactive gases. and applying appropriate sputtering power. No mention was made of total

or partial operating pressures. gas flow geometry. or the specific discharge kinetics. It

will be clear in this and the next chapter that each of these issues is both critical and

nontrivial.
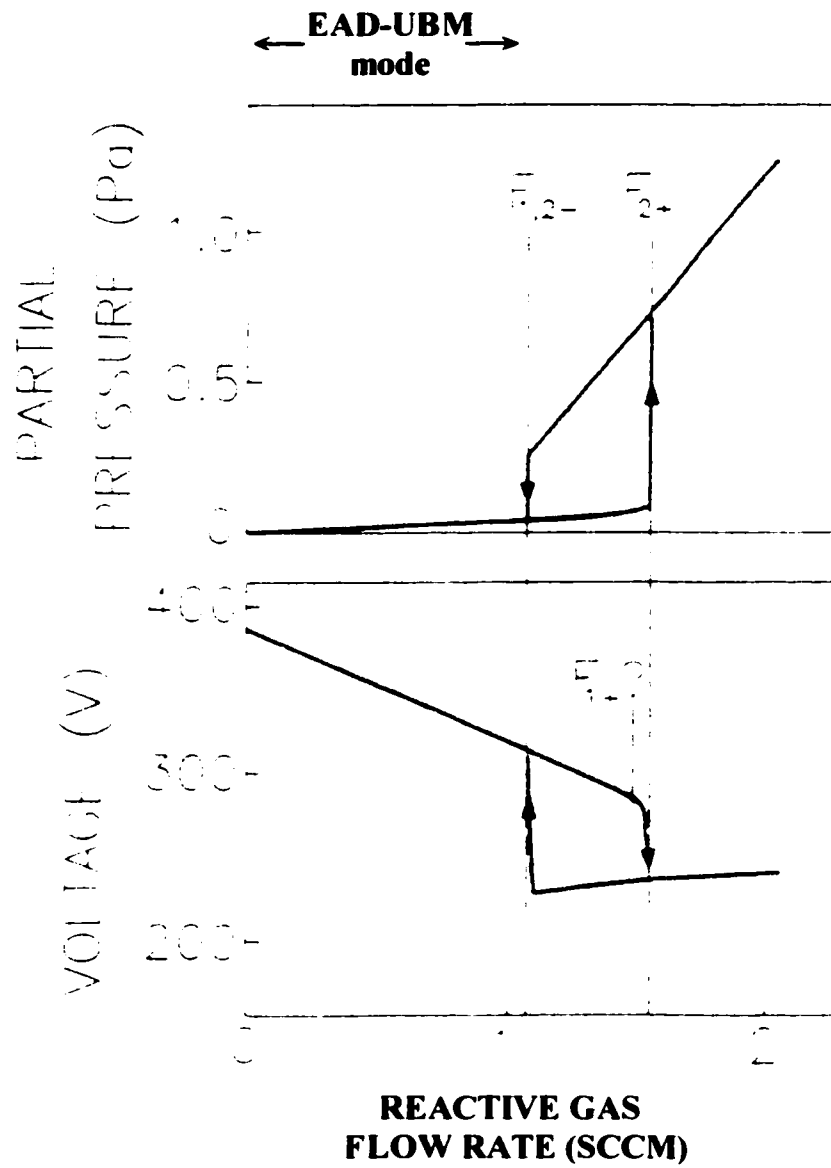
Figure 4.2: generic hysteresis behavior for various parameters monitored in the reactive magnetron sputtering of a metal target.

Much of the difficulty in establishing a viable process for reactive sputtering of

such complex materials resides in the instability of the metal target surface in

experiencing various degrees of target "poisoning." or surface oxidation. during

magnetron operation. As the metal target surface becomes increasingly oxidized. the

sputter yield will drop to that of the corresponding metal oxide. This reduced sputter

yield will. in turn. result in a smaller demand for the reactive gas. As a result. the partial

pressure of the reactive gas in the sputtering chamber is observed to increase. as shown in

Figure 4.2(a).

A characteristic which is observed for reactive D.C. magnetron sputtering of a

metal target is the "hysteresis" of the metal target/cathode self-bias potential as a function

of the partial pressure of the reactive gas within the sputtering chamber. This behavior is

determined by the metallic-mode/oxidized-mode transition. The behavior of a reactive

sputtering system is hysteretic from the operator's point of view. because the monitored

parameter is the oxygen input. or partial pressure. or deposition rate. rather than the

actual state of the target surface. The state of the target surface is the actual physical

parameter of interest here. and it will generally share a unique relationship to the target's

operating voltage. for a given set of process conditions. The observed target potential

will demonstrate a hysteresis as a function of reactive gas partial pressure. because. in

any case. a finite amount of time is required to equilibrate the target surface to a new gas

environment. However. in many cases. the target hysteresis will. in fact. reflect two

distinct states of a more-or-less dynamic steady state for a given set of process

conditions. The actual extent of the hysteresis reveals nothing more fundamental than a

composite of the general process conditions used. e. g.. the target material. the pumping speed. the gas flow rates. the sputtering power. the gas flow geometry. etc. The target self-bias. though. can provide much information about the relative state of the target surface.

Aside from the difficulties in achieving run-to-run reproducibility. due to target poisoning. the lack of control over oxygen mobility in DC reactive sputtering systems can lead to the same problems demonstrated earlier in RF sputtering: in particular. negative oxygen ion bombardment. While the creation of highly energetic (100+ eV) negative ions produces highly visible effects in unbalanced "Type II" magnetrons of the sort used herein. the tendency can be observed in a wide variety of metal oxide sputtering systems.

The use of A.C.. pulsed D.C.. or bipolar sputtering configurations allows for a degree of target poisoning to occur without compromising the stability of the sputtering plasma. However. these latter techniques will not obviate the instability in the relative sputtering yields that occurs when performing reactive deposition from widely disparate metals. such as in the case of the Bi- or Pb-containing perovkites.

In implementing the highly non-equilibrium sputtering methods used here. SBT does offer the dubious advantage of allowing one to monitor effects of the reactive sputtering environment through the readily altered compositional and structural characteristics of the resultant films. However. the process of identifying effects is problematic. though. since sputtering readily provides the conditions to form a variety of undocumented stable and metastable phases. whereas. there is little information available on even the equilibrium phase space of SBT.

While many reasons have been given for why metallic-mode sputtering is or is not possible for these ferroelectric perovskite materials. it has been determined in the present work that the essential difficulty may be reduced to the following:

1.) In non-activated sputtering methods. the arrival rate of oxygen at the substrate. required for proper stoichiometry. is so high that target poisoning cannot be avoided.

2.) In activated sputtering processes. an increased sticking coefficient of oxygen at the substrate may be achieved. but it is normally accompanied by increased ion bombardment. which resputters the volatile species at the depositing film.

Neither of these options provides for a reproducible process in practical system designs. It is also a practical reality that none of the previous process geometries cited in the literature have been capable of overcoming this dilemma. The present research finds that this inability is due both to the described gas flow geometries. as well as to the basic processing environments that were previously used.

The dilemma cited above has been resolved in the present work through the implementation of an apparatus and method that has not been suggested in the previous vapor deposition literature. In fact. up to the present. the use of "Type II" unbalanced magnetron sources for the on-axis deposition of Bi- and Pb-containing perovskites would be considered antithetical. due to the operational characteristics typified in Figure 3.2. That such an approach is found viable in the present work is very much dependent upon

the discovery of a new mode of operation for magnetron sputtering. which will be more thoroughly discussed in the next chapter.

While other target configurations were attempted. the configuration of Figure 4.3 was ultimately relied upon as the most promising. This figure also displays other elements of the chamber design that were found critical to attaining the method developed. The tailoring of the sputtering and reactive gas flow geometry was critical to the realization of the optimized metallic-mode reactive sputtering process. It may be noted from Figure 4.3 that the reactive gas is injected uniformly and directly towards the substrate. whereas the Ar is injected around the sputtering target. so as to effectively provide Ar as the primary gas for operation of the discharge. This latter geometry provides an additional non-equilibrium growth characteristic to the present process. since the chemistry performed at the substrate by the reactive gas may be largely avoided at the target; gas pressures are in steady state. but never equilibrated.

As is depicted in Figure 4.3. the target solution ultimately developed consisted of two separate target materials: a pure Ta (99.999%) and a composition of Bi-Sr intermetallics. Once the metallic-mode process was realized. these target materials were found to offer the greatest reproducibility in the deposition of SBT. and also to offer a promising combination for future incorporation into a single mosaic target. for further process simplification.
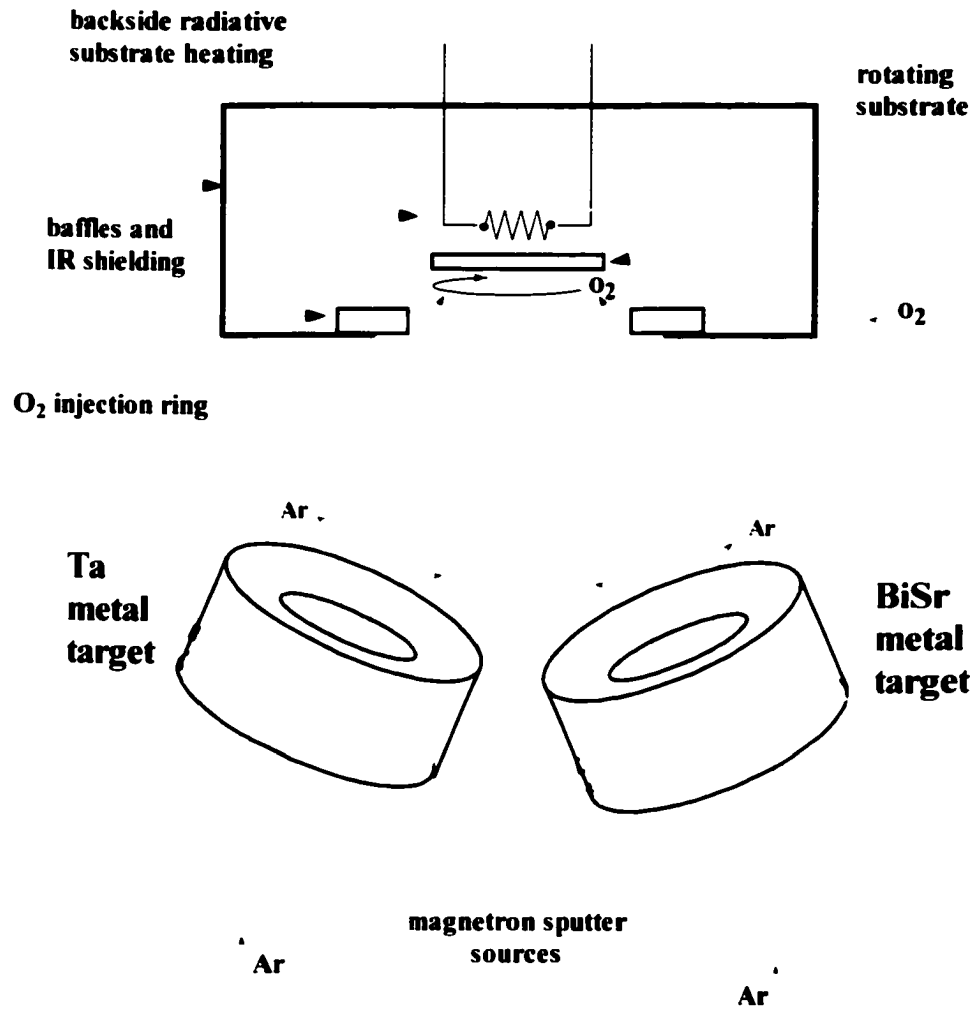
Figure 4.3: DC sputtering chamber configuration
used in work presented in this chapter.

4.4.1 Source/Target Development

The effective sputter yield of plasma-sputtered Bi is very high due to both its

intrinsic – single particle – sputter yield coefficient. as well as its poor thermal

conductivity. This poor thermal conductivity leads more easily to surface heating. thermal spikes. and sublimation in the environment of a sputtering plasma. Earlier experiments by the author involving reactive co-sputtering of elemental Bi and Ti for the formation of BiT. indicated that this high sputter yield of Bi is highly sensitive to small degrees of oxide target poisoning. Earlier experiments in sputtered SBT also indicated a high sensitivity to target poisoning. even when all magnetron sources were purged with high flows of argon (>10 sccm). The instability in film growth. experienced in the previous work on RF-sputtered SBT. due to the volatility of Bi at $T_{sub}> 400$ °C. becomes compounded by the additional sensitivity of sputter-yield to target poisoning. It became apparent that highly localized gas flows. which help to distinguish this research from previous reports on sputtered perovskites. were still not adequate to stabilize the sputtering rates of the various metals.

4.4.2 Target Fabrication

In response to these observations of the instability inherent in cosputtering Bi. the author developed an all-metal target approach with the aim of avoiding such process instability. The success of work presented in this chapter is. in part. due to exploitation of the intermetallic phases that exist in the Bi-Sr system. The election to undertake this approach was made due to several anticipated benefits:

    a.   achieving an equilibration of the relative sputtering yields for bismuth and strontium. thereby achieving assured stoichiometry in the vapor flux.

b. acquiring the ability to sputter from strontium metal without the difficulty of handling and maintaining a pure strontium target. and

c. exploiting the high secondary electron coefficient of strontium.

Fabricating targets of the Bi-Sr intermetallics required a fair amount of development work. due to a combination of many factors. including the highly exothermic nature of the phase formation and the active nature of the metals involved. For the solution ultimately developed. a cylindrical high pressure vessel was fashioned from 316 stainless steel. which was subsequently fitted with a sleeve-like heating element. This target-casting vessel was required to be sealed. so as to prevent boiling of the bismuth during the exothermic formation of the Sr-Bi intermetallic.

Many studies have been performed to reveal the dependence of sputter deposition upon the microstructural properties of metal targets. most of this work addresses the significant effect of grain size and orientation in elemental targets. However. little work has been performed to establish the basic characteristics that qualify sputter deposition from an intermetallic target. From basic considerations of the physics of sputter bombardment – i.e.. knock-on. thermal spike. and intermediate regimes – as well as from consideration of bond energies. one may easily deduce that the sputter yield of an intermetallic is not a composite of the two separate sputter yields for the separate elements: instead. it must be a single sputter yield representative of the interatomic bond energies of the intermetallic. This is good. for we would like to avoid the problems that

may be associated with sputtering an inhomogenous target material that contains separate

phases with disparate sputter yields.

target
composition
range

"A"

Figure 4.4: Bi-Sr phase diagram, with composition range of targets used.

The phase diagram of the Bi-Sr system, Figure 4.4, exhibits several intermetallic

phases. While a number of metal targets were fabricated that possessed a bimetallic

composition corresponding to the target composition range in Figure 4.4. a reproducible relationship between the target composition and phase development/composition in the films deposited from these targets could not be definitively established until the novel developments of this thesis work were put into place. These developments. as will be revealed in this and the following chapters. allow for the optimum target Bi-Sr ratio to actually be that of the desired nominal film composition: in other words. the problems with re-sputtering and volatilization of Bi in normal sputtering arrangements was overcome. The optimum target composition in this work thus evolved to be nominally that of the desired film composition. which corresponds to the region "A" in the phase diagram of Figure 4.4.

Aside from equalizing the sputter yield of bismuth and strontium. another. unanticipated. benefit of utilizing the Bi-Sr intermetallics is the relative resistance of such alloys to oxidation. This quality of the intermetallics made the handling of the Bi-Sr target considerably less troublesome than if a pure Sr target had been used.

4.4.3 Electrical Characteristics of Targets

Electrical characteristics describing the cathode self-bias vs. degree of target poisoning are given in Figure 4.5. The data given in Figure 4.5 was acquired by allowing the target surface enough time to achieve a dynamic equilibrium with the sputtering environment and partial pressures listed. Hysteresis curves are rarely constant. but are. rather. a function of the history of the specific target and chamber in question. As such. and because the targets were never allowed to become genuinely poisoned. the curves
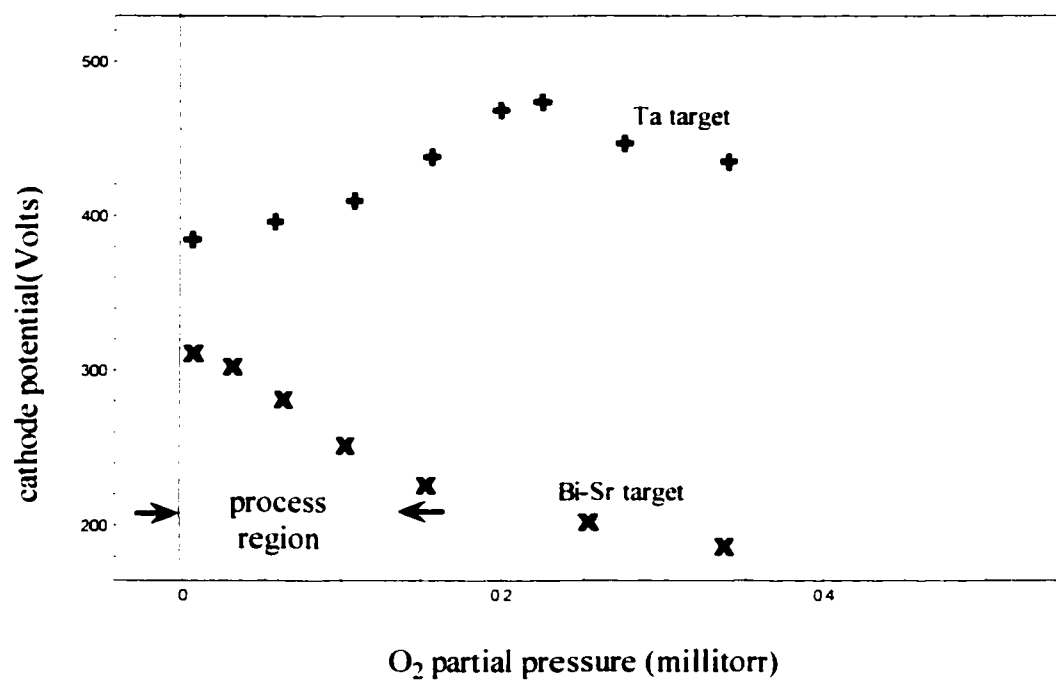
Figure 4.5: Target voltage vs. oxygen partial pressure for reactive sputtering of Ta target and SrBi target.

presented are singular rather than hysteretic. Various hysteretic curves with similar

extrema can be observed. with the degree of hysteresis being primarily a function of the

time given for stabilization of the sputtering system.

One may note that the relationships of target self-bias to oxygen partial pressure

given in Figure 4.5 do not extend far into the oxygen-rich regions of given parameter

space. This is because the curves seen will generally continue toward either a somewhat

asymptotic value. or an abrupt impedance and plasma outage. depending on the metal. In

either case. such behavior indicates the build-up of excessive oxidation at the target

surface. This fully poisoned condition was not implemented or recorded for this work. as

it typically takes either excessive sputtering or a fresh target. due to the reactivity of Sr in

the Bi-Sr target. to restore original target performance. and is of little practical interest

here.

The behavior of the two sources in Figure 4.5 indicates a significant difference in

the operational characteristics of the Ta and Bi-Sr sources. The point of operation in the

target voltage curve indicates the degree to which the system is being operated in the

metallic mode. In the present work. oxygen flows were always maintained sufficiently

low to allow the cathode/target self-bias to remain well within the "non-poisoned" region

of the voltage curve. As such. the entire target surface remained shiny and metallic. with

no evidence of oxide. throughout operation at the standard pressures (Table 4.1) used.

This is a very important result of the present work. for it shows that the

irreproducible region of process space. corresponding to higher oxygen pressures at the

target. may be avoided altogether. The prevention of oxygen at the target surface

provides two crucial results: (a) the tenuous dependence of sputter yield on degree of

target oxidation may be avoided altogether. and (b) the production of negative ions. with

subsequent acceleration and re-sputtering of the depositing film. can be essentially

eliminated.

UBMII METALLIC MODE	
Ta target power	30-50w
Bi-Sr target power	15-40w
Bi-Sr target composition	7-28%
O_2 partial pressure	0.05-0.5 mTorr
Ar + O_2 total pressure	1.5-7mTorr
flow rate	~15sccm
substrate temperature	R.T. - 500 ^{0}C

Table 4.1: Range of deposition conditions

4.5 Phase Development for D.C. Reactive Sputtering

4.5.1 Development and Characterization of Sputtered Bi_2O_3 Seed layers

While SBT ferroelectric thin films were successfully obtained using standard

electrode materials as the substrate. various advantages in repeatability and control were

found in the implementation of seed layers. at higher deposition temperatures. Because it

was witnessed that slight variations in the initial substrate conditions produced extremely different modes of film growth under such energetic growth conditions. it was determined that the initialization of heteroepitaxy could be more easily controlled by means of a seed layer. Such a seed layer should already possess a high accommodation factor for the adsorbing bismuth atoms. The simple choice of seed layers for this function was Bi_2O_3. and studies were performed using exceedingly thin films (<10 nm) of this material.

To verify the initially observed relationship of growth anisotropy to substrate conditioning. Bi_2O_3 was deposited by reactive sputtering onto a shadow-masked 2" (100) Si wafer already deposited with the standard Pt-electrode sequence. A shadow mask was used to divide the wafer with a straight and well-resolved step. so as to determine how definitive was the relationship between the underlying surface chemistry and the mode of growth in the subsequently deposited SBT layer. The deposited Bi_2O_3 layer thickness was verified via stylus profilometry (Dektak IIa) to be <50 Angstroms (below the resolution limit of the instrument). Visual inspection gave no evidence of the Bi_2O_3 layer. indicating again that it was on the order of monolayers thick. After depositing the masked Bi_2O_3. the wafer was deposited with SBT at 450 °C. The substrate was rotated continuously during both (shuttered) presputtering and deposition to ensure that the two sides of the substrate were exposed to the same environment.
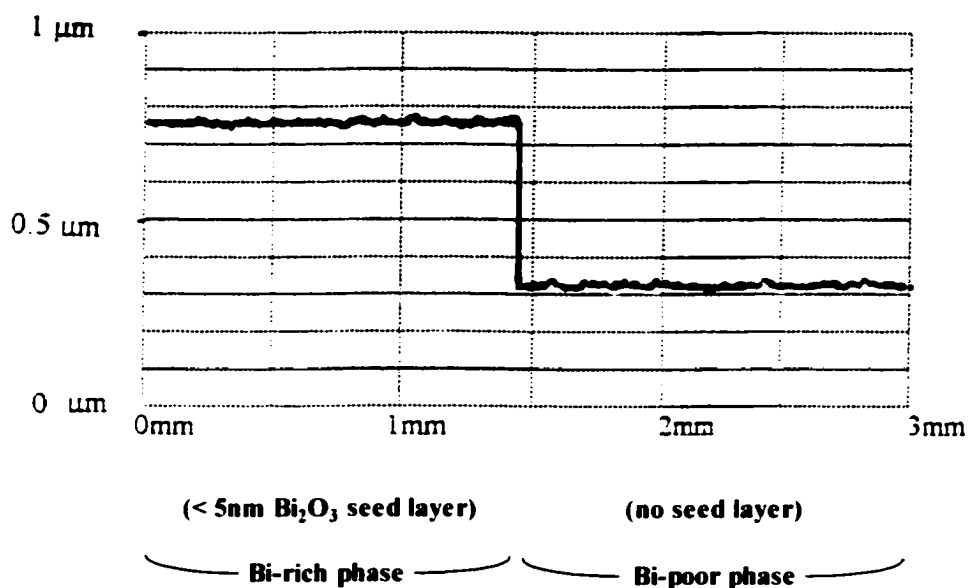
Figure 4.6: Stylus profilometry scan of step-function in
growth rate due to Bi_2O_3 seed layer.

The results of this study establish incontestably that large anisotropies in film

growth rate and composition occur as a result of initial substrate chemistry in these

energetic growth environments. The resulting step function was measured via stylus

profilometry. As indicated in Figure 4.6. the previously indiscernible Bi_2O_3 step resulted

in a precisely delineated step in the growth rate of the SBT-type material. corresponding

exactly to the original shadow mask. This step revealed a more than two-fold increase in

thickness and, hence, growth rate as a result of Bi_2O_3 seeding. In later experiments, it was found that this step-growth difference could be more than five-fold with appropriately increased bismuth vapor flux. Given the rather novel circumstances of this process, it may not be surprising that no prior account of this dramatic increase in growth rate, as a result of functionalizing the surface with a few-monolayer seed layer, has been found in the vapor deposition art.

The two sides of this wafer were analyzed with XRD and XRF to determine differences in phase and composition. The XRD results, in Figure 4.7, reiterate the findings of the x-ray fluorescence studies, which revealed Bi fluorescence peak intensities taken from the thicker side of Figure 4.6 to be anywhere from 3 to 5 times the Bi peak intensities taken from the thinner side. These results would suggest a much larger percentage of elemental Bi in the thicker side of the grown oxide step, though no precise compositions were calculated from these peak heights. The very (1 1 1)-oriented fluorite peaks of 4.7(a) have been well established, in the present work, as corresponding to excessive Bi-content in the grown film. The limited crystallinity of Figure 4.7(b), on the other hand, is a common and definitive indication of Bi-poor material.

The findings here relate to previous studies into the effect of particular platinum-terminated substrates upon the growth of SBT. These reports by Kim, *et al.* and by Im, *et al.* were based upon Mass Spectroscopy of Recoiled Ions (MSRI), wherein ions produced by sputtering the grown film with an Ar^+ beam are analyzed with a mass
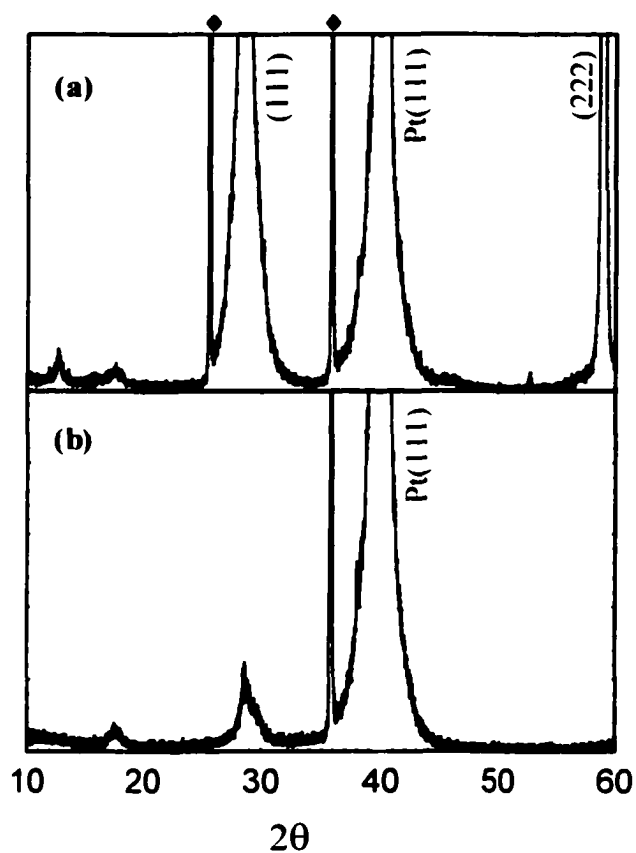
Figure 4.7(a) & (b): XRD 2-θ scans for the two sides of the step-growth shown in Fig.4.5. with (a) the high-growth-rate side producing a very Bi-rich phase. and (b) the low-growth-rate side producing a Bi-poor phase.

spectrometer (Kim *et al* 2000) (Im *et al* 1998). They studied the effect. on SBT growth. of the various elements utilized in platinum electrode stacks. Similarly. Dhote. *et al.* of the same group of researchers. reported on the incorporation of Bi onto $YBa_2Cu_3O_{7-x}$ in SBT growth. using the same characterization technique (Dhote *et al* 1999). These reports enabled further verification of earlier reports that. in Pt electrode stacks that utilize Ti metal as an adhesion layer to the underlying Si substrate. Ti metal would diffuse through the Pt electrode to the SBT/Pt interface (Seong *et al* 1998). In the studies by Im and Dhote. which both used ion beam sputter deposition for the SBT films. it was concluded that the Ti and Si both reduced incorporation of Bi. during growth of SBT. as a result of competition for available oxygen at the growth interface.

However. the results obtained in this section. combined with some basic thermodynamic reasoning. are found to contradict these previous reports. First. a general consideration must be raised concerning the relevance of metallic Ti or Si in the $5X10^{-4}$ Torr oxygen background used in the reported work. It is a well-known state of affairs that a monolayer of oxide will form on such materials. with relatively high-magnitude heats of oxidation. in time periods on the order of a second. when placed in oxygen pressures two orders-of-magnitude lower than that used in these reports. Noting that deposition rates are normally lower than one monolayer/second. and that the diffusion rates of Ti or Si would be considerably smaller yet. it is not apparent how either Ti or Si could exist at the growth interface in a reduced state.

In addition. the argument that Bi remains reduced due to the oxygen scavenging ability of Ti or Si is essentially based on a premise of mass action in homogenous

reaction scenarios: i.e.. the amount of oxidized Bi created will be inversely proportional to the amount of Ti or Si present. As is revealed in the studies performed in the present work. this is clearly not the case. The quantity of Bi incorporated into the growing SBT film is primarily determined. instead. by the accomodation. for Bi. of the specific SBT-type oxide phase originally nucleated. That this accomodation of Bi is an issue of discrete phases may be witnessed in the fact that an abrupt transformation to a Bi-rich phase occurs on the Pt substrate. even when the initial Bi_2O_3 seed is deposited as a smooth lateral gradient. rather than as a step.

It should also be pointed out that. if Ti metal were arriving at the growth interface in quantities sufficient to deplete the available oxygen. one would expect a comparable contribution of TiO_x to the resultant film thickness. which is not evident in the observed growth-rate disparity.

Finally. it is submitted here that. whereas the existence of Ti at the point of heteroepitaxy does reduce Bi incorporation into the growing SBT film. this effect results from the low accommodation of the TiO_x interface that will inevitably present itself. rather than from a reducing Ti metal. This view is consistent with the author's experiences in depositing SBT onto other oxide substrates. such as fused silica or thermally oxidized silicon. at $T_{sub}>400$ °C. These latter substrate materials were also dramatically prone to nucleating Bi-poor SBT phases. relative to deposition onto a Pt surface. In fact. in terms of free energy. the Pt substrates can be expected to have a fairly high affinity for Bi. given the corresponding chemical activity between the two elements.

On the other hand, the free energy for any of the high-temperature oxides treated here can be regarded as quite low in the adsorption of either Bi or Bi_2O_3.

These observations indicate that difficulties, experienced here and elsewhere, in controlling the incorporation of Bi into vapor deposited SBT films, with suitably high substrate temperatures for as-deposited growth (T_{sub}> 400 °C), are based upon rather permanent issues that are general to the SBT material itself, rather than a specific contaminant.

These step-growth experiments also reveal that there may be difficulties in characterizing certain growth behavior of the SBT phase as "adsorption-limited", as SBT deposition work in pulsed laser deposition has been described. The premise of such a growth process is that the material phase in question provides a thermodynamically preferred composition, which, in turn, manifests in a self-limited incorporation of some relatively volatile component, such as Bi. While it should be remembered that the processes used here are unusually energetic, some rather simple conclusions can be drawn from the results of Figures. 4.6 and 4.7. One conclusion to be drawn is that, in the non-equilibrium vapor deposition methods, the adsorption of the Bi vapor may be more readily determined by a competing phase than by the SBT phase. As such, an overpressure of Bi vapor will not necessarily favor growth of SBT. As SBT does not lend itself to the gentler forms of vapor deposition, such as standard MBE or e-beam evaporation, it would appear that such competing phases might present a continuing issue in the vapor deposition of SBT. Another interesting conclusion that may be drawn from Figures 4.6 and 4.7 is that, in these sort of energetic processes, a momentary fluctuation

in the surface composition of a growing SBT film may initiate a separate phase of much different composition. In much more equilibrated processes, such as PLD, where relatively high total and O_2 partial pressures, and thermalized neutral plasmas, preclude heavy bombardment of the substrate by either ions or electrons, these issues may not be as evident; but, they can still be expected to exist.

The results for these initial studies in seed layers show that the "volatility problem" for Bi, at least in the more energetic vapor deposition of the Bi-layered perovskite, SBT, can be largely determined by the initial nucleation stages of film growth, and, thus, by the initial substrate conditions. While incorporation of Bi_2O_3 as a buffer layer between the Pt and SBT layers has been performed previously for both sputtering and solution chemistry deposition of SBT, the reasons expressed for doing so have varied. However, in none of these past cases were intermediate layers reported to produce a difference in growth rate or in Bi adsorption. The prior use of intermediate layers has been described within the context of buffer layers, diffusion barriers (Lim and Kalkur 1997), and Bi-compensation layers. In a report by Hu, et al. a ferroelectric $Bi_4Ti_3O_{12}$ (BiT) layer and SBT layer were subsequently deposited with solution chemistry (MOD). As this was spin-on deposition, adsorption of bismuth was not an issue: however, the BiT layer was found to promote 50 °C-lower temperature nucleation of the ferroelectric SBT phase, as compared to spun-on SBT films without the BiT layer (Hu and al 1999). As with other MOD and sol-gel work utilizing Rapid Thermal Annealing (RTA), it is unclear how the low substrate temperature (T_{sub}= 600 °C) purportedly used in this account could be verified in such an inherently non-equilibrium

process. given the complicated emissivity issues of the multilayer stack (Hu and al 1999). However. the use of the layered perovskite. BiT. as a seed layer could have a very significant effect. in vapor deposition of SBT. by encouraging nucleation of the SBT phase rather than that of the MF phase.

The effect of the substrate on the incorporation of bismuth in SBT growth has been addressed by Matsuki. *et al.* who deposited a Bi_2O_3 "crystalline buffer layer" as a means of preventing formation of a bismuth-poor film (Matsuki). The Bi_2O_3 films used by Matsuki were significantly thicker (20nm) than those used here. and required polycrystalline. as opposed to amorphous. Bi_2O_3 for the desired effect. However. since the "amorphous" and "crystalline" buffer layers were also differentiated by the use of a reducing. pure Ar. sputtering environment. it is unclear whether or not there were other determining factors. e.g. less oxygen and more metallic bismuth in the deposited film.

The aim in the present sputtering work. though. was to make the Bi_2O_3 layer so thin as to be insubstantial in the overall composition of the SBT – or Pt electrode – layer. As in the case of the demonstrated step-growth. one could thereby control the material phase and composition purely as a function of the initial chemistry of the polycrystalline substrate surface. Because of this aim. thicker Bi_2O_3 layers were deemed undesirable. In subsequent deposition runs of SBT. <5nm seed layers were normally deposited prior to deposition of the SBT layer.
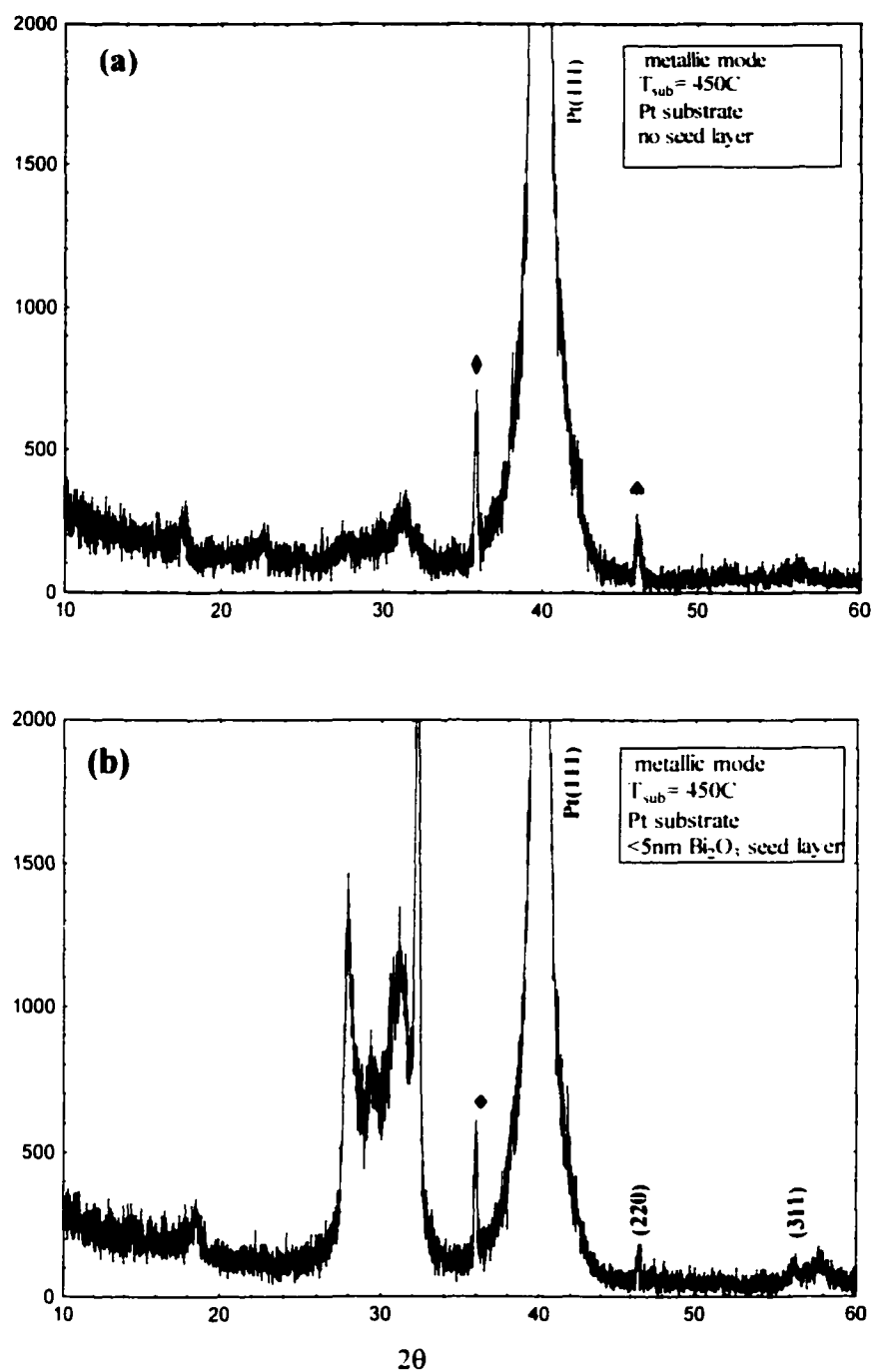
Figure 4.8(a) & (b): XRD 2-θ scans for metallic mode sputtering of SBT onto Pt substrates at the standardized substrate temperature of 450 °C, showing (a) the bismuth-deficient phase developed on bare platinum substrates, and (b) a phase of nominally SBT composition obtained with the bismuth seed layer.

In subsequent SBT growth. the seed layer used for the D.C. sputtering of SBT was eventually formed directly from the Sr-Bi metal target. yielding a compound of nominal composition. $Sr_2Bi_6O_{10}$. which was thought a favorable seed-layer choice for several reasons: (1). it could be conveniently deposited in the existing experimental set-up: (2). due to the affinity of the two metals. the SrBiO compound could be expected not to sublime or dissociate at significantly higher temperatures than Bi_2O_3: and. (3). the SrBiO compound could be expected to better resist the catalytic dissociation and diffusion of Bi atoms into the underlying Pt substrate. thus maintaining Bi atoms at the SBT growth interface.

The XRD data of Figure 4.8(b). shows that a rather dramatic increase in Bi-incorporation. over the seed-less growth results of Figure 4.8(a). had indeed been obtained in SBT growth efforts wherein the vapor flux was known to be of the desired stoichiometry. However. despite the incorporation of the SrBiO seed layer. higher temperature processing. above 400 °C. continued to render difficult the compositional control required for growth of the ferroelectric SBT phase. This difficulty is evident in Figure 4.8(b). which is found to be a recurring high-temperature Bi-deficient phase. That this is a high temperature phase was evident in that it is not altered after a 4-hour anneal at 750 °C.

4.5.2 Use of Ta_2O_5 as a Diffusion Barrier

While the higher substrate temperatures could also cause increased Bi-volatilization during film growth, previous observation of growth behavior indicated that the Bi-deficiency might easily be due, yet again, to the heteroepitaxial difficulties of initial nucleation/growth processes at the original interface. Though the sublimation and resputtering of the Bi_2O_3 seed layer could be expected to be greatly suppressed with the addition of Sr to the seed layer, the interfacial interactions of the underlying Pt electrode with the several SrBiO monolayers is far less straightforward. It was clear that some modification of the seed layer, due to the Pt interface, was still quite likely to be occuring at the higher substrate temperatures used, possibly due to alloying of Bi with the Pt electrode or a varying contribution from the Ti or TiO_2 adhesion layer under the Pt layer. While the $SrBi_2O_3$ seed layers just discussed were instrumental in achieving run-to-run reproducibility, the high activity of Bi in standard electrode metals such as Pt was still an issue.

In the spirit of controlling the growth mode through interfacial chemistry, rather than through compositional supplements, it was elected to place a relatively inert diffusion barrier between the SrBiO seed-layer and the Pt layer. A desired property of the diffusion barrier would be that it could be effective as an exceedingly thin interfacial layer, so that, like the Bi_2O_3 seed-layer, it could not have a noticeable effect on the composition of the SBT film, except through heteroepitaxial interactions. Also, such an exceptionally thin diffusion barrier would not make a significant *bulk* contribution to the electrical properties of the resultant capacitor structure. Using a Ta_2O_5 buffer layer for

this purpose was an appealing option, since it could be easily implemented in any SBT

vapor deposition process, and presented the least possibility of complicating

characterization efforts. As in the case of Bi-containing seed layers, Ta_2O_5 seedlayers

have been used in solution chemistry work in SBT research (Kim *et al* 2000). Because of

the limitations of depositing very thin layers with sol-gel or MOD, the Ta_2O_5 layers in the

latter work, by Kim. *et al.* were rather thick (50 nm) and would hence have an effect on

more than interfacial issues. These researchers found that the Ta_2O_5 over-layers inserted

between the Pt electrode and SBT film resulted in the emergence of strong (00*l*) peaks

corresponding to the lower-P_r, c-orientation of SBT. Here. however. the Ta_2O_5 layer was

to be inserted between the SrBiO layer and the Pt electrode layer, thus providing an

effective SBT composition, while simultaneously providing the functionality of both the

Ta_2O_5 diffusion barrier and the SrBiO seed layer.

In this work, heterostructures were deposited, consisting of the thin film stack.

Pt/(<5nm Ta_2O_5)/(<5nm SrBiO)/SBT. The benefit of inserting the interfacial Ta_2O_5 layer

was, as in the case of the SrBiO layer, immediately apparent. An XRD scan of an SBT

stack of this configuration is shown in Figure 4.9. In this figure, the Ta_2O_5 and SrBiO

layers were deposited at T_{sub}=200 °C, while the SBT layer was deposited at T_{sub}=450 °C.

As can be seen, the same MF phase development observed in the previous chapter on RF

sputtering, is evident here as well. However. The XRD peaks in Figure 4.9 indicate that

much of the transition of the MF phase to the ferroelectric SBT phase has already taken

place. Of the four primary peaks that designate the (a)-oriented SBT. only the (115)

reflection has remained in the MF phase location, so that the as-deposited film of Figure

4.9 may be expected to be weakly ferroelectric as in the case of similar as-deposited phase development in Figure 3.8.

The as-deposited film of Figure 3.8. deposited by the RF sputtering work in the last chapter. consisted of a capacitor stack deposited on 1/16" fused silica plate. so that there was some ambiguity as to the thermal gradient across the thickness of the SiO_2 insulator in the energetic sputtering environment. In the case of Figure 4.9. however. the thin film stack has been deposited on a Si (100) wafer. so that there was no such ambiguity. As in the case of Figure 3.8. it may be reasonably concluded that the XRD data of Figure 4.9 corresponds to at least 700 °C equilibrium phase development. This implies that we can achieve 700 °C phase development at a 450 °C substrate temperature. a significant decrease.

An important aspect of the phase development of Figures 4.7- 4.9 is that it is reproducible and. hence. tailorable. Equally important is that this phase development is quite homogenous across the on-axis-sputtering field of the "Type II" unbalanced magnetron source. Given the previous behavior of these unbalanced magnetron sources. as consistently and extensively reported in the existing literature. and as illustrated in Figure 3.2 of the previous chapter. the homogeneity ad stoichiometry transfer of the presently developed reactive sputtering process are quite unexpected.
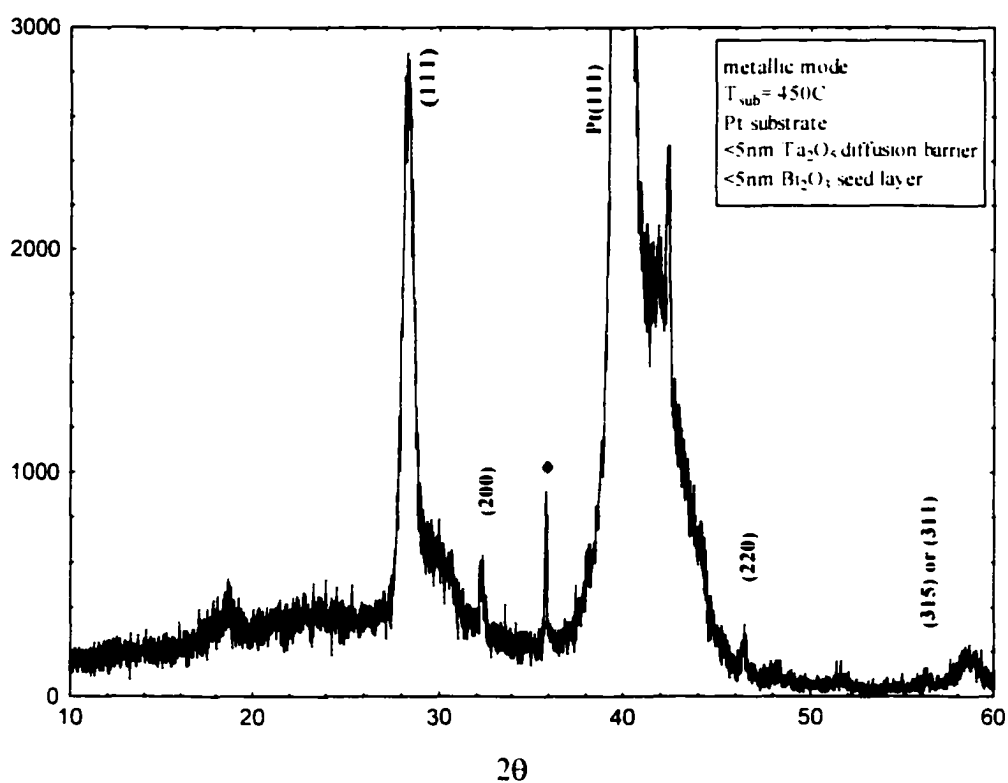
Figure 4.9: XRD 2-θ scan of MF-SBT transitional phase. as-deposited at 450 °C. Compositional control is enabled by a (<5nm)Ta₂O₅/(<5nm)SrBiO seed layer at the Pt/SBT interface.

OPTIMIZED UBMII-EAD METALLIC MODE	
Ta target power	40w
Bi-Sr target power	35w
Bi-Sr target composition	28%
O_2 partial pressure	0.05mTorr
Ar + O_2 total pressure	2.o mTorr
flow rate	~15 sccm
substrate temperature	450 ^{0}C

Table 4.2: sputtering conditions for optimized metallic-mode process.

A subsequent anneal. at 750 ^{0}C. of the as-deposited films corresponding to MF-type

phase development resulted in SBT phase development. as evidenced in Figure 4.10.

However. as may be seen in Figure 4.10. the resulting annealed material. when deposited

on Pt electrodes. would typically result in a x-ray reflection that could not be definitively

identified. such as the peak occurring at around 29.7 ^{0} in Figure 4.10. Such evidence of

non-phase-pure SBT is a reflection of the inability to prevent Bi loss into the underlying

Pt electrodes. Consequently. further development of the ferroelectric phase could not be

obtained by anneals at the typical 800^{0}C. since Bi loss would then incur the further

growth of Bi-deficient phases.
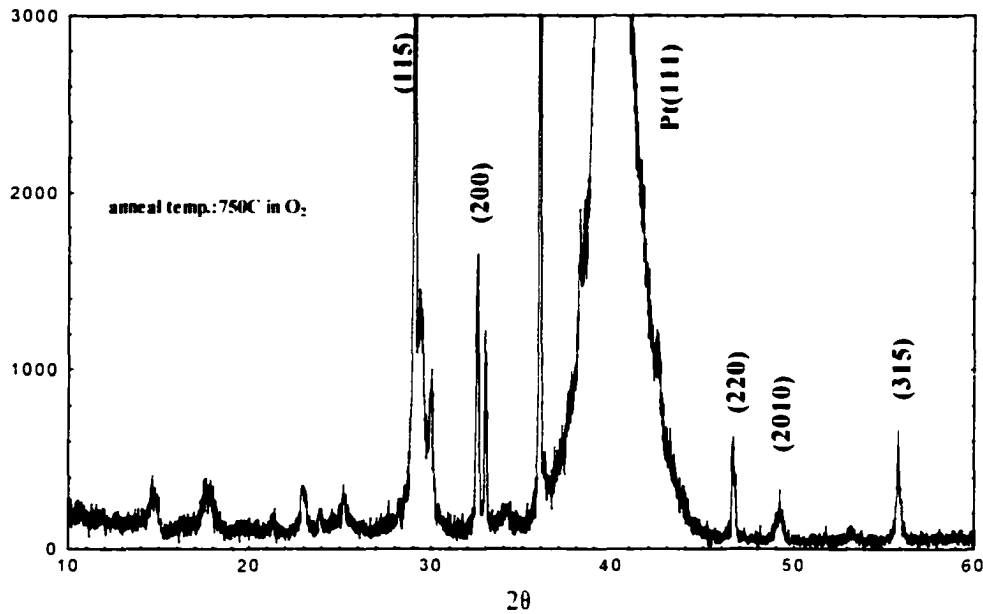
4.10: XRD peaks for annealed SBT deposited by new method.

4.6 Ferroelectric Properties

The relationship between phase development and ferroelectric properties became

sufficiently understood in the previous RF sputtering work of this dissertation. and was

mirrored in the present work on D.C. reactive sputtering of SBT. In the processes studied

here. the higher-P_r (115)-oriented SBT dominates film growth on either polycrystalline

or amorphous substrates. Of greater practical import is the hard-won understanding that.

in non-equilibrium growth methods. the many nearby phases that "look like" ferroelectric

SBT in the x-ray diffraction data are. in fact. not ferroelectric. Empirically speaking. the

X-ray reflections of a potential (a)-oriented SBT film must be fairly precisely identifiable as the SBT phase, or it can be expected that it is a separate phase that may be undocumented. This state of affairs places into doubt many of the previous reports of deposited SBT – or similar ferroelectrics – by such non-equilibrium methods, wherein the only evidence is (frequently vaguely presented) X-ray or electron diffraction data.

Since the relationship between XRD data and phase development of SBT had become well established for the methods explored, ferroelectric hysteresis testing was performed on a fairly selective basis in the D.C. sputtered films. Also, once on-axis, metallic-mode sputtering was successfully developed for SBT, the formation of the ferroelectric SBT phase, through a post-deposition anneal in oxygen, became a relatively straightforward process with low-temperature deposition ($T_{sub}<$ 300 °C). Ferroelectric P-E data for a SBT capacitor fabricated at room temperature, and annealed at 750 °C, is shown in Figure 4.11, which yielded a remnant polarization of $2P_r=7.8$ $\mu C/cm^2$. Relatively little effort was invested in establishing comprehensive performance data on the F.E. properties of a post-anneal process, however, as such post-anneal approaches hold little promise of any great advantage, compared to the establishment of a reproducible as-deposited SBT process.
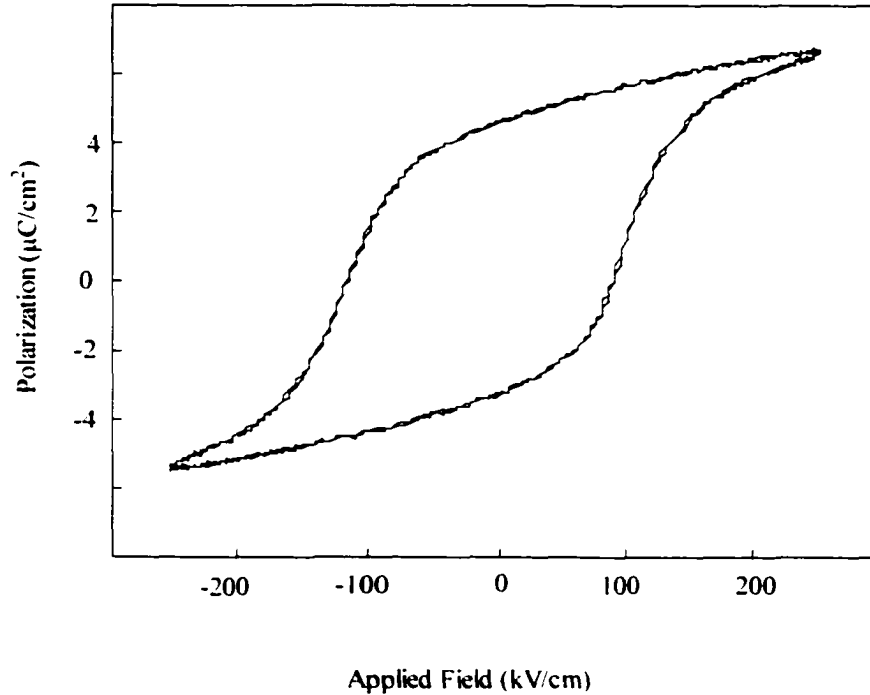
Figure 4.11: F.E. hysteresis of DC metallic mode sputtered
SBT in a Pt/SBT/Pt/TiO$_2$/SiO$_2$/Si(100) capacitor.

It may be noted that the coercive field required for switching in the capacitor of

Figure 4.11 is quite high ($2E_c = \sim214$ kV/cm under a 250kV applied field). It is found

that Sr-deficent films deposited by more equilibrium methods, such as by sol-gel or

MOCVD, display such increased coercive fields (Dawley 1999). This observation is

consistent with the conclusions drawn from the XRD data in this chapter, namely, that the

films deposited in the optimized process are still either Bi-rich or Sr-poor, depending on

sputtering power delivered to the Bi-Sr target, due to the successful replication of an only

somewhat Bi-rich metal target composition. Hence, increasing power to the Bi-Sr

sputtering source, to increase Sr content in the deposited films, would also unfavorably

increase Bi content. A straightforward improvement of this situation, now enabled in the

presently developed sputtering process, would be to fabricate a new Bi-Sr target that

reflects this faithful transfer of target composition to the deposited film. Such replication

of target stoichiometry reveals the dramatic improvement over earlier D.C. sputtering

experiments that were conducted in this work ostensibly under very similar conditions,

wherein even sputtering targets of exceedingly Bi-rich compositions resulted in Bi-poor

films.

It may be expected that the transitional phase of Figure 4.9 is weakly ferroelectric,

just as the, essentially identical, as-deposited phase of Figure 3.14. However, there is

little point in investigating such properties. Not only is it difficult to discern such weakly

ferroelectric properties from other charge transfer mechanisms in the complex capacitor

heterostructure, it is also difficult to conclude that such mechanisms are not to blame

when the weak ferroelectric behavior is not observed.

4.7 Conclusions

While a multitude of deposition approaches were tested in this research, many of

which will not be discussed in this thesis, it is noteworthy that much of the phase

development for the SBT and non-SBT compositions was quite similar across a broad

spectrum of vapor deposition environments. The results of this chapter appear to confirm

the general nature of the metastable fluorite (MF) phase development suggested in the

previous chapter.

BENEFITS OF METALLIC-MODE

In addition to the benefits of developing a metal-target reactive sputtering process, mentioned earlier, additional benefits are allowed by the metallic-process mode reactive process:

1. higher density films

2. elimination of particulate problems associated with ceramic targets

3. in developing a true metallic-mode reactive sputtering process for the first time in any sputtered ferroelectric, establishing a more stable and repeatable process for the general deposition of multicomponent oxides.

4. possibility of revealing nature of film growth kinetics in energetic processes through manipulation and monitoring of reactive gas in low transition flow; something not possible with RF sputtering or DC sputtering of oxidized targets.

5. refinements and increased control offered by metallic mode sputtering

6. crucial elimination of a substantially modified surface layer on the target surface, allowing run-to-run repeatability

7. possibility of increased deposition rate at lower powers, as compared to poisoned targets

8. possibility of effectively increasing adatom mobility at the substrate

While many other issues are typically cited, the real difficulty in implementing a metallic-mode sputtering process for ferroelectrics in previous sputtering set-ups must

ultimately rest on one primary dilemma. On one hand, at higher gas pressures, the target

will significantly poison for any practical flow rate, even using the highly controlled

delivery of the present experiments. On the other hand, the low total and oxygen partial

gas pressures required for implementing metallic-mode sputtering also result in reduced

films, or, in activating processes, energetic plasma species that resputter the growing

film. The method and apparatus ultimately here developed for reproducible metallic-

mode D.C. reactive sputtering of SBT constitutes an independent subject of study, and

will be treated more fully in the following chapter.

5. THE DEVELOPMENT OF ELECTRON-ASSISTED DEPOSITION (EAD)

5.1 Preliminary Observations

The experimental conditions described in the last chapter are accomplished

through a rather dramatic reversal of the behavior associated with a "Type II" unbalanced

magnetron. Such "Type II" UBM's are well-recognized and documented for providing

unusually high ion-bombardment in on-axis. or near-axis. deposition (Howson and J'Afer

1990: Howson 1997) (Sproul 1993) (Telling *et al* 1998). Primary applications for these

sources have been in tool coatings and other such applications wherein a high degree of

ion peening and re-sputtering at the depositing film is beneficial. As such. these

sputtering configurations have not been reported for use in film growth applications that

are sensitive to ion bombardment. such as for multicomponent oxide materials or single-

crystal epitaxial growth. as this would result in more defective films than in conventional

balanced-magnetron sputtering. The research communities for these more delicate

applications noted the undesirable effects of "Type II" UBM sputtering quite quickly. and

as a result. only the opposite. non-energetic. "Type I" UBM's have been reported for on-

axis sputtering of such complex materials as the High-T_c super-conducting oxides or

perovskite ferroelectrics. The successful development here of "Type II" UBM's. for on-

axis sputtering of such damage-sensitive oxides as SBT. marks a fundamental transition

in the behavior of plasma-based sputtering sources.

An attempt was made to reveal the possible mechanisms behind this behavior.

Studies were performed to establish the relationship of such I-V behavior to variables of

target composition. total pressure. partial oxygen pressure. and substrate position. It was

found that there is a sound basis for qualifying this method as the first example of what

can be termed. Electron-Assisted Deposition (EAD).

5.1.1 Activation of Chemistry in Energetic Deposition Processes

The relationship between degree of oxidation and oxygen partial pressure has

been explored in previous reports on the plasma sputtering of multi-component oxides.

with somewhat predictable results. Prominent groups. such as those involved in the

sputtering of PZT found that the degree of film oxidation could be increased to a

desirable level by increasing the oxygen partial pressure: and in fact. due to the low-

magnitude heat of oxidation of lead (still slightly greater than that of bismuth). rather

high partial pressures of oxygen (15 mTorr) were required to form acceptably transparent

films (Sayer 1986). The recitation here that more oxygen allows higher oxidation of the

growing film might sound somewhat mundane.

However. this straightforward perception of how oxygen interacts in a magnetron

plasma is found to be overly simplistic in the present work. In Figure 5.1 are absorption

spectra for a series of SBT films deposited during the RF sputtering segment of this

dissertation work. The films were deposited on fused silica at room temperature. while

consecutive deposition runs were conducted with successively lower partial pressures of

oxygen. As was apparent on observing the transmission of these films. and is now

apparent in these absorption spectra of Figure 5.1. the SBT deposited at a significantly

higher oxygen partial pressure actually demonstrated a marked increase in neutral density

optical absorption. Such neutral absorption is a clear demonstration of a decrease in

oxidation, and representative samples were subsequently annealed in oxygen to

demonstrate the disappearance of such absorption. A recent report seems to imply

similar behavior in the magnetron sputtering of GeO_2 by Njoroge. *et al.* (Njoroge *et al*

2000). However, the latter researchers concluded that the paradoxical appearance of an

increased elemental Ge content in the GeO_2 films – noted by a corresponding increase in

XRD reflections – was, in fact, due to the presence of more amorphous – rather than
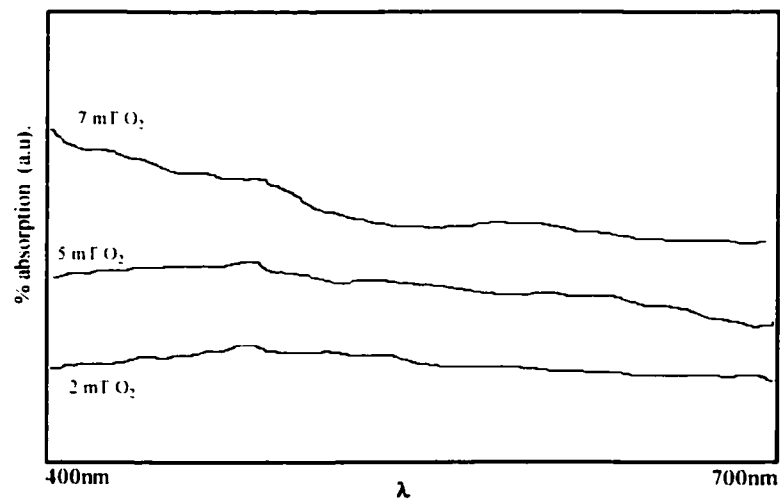
Figure 5.1: Optical absorption of RF sputtered SBT
films as function of O_2 partial pressure.

crystalline – Ge in the films deposited at lower partial pressures of oxygen. The latter researchers did not entertain the possibility that lower oxygen pressures may beget less reduced films due to activation by a lower pressure plasma environment. This possibility is intimately connected to why the unbalanced magnetron approach has been actively implemented here.

As indicated. in Figure 5.1. by the counter-intuitive relationship between O_2 partial pressure and resultant film oxidation in the RF sputtering experiments above. activation of surface chemistry by the plasma environment can clearly play a dominant role in determining the chemistry of the growth interface. Similarly. free or quasi-free electrons undoubtedly play an important role in reactive film growth for any such plasma-assisted deposition method. Yet. the effects of such electrons are seldom discussed. let alone characterized. The question arises as to whether one might possibly develop a process that would establish a distinguishable electron-assisted deposition (EAD) method. where film growth characteristics are dominated by electron bombardment of growing thin film.

5.1.2 Previous Electron-Assisted Processes

To distinguish an EAD process from a plasma-assisted deposition process. we must be able to clearly demonstrate electron-dominated bombardment of the growing film. Also. if EAD is to be a meaningful term. we must be able to clearly differentiate the results of the EAD process from that of either plasma-assisted growth or an ion-assisted deposition (IAD) process. Obviously. verifying a substantial bombarding

electron current by grounding it through the growing film is of little practical use. nor would it isolate the effects of bombardment from the (unwanted) effects of conduction.

There is not found. in the vapor deposition literature. any account of another research group reporting what one may claim as an EAD process. Potential reports of an EAD process do not satisfy the above conditions. in that they fail to demonstrate a verifiable method for eliminating the ion contribution. nor do they demonstrate a resulting growth process that may be distinguished from that of low energy ion bombardment. Some recent reports are based upon experimental efforts in "electron-beam assisted deposition" of CeO_2 on silicon. by way of installing a secondary thermionic filament near the substrate. in an existing e-beam evaporation system. These prior accounts of electron-beam assisted deposition resulted in the observation of a lowered epitaxial temperature for the growing oxide film (Inoue and al 1997; Inoue et al 1999: Inoue et al 2000). However. such effects as a lowering of the required epitaxial growth temperature are not distinguishable from the effects readily obtained with low-energy ion bombardment.

Also. to assert solely an electron contribution to the lowered epitaxial temperature. the Inoue group discounted an ion contribution by diverting the electrons with bending magnets. and observing the diminished effect of only the remaining negative ions. Yet. this is not a convincing description. as it does not account for the creation of positive ions. or weak-plasma interactions created by the electrons. Under such circumstances. the low-energy positive ions – created by the secondary beam and elsewhere – will not be separated from a secondary electron beam by such bending

magnets. but will tend to follow the negative space charge of the electrons. The Inoue group assumed negative ions were the only ions at issue. since there is no discussion of the effects of O^+. O_2^-. or Ce^- in their published reports. One can expect negative oxygen ions may dominate ion production at oxide surfaces of the e-beam deposition hearth. However. the low-pressure. gas-phase interactions of the secondary electron beam. with both the injected oxygen and the dissociated CeO_2 vapors near the substrate. will typically favor production of positive ions. The contingencies here are quite different from those of the well-developed 270^0-deflection e-beam sources. where acceleration forces are much greater. and the positive ions *do* follow the electron beam. only. *most* positive ions cannot traverse the full 270^0 and enter the narrow beam aperture-stop. It should also be remembered that. in such e-beam evaporation systems. the effective pressure at the substrate. due to both oxygen flow and depositing metal/metal oxide vapor. will be higher than what is read at the pressure gauge. which implies a higher production of positive ions. Due to these. and other. considerations. it is thus not clear how large the positive ion population is. or what part it plays in the altered growth conditions of the preceding reports.

The preceding contribution of positive ions will be multiplied in the circumstance that the growing film is an oxide insulator. It is a frequently troublesome aspect of such energetic vacuum processes that thin film oxides. due to positive electron affinity. low aspect ratio. and inherently high capacitance on conducting substrates. readily develop an electron sheath as in Figure 5.2. If electron bombardment of the insulating film is the goal. then such charge build-up will certainly occur. The field seen by the electrons on
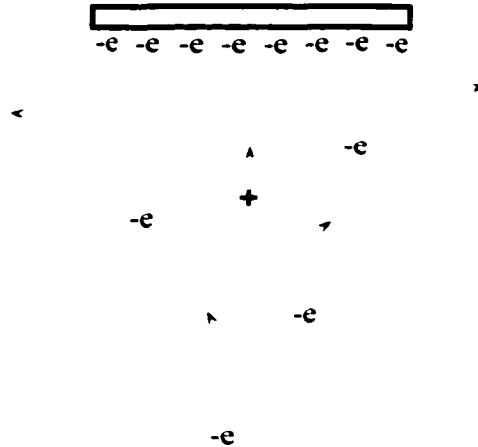
Figure 5.2: Normal. untrapped electron bombardment of a dielectric substrate during vapor deposition. wherein charge arrival at the growing film must equalize.

the process-side of the growing insulator will then be quite different from the ground potential of the substrate holder. If the impinging electron beam is not to be repelled from the charged-up oxide film - and proceed to conducting portions of the substrate. substrate fixture, or chamber - some form of charge compensation at the oxide growth interface must occur. Because development of a surface charge potential will occur on even the most fractured thin film oxide insulators. leakage current to the grounded substrate cannot account for such charge compensation (unless the oxide material was so

defective that it performed as a semimetal). The typical form of charge compensation is through attraction of positive ions. and the negatively-charged oxide growth interface can be expected to promote an equalization of the arrival rate for positive ions and negative charge. similar to any floating plasma probe. In this way. even a relatively limited production of positive ions becomes relevant to the growth conditions. In addition. at 10^4 to 10^5-times the mass of an electron. the impact of ions such as O^-. O_2^-. and Ce^-. can readily overshadow the effect of electrons on the growth interface. The charging up of the growth interface of an insulating oxide may. in itself. have an interesting effect on epitaxy. but it is difficult to imagine a basis for discounting an ion contribution in either the described experimental set-up or results of this e-beam process. Recently. another group has performed similar "electron beam-assisted" thin film growth experiments in dual ion beam deposition of CN. and has used arguments similar to those of the Inoue group (Kim *et al* 2001). However. the difficulties are essentially the same in view of the highly plasma-like environment at the growth interface.

As is suggested in these previous accounts. the overall difficulty in developing a true EAD process resides in the difficulty of providing an actual electron gas directly incident on the film growth interface. rather than what is better described as low-density plasma interactions. while simultaneously utilizing a materials process that allows positive identification of electron-dominated growth behavior. Because most conducting materials possess the lower bond energies of metallic bonds. and tend to be relatively low-temperature phases. the higher temperature insulating and semiconducting compounds appear to be more likely candidates for discerning the effects. and. hence.

benefits of an EAD process. In addition. the use of conduction through the film to establish an electron current simultaneously adds an unknown contribution due to ohmic heating.

Unfortunately. deposition of these compounds with suitable low-pressure deposition methods will usually involve reactive vapors that are likely to interact with the electrons. producing ions that easily dominate the growth process. In addition. such compound materials will typically be prone to charging effects under electron bombardment. thereby reducing the surface interactions of the electron beam in a manner that is difficult to monitor or manipulate.

5.2 Establishing as EAD Process with a UBM Discharge

5.2.1 Experimental Considerations

The use of unbalanced magnetrons of the "Type II" category is well-known to produce a large flux (around 5 mA/cm^2) of positive ions to a substrate in the on-axis sputtering of metallic materials. Charge transfer processes for such UBM sputter sources in an oxygen-containing environment are much less characterized. presumably because the build-up of an insulating layer on the substrate makes it difficult to reliably infer electronic behavior on the plasma-side of the insulating film. Another possible reason for the scarcity of data concerning Type II magnetron sources in oxidizing processes is the apparent unsuitability of such sources for depositing most industrially important oxides.

In this research. the electrically conducting relief structures built into the electrically floated substrate holder can allow a somewhat reliable means for eliminating

the electric potentials that might build across the growing dielectric film. However, it should be noted that the self-bias potentials obtained are necessarily only the low end of the voltages that will exist at the dielectric growth interface. Because of this latter reality, the trends observed in these electrical studies were sufficient to provide some rather fundamentally important, and novel, information about reactive sputtering processes.

Because of the aforementioned limitations on monitoring the substrate I-V characteristics, grounding of the substrate to monitor substrate current was seen as a pointless exercise. Such an attempt would fundamentally alter the sputtering environment, as well as provide unreliable data due to the unknown impedance of the growing film. However, at the high self-biases witnessed, the voltage drop across the insulating film should be fairly insignificant, given the high impedance of the substrate/voltmeter system. One reason for comfortably asserting this is that, at a few hundred Angstroms film thickness, the field within the insulating film would be in the Megavolt/cm range for even a 2-volt difference. This would result in more than enough leakage current, over several cm^2 of substrate area, to dissipate the potential for even the highest quality films.

While performing in-depth probe studies of the plasma characteristics of the constructed unbalanced magnetrons was beyond the scope of the present work, attention was paid to the plasma characteristics that could be inferred from the floating bias voltage of the 2" diameter substrate and the I-V characteristics of the magnetron discharge. As depicted in Figure 4.3 the substrate was suspended directly over the deposition axis of both magnetrons. Behavior of the unbalanced magnetrons appeared to be quite similar to

the behavior reported originally in the work of Savvides and Window, as well as later

work, in that normal operation with a metal target gave peak floating voltages between 25

to 30 Volts D.C. in the on axis position (Window and Savvides 1986) (Telling *et al* 1998)

(Spatenka *et al* 1999). Similar to the earlier work, the peak bias voltage was found to

occur in the on-axis position, with the bias voltage increasing as a function of decreasing

sputtering pressure, down to around 2 mTorr, where both operating current of the

magnetron discharge and the substrate self bias voltage dropped sharply with decreasing

pressure. Given the disparate UBM designs utilized in the various studies of these

sources, it is interesting to note the similarity of their behavior. This similarity in

behavior suggests that the one may understand much of the operating characteristics of a

magnetron design simply by knowing its general magnetic field shape.

There is a general consensus, in the previous literature dealing with the normal

"Type II" UBM operational mode, that the plasma characteristics of the sputtering

discharge are extended to the substrate, so that that the environment in the vicinity of the

substrate, as in Figure 5.3, in normal UBM operation, is "plasma-like". In such an

instance, an ion sheath may be expected to form adjacent to the substrate, and the

substrate negative self-bias may be regarded as an acceleration potential, resulting in a

fall region for positive ions. The actual magnitude of this acceleration potential will then

be the difference between the floating substrate potential and the plasma potential in the

adjacent ion sheath. The plasma-potential will be close to zero, and, classically, slightly

positive, if the environment is indeed plasma-like (i.e., roughly neutral). While there is

difficulty in explaining the fairly negative plasma-potentials observed in the earlier UBM
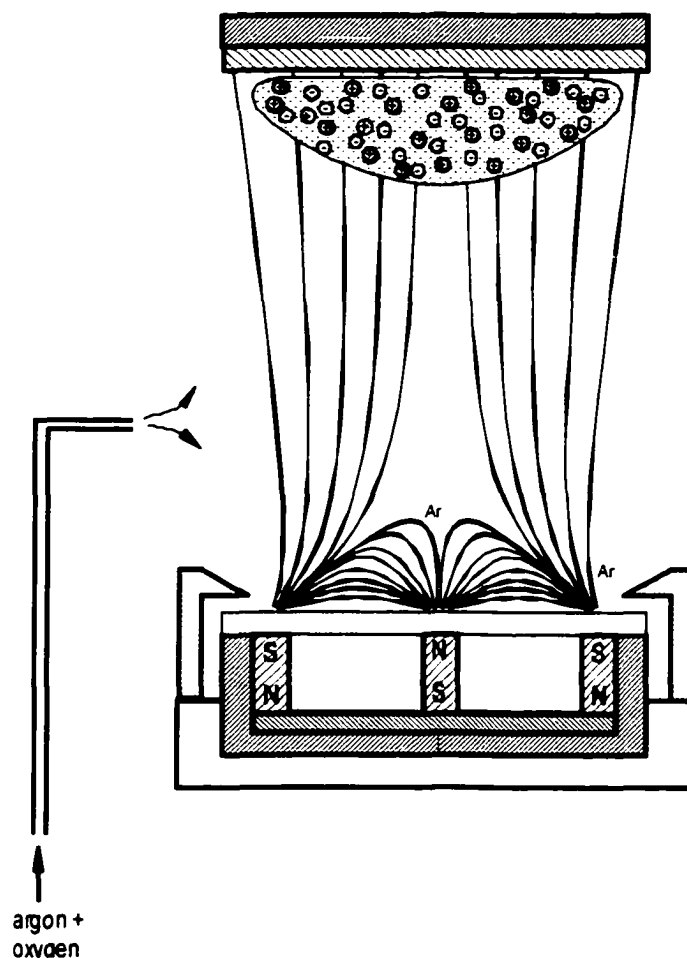
Figure 5.3: illustration of magnetron in normal
UBM mode of operation.

experiments in the "normal" mode. they do provide an acceleration potential with respect

to the substrate. and the presence of heavy ion bombardment is very evident in the

deposited films. as is evident in Figure 3.2. Hence. because of the relatively low (in the

present context) self-bias voltages involved. and the evidence of high positive ion numbers. charge compensation at the substrate may be primarily attributed to simply the equalization of charge arrival.

However. this observation of the generic nature of I-V characteristics for UBM magnetic design is more appropriate for the "simple" sputtering of a metal. Studies performed in this work establish that the situation can be dramatically different in the DC reactive sputtering of a dielectric. For these studies. I-V characteristics in DC reactive sputtering were obtained using the highly non-equilibrium gas flows described in conjunction with Figure 4.3. thereby attaining a condition of stable and reproducible "metallic mode" reactive sputtering. and co-sputtering. of the Sr-Bi and Ta targets described in Chapter 4. The surprising observation made in these experiments was that the substrate self-bias could increase roughly an order of magnitude. Substrate self-biases of over –200 VDC – as opposed to transient surface potentials one might observe in an RF process – were regularly observed in the metallic-mode reactive sputtering of SBT. far higher than those previously reported in sputter deposition.

5.2.2 Basic Behavior in the EAD Mode

This section introduces some of the basic attributes of what will be shown to be an Electron-Assisted Deposition (EAD) method. that is demonstrated here using a "Type II unbalanced magnetron" (UBM) sputtering source. Figure 5.4 helps to illustrate the basic nature of the transition from the normal UBM operational mode to that of the "EAD-UBM" operational mode. The previous behavior of the normal UBM mode

observed in the R.F. sputtering studies of Chapter 3 revealed the heavy ion bombardment and ion-beam characteristics for which these "Type II" UBM sources have become well known and extensively studied, for either R.F. or D.C. sputtering processes. As is illustrated in the deposition and composition profiles of Figure 5.4, the previous effects of heavy ion bombardment have been dramatically reversed in the on-axis portion of the substrate. Rather than the deposition zone that corresponds to on-axis sputtering being almost completely depleted of bismuth, there is actually a dramatic *increase* in the bismuth content with respect to the peripheral off-axis deposition region.

It is also evident, in Figure 5.4 that the inhomogeneity of the normal UBM mode of Figure 3.2, a general characteristic of normal UBM mode operation in reactive systems, has essentially disappeared. However, this behavior does not mark a return to the less energetic environment of conventional "balanced" magnetrons. This may be recognized by noting that the on-axis region of the substrate, in Figure 5.4, is simultaneously being bombarded by electrons, to the extent that it is floating, in this case, at a substrate self-bias potential of $V_{sub} = -180VDC$. This D.C. voltage is clearly, assuming an actual plasma-like environment at the substrate, far in excess of the acceleration potential sufficient to produce the eroded profiles typical of normal UBM operation, which is captioned in Figure 5.4.

reduced Ta/Sr compounds

predominantly SBT composition;
increasingly Bi-rich toward center

transition region

SUBSTRATE

normal
UBM mode

V_{sub}= -27 VDC

substrate
composition
profile; % Bi
content
(a.u.)

0

substrate
thickness
profile
(a.u.)

0

V_{sub}= -180 VDC

TARGET
DIAMETER
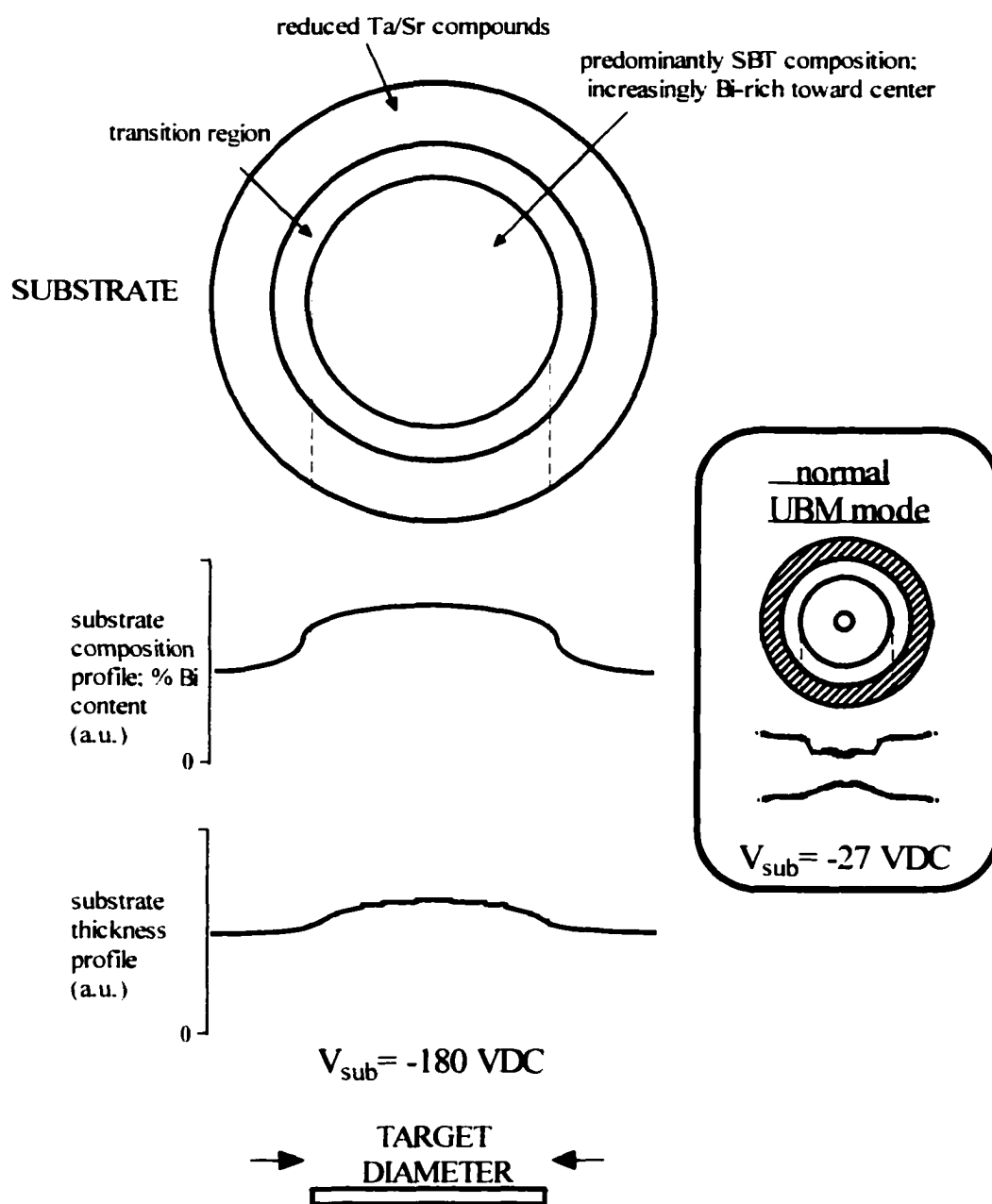
Figure 5.4: Substrate stoichiometry/oxidation/thickness profile for the EAD mode at very low oxygen partial pressures. Characteristics for the normal UBM mode are in the smaller caption.
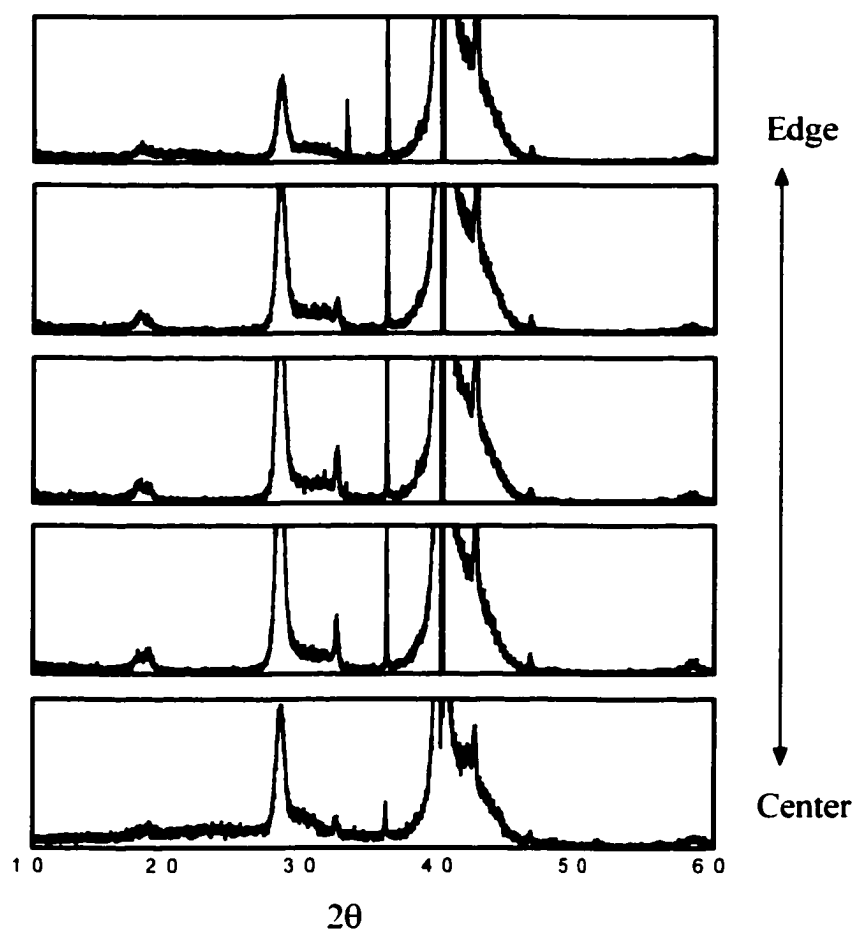
Figure 5.5: XRD series characterizing uniformity of substrate from center to edge of the on-axis zone. T_{sub}=430C.

Another important aspect of the EAD deposition profile typified by Figure 5.4 is that, in very low oxygen partial pressures (<0.05 mtorr), only the on-axis region of the substrate is observed to be a stoichiometric oxide, while the reactively deposited film outside of this irradiated on-axis area, is very reduced. In SBT deposition, this same

reducing environment will, nonetheless, still result in the desired bismuth content in the irradiated on-axis area of the substrate. This latter development dramatically illustrates the activating nature of the high electron flux that is incident on the growing film, so that the deposition process is essentially an *activation-limited growth* process.

Relative to the films deposited in the normal UBM II mode in Figure 3.2, the much increased homogeneity of the films deposited by the EAD method, apparent in the results in Figure 5.4, is further evident in the far greater phase homogeneity observed in the resulting XRD data, in Figure 5.5. These XRD scans were taken from a substrate that was stationary during deposition. In Figure 5.5, the MF phase, described in chapters 3 and 4, consistently emerges in the sampled regions, which range from the center of the on-axis region to its edge.

It is argued, in this chapter, that the "EAD-UBM" process, as introduced above, provides a combination of effects that satisfy the previously submitted criteria for establishing, for the first time, a true EAD process. As will be further supported, the environment at the growth front demonstrates the required conditions that, first, there is verifiable energetic bombardment of the growing film that is clearly dominated by electron current, and, second, the results of the energetic bombardment are clearly differentiated from the effects of ion, or plasma, bombardment.

5.2.3 The Departure From a Plasma-like State

The classical discharge concept, the "anode fall" region, does not apply well to the experimental conditions of the EAD-UBM mode. The typical expectation of such a

-200 VDC electrostatic surface potential in a sputtering environment is to expect nearby positive ions to accelerate through a fall region to bombard the surface at close to 200 eV. If the 200V self-bias could be vaguely perceived as the acceleration voltage for positive ions. then one would expect to see heavy resputtering of the Bi at the growing film. rather than an *increase* in the Bi adsorption rate. as in Figure 5.4.

The analysis of floating potentials in UBM sputtering has been. in all reports up until the present. treated within the context of ambipolar diffusion and general plasma behavior. Under these assumptions. we should be able to estimate how the floating potential will be related to the electron temperature. T_e. of the ambipolar environment. Accordingly. we might use the Bohm criterion to predict T_e as a function of the floating potential. as was discussed in Chapter 2. Because the electron temperature distribution might be multi-modal. and. typically. bi-modal. an estimate of this relationship . following Penfold. allows for a summation of Boltzmann factors:

$$[\ \Sigma \, a_j \, e^{-V/Tj} \ ]^{-1} \ = \ 108(M/40)^{1/2} \quad \text{where } \Sigma \, a_j = 1 \quad (1)$$

where M is the ion mass in a.m.u. and T_j correspond to the electron temperature of each Boltzmann-like electron energy distribution present. For the argon sputtering gas used here. we find that. for $V_f = -200$. the single-mode electron temperature is $T_e^{low} \cong 43$ eV. If we assume a second electron population exists with higher temperature. T_e^{high}. which would typically be expected. then the temperature. T_e^{low}. of the first electron population may be lower and becomes increasingly insignificant as T_e^{high} increases far above 43 eV.

A common interpretation of the above relation, and experimentally observed V_f, would then be that a relatively small percentage of secondary electrons have retained close to the full cathode potential after escaping from the trap region near the cathode(Sheridan *et al* 1991) (Sheridan *et al* 1990) (Penfold 1995). However, there are several difficulties in appealing to this explanation in the present context.

Foremost of the inconsistencies in assuming the above relation (1) describes the observed EAD mode is the fundamentally different unmagnetized plasma environment for which the Bohm criterion and the above relation are formulated. More centrally, though, a seven-fold increase in the negative floating potential clearly cannot produce the dramatically reduced re-sputtering of Bi at the growing film, as observed, if the Bohm sheath criterion were remotely valid and the environment at the substrate were vaguely plasma-like. One could argue that ion bombardment has effectively disappeared because plasma density at the substrate has been, somehow, significantly diminished: however, this would require a commensurate decrease in the local electron density. By all indications, the opposite has occurred, and the EAD transition marks a significant increase in electron creation at the cathode, where both cathode current increases, and the proportion of the resultant current that is electron current appears to increase significantly, as well. Also, as discussed in Chapter 2, the ambipolar diffusion rate, $D_{\perp a}$, of electrons escaping out of the closed UBM magnetic trap, at these low pressures, may be expected to be higher than the diffusion constant, $D_{\perp e}$, of electrons alone, so that a decreased ion population would not, according to relevant theory, result in increased electron diffusion from the trap.

A reconciliation of these observations is obtained if the substrate environment in the EAD mode is considered to be accurately described. not as a plasma state. but rather. as a magnetically confined electron gas. This latter qualification would provide a novel basis by which successful EAD processes could be implemented. Following sections will further assess the likelihood of this qualification.

5.2.4 EAD-UBM Environment as Two Functionally Distinct Regions

The schematic in Figure 5.6 is presented to aid in this presentation of the EAD-UBM mode. as well as to differentiate it from normal UBM operation. depicted in Figure 5.3. The assembly of electrons in the volume between the cathode and the substrate. as indicated in figure 5.6. are no longer characterized as diffusing within a body of plasma. Instead. the behavior of the electrons is shown as essentially a magnetically confined electron gas. In addition to this qualification of the substrate environment as that of an electron gas. another substantial qualification of the EAD-UBM environment is introduced here. which is based on the observation that the EAD-UBM environment is a combination of two functionally distinct. centro-symmetric volumes. These volumes. 'A' and 'B' in Figure 5.6. can be generally delineated by the termination of their respective magnetic field lines. One may note that. in the illustrated magnetron field. the magnetic field lines may be characterized as either terminating only at the cathode surface. or as terminating also at the electrically floating substrate fixture.

oxygen argon
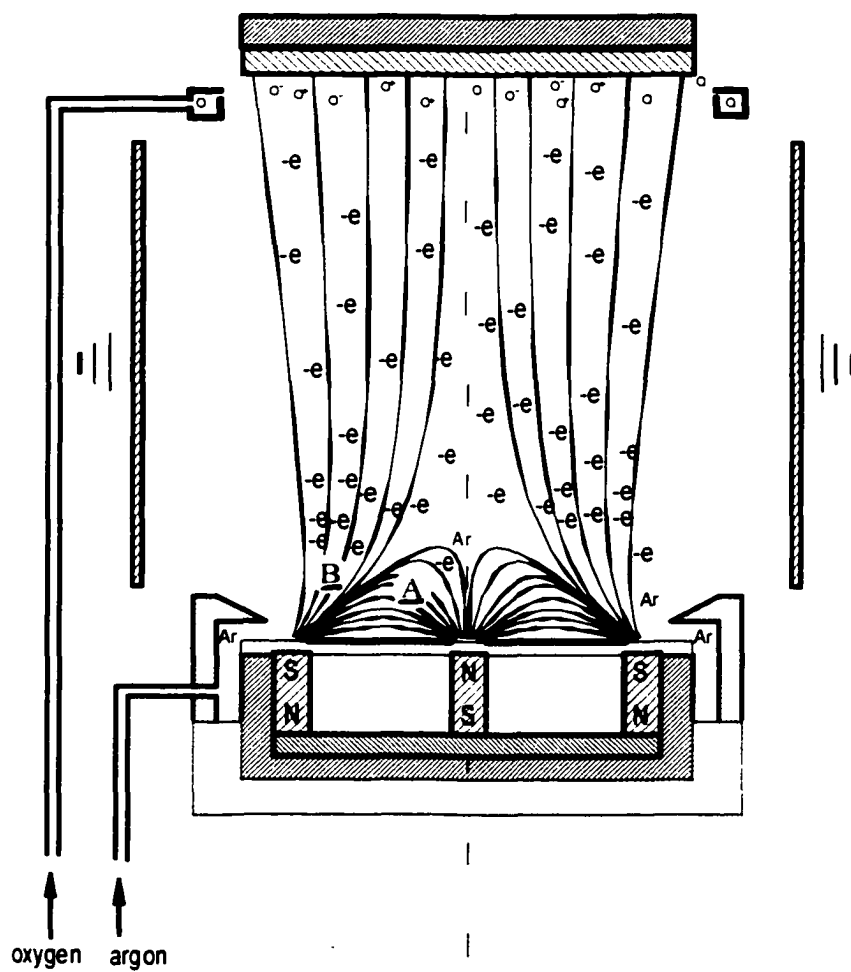
Figure 5.6: proposed environment of magnetron EAD-UBM mode of operation, with excess electron flux emitted at the target, <3 mTorr pressure, and a differentiated gas flow pattern.

These two distinct regions of the magnetic field are designated. in Figure 5.6. as

'A' for the trap of the magnetron sputtering plasma. and 'B' for the EAD electron trap

that communicates directly with the substrate. In this division. the cathode is in direct

communication with both 'A' and 'B' regions. and thus. must similarly provide two

separate. concentric. areas that are also functionally distinct. As is evident in the figure.

the EAD trap. 'B'. terminates at the cathode in the form of what is essentially a magnetic

mirror. as characterized by the magnetic cusp and commonly used. in various forms. in

tokamaks and other plasma studies. Since no plasma sheath can exist at this cusp. any

electrons entering the cusp region of 'B' will be in direct communication with the

cathode's negative potential. and will thus migrate in the opposite direction. toward the

substrate. Because the EAD trap. 'B'. completely isolates the magnetron plasma trap.

'A'. from the grounded surfaces in the chamber. any electrons created in the magnetron

trap must enter and. somehow. migrate out of the EAD trap before finding ground. This

observation that the EAD-UBM environment is a combination of two functionally

distinct trap regions provides a structure in which the plasma-like properties of the

sputtering discharge can be effectively isolated from the mechanisms at work near the

substrate. However. such a lack of homogeneity. in the EAD-UBM environment. also

further diminishes the relevance of the available analytical approaches.

5.2.5 Importance of the Secondary Electron Coefficient

The EAD-UBM mode is. in great part. reliant upon the creation of a

disproportionately high flux of electrons. That this is the case may be deduced by

observing the relationship of the observed substrate self-bias to the percentage of Sr

incorporated in the Sr/Bi alloy sputtering target. As is apparent in Figure 5.7. there is a

transition to the EAD-UBM mode of operation as the Sr content of the target is increased

above roughly a 20% content. As the high secondary electron coefficients. δ_{se}. of the

Group IA and Group IIA metal oxides is well established. the emergence of the EAD-

UBM mode may be reasonably attributed. in part. to an unusually high flux of electrons

injected into the UBM's magnetic field.

The mechanism entertained results from experiences in witnessing dramatic

changes in magnetron plasma behavior as a function of the secondary electron coefficient

of the target surface species. The secondary electron coefficient. δ_{se} . is defined here. as

elsewhere. as the ratio of the number of electrons emitted from a surface to each incident

electron. Thus. if one electron is emitted from a surface for each incident electron. the

secondary electron coefficient of that surface is unity. Of course. these coefficients must

be determined in a vacuum. and the coefficient will change significantly as a function of

both the energy of the incident electron and the temperature of the material surface. as is

indicated in Figure 5.8.

The significantly higher secondary electron coefficient most metal oxides possess.

relative to the respective metal. may be easily witnessed in the DC reactive sputtering of

many metals through the self-bias of the magnetron cathode. These observations can

then form a basis for characterizing "metallic-mode" sputtering behavior. While the

signature I-V characteristics for reactively sputtering any one metal will be determined by

► EAD-UBM mode
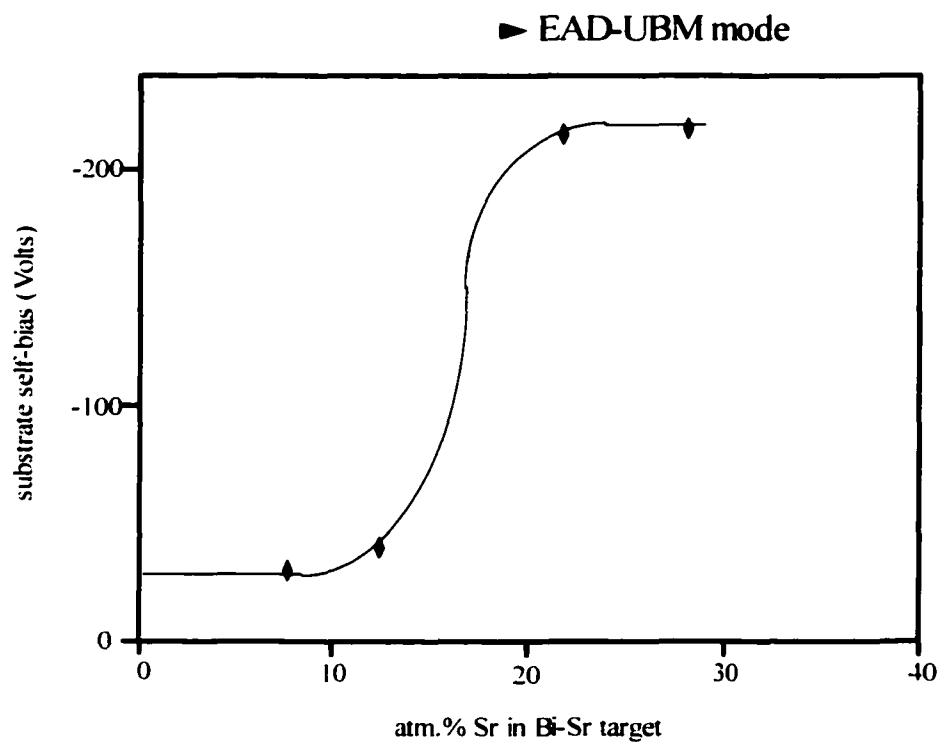
Figure 5.7: Self-bias voltage of the floating substrate vs %Sr in target.

a complex interplay of many plasma/surface interactions, it is not uncommon to find

slight oxidation of the target surface to result in a 20%-decrease in the target potential.

This latter drop in cathode voltage may be attributed primarily to increased electron

emission from oxidized atoms at the target surface.
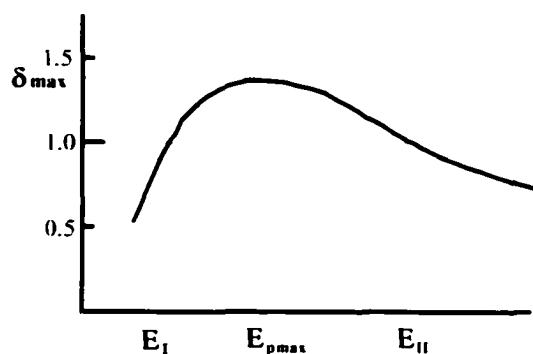
Figure 5.8: Graph illustrating the secondary electron characteristic of material/vacuum interfaces. A characteristic emission of secondary electrons as a function of primary electron energy is given.

Consultation of references on secondary electron coefficients. δ_{se}, gives an indication of the tendency for metal oxides to possess significantly higher secondary electron coefficients than the corresponding metal. However, it should be kept in mind that the values given in Table 5.1 are only the barest indication of the situation encountered in the present study. Whereas one may observe from Table 5.1 that the coefficients of MgO are quite high, these properties are found to significantly multiply for a fresh, vacuum-cleaved, plane. The effective secondary electron coefficients for the same metal oxides when incorporated into a metallic matrix, and immersed in an oxygen-containing magnetron plasma, will likely be significantly higher, yet.

Material	δ_{max}	E_{pmax} (eV)	E_I (eV)	E_{II} (eV)
Ag	1.5	800	200	>2000
Al	1.0	300	300	300
Li	0.5	85	none	none
Pt	1.6-1.8	700	350	3000
Bi	1.2	550	none	none
Ta	1.3	600	250	>2000
MgO	3-15	400-1500		
MgO (vacuum cleaved)	21-25	1500		
SiO$_2$ (quartz)	2.1-4	400		
"Glasses"	2-3	2-3		

Table 5.1: Some known values of the secondary electron coefficient. δ_{se} . for selected materials .

While the D.C. sputter processes developed here operate in a relatively extreme metallic mode. it should be remembered that one can not obtain reliable secondary electron characteristics of pure. highly reactive metals such as Sr. without studying a fresh surface of the metal in a UHV environment. Oxygen gettering by such Group IA and IIA metals is too efficient to allow a completely pristine metal surface in any practical oxide process. This latter reality does not compromise the operation of a highly metallic mode in the present work. For one. the Sr-Bi target is predominantly Bi in a Bi intermetallic. Any dispersed SrO will not enjoy the low sputter yield of a SrO precipitate. but will be sputtered as quickly a its surrounding matrix. Secondly. and

perhaps of key importance. what oxidation of the target Sr does occur will do so

primarily outside of the target erosion track. namely at the target center and edge. These

relatively unsputtered areas of the target correspond. also. to the target surfaces which

emit relatively orthogonal magnetic field lines. as may be seen in Figure 5.6. where field

cusps exist at the target center and target perimeter. Thus. electrons released from these

areas of relatively high SrO contamination will readily escape toward the substrate.

5.3 Analysis of Diffusion and Transport in the EAD-UBM Mode

The efficient production of a high electron flux in a magnetic trap does not. in itself.

explain the high floating potentials observed in this EAD process. At the dimensions of

the current system. it takes very little surface charge to redirect a high flux of low-energy

electrons to a nearby. grounded surface. The establishment of roughly an order of

magnitude higher floating potential in the EAD mode indicates that the magnetic trap of

the "type II" UBM is far more capable of trapping electronic charge than was previously

suggested. To understand how this EAD mode arises. it is appropriate to look back at the

normal UBMII mode to find limiting factors that might prevent such efficient electron

confinement. The availability of positive and negative charge that provides the "normal"

conditions must. of course. be contingent upon issues other than the magnetron source

design.

On observation of the relatively efficient trapping of the UBM-EAD mode. we

can assert that there must be some limiting mechanisms that prevent such efficient

electron trapping in the normal UBM mode. These limiting mechanisms in the normal

UBM mode might be logically assessed as either interactions that allow the gas-phase

electrons to escape the magnetic field-lines, or. interactions of the electrons with the

substrate that allow electron loss.

To aid in explaining the energetic sputtering environments encountered here, an

illustration of many of the different dominant mechanisms proposed is presented in

Figure 5.9(a) for the normal UBM mode, and Figure 5.9(b) for the UBM-EAD mode.

Figure 5.9(a) is a representation of the environment at an electrically floating substrate in

the normal "Type II" UBM methods reported, which have dealt primarily with deposition

of metallic materials, such as metals and metallic nitrides. Figure 5.9(b) is a

representation of the environment at an electrically floated substrate in the EAD process

developed here, which may be enhanced by the formation of an insulating thin film on

the substrate surface.

The illustrated mechanisms, in Figure 5.9, that are used to describe the transition

between these two modes are as follows: electron/ion gas phase interactions (A),

primary/secondary electron exchanges (B), surface/sub-surface migration of electrons

(C), ion bombardment and related charge compensation (D), and field/thermionic

electron emission (E). Various elements of Figures. 5.9(a) & (b) must be regarded as

descriptive tools, rather than precise representations. For instance, there is no point in

attempting to display the various Larmor radii of the electronic charge, nor the possible

Larmor potentials due to the magnetic field. The stray electrons depicted in the substrate

volume designate the essentially metallic nature of the underlying substrates. However,

the density of electrons at the substrate surface in Figure 5.9(b) denotes the presence of
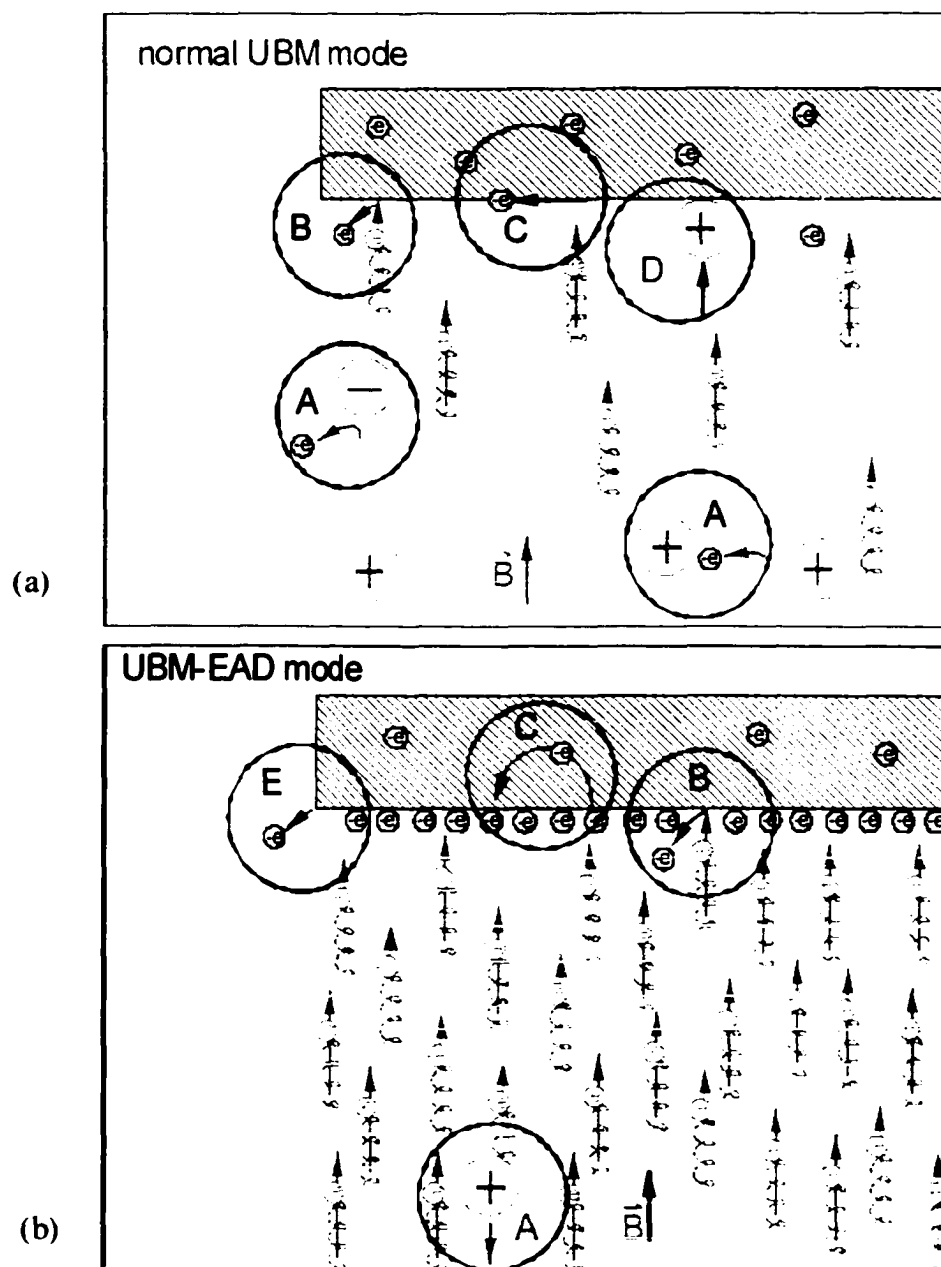
Figure 5.9(a): Schematic of the plasma-like environment near a floating substrate
in previously reported "Type II" UBM sputtering methods. Various dominant
mechanisms of charge transfer are shown.

Figure 5.9(b): Schematic of proposed mechanisms that dominate charge
transfer in the UBM-EAD mode developed in the present work.

an insulating oxide surface layer, with accompanying surface charge that may vary

considerably, and, infact, reverse, as a function of primarily the local electron interactions

and the secondary electron characteristics of the oxide surface layer. The elements of

these two figures will be discussed throughout the remainder of the chapter.

5.3.1 Interactions with the Substrate

The unknown contribution of space charge to the behavior of magnetron

sputtering discharges has been addressed very little in the existing plasma sputtering

literature. The effects of space charge in the vicinity of the substrate are even less

discussed. This is because it is quite difficult to assess space charge contributions in the

highly synergistic environment of a reactive magnetron discharge, where such

characterization means as Langmuir probes can fundamentally alter the monitored

discharge environment. However, the electron-dominated environment of the present

EAD process may allow for some simplification. With the very high electron emission of

the Sr-containing target, combined with the efficient trapping provided by the UBM

magnetic field, the electron density within the UBM environment appears to reach a

critical saturation level. This is to say that, at some magnitude of electron density,

electrons arriving at the substrate do so largely in response to electron space-charge,

rather than to ambipolar effects. Otherwise, such magnetically guided electrons would

not accelerate toward the remote and highly negative substrate, but would instead occupy

a relatively positive vacuum region between target and substrate, diffusing toward

grounded chamber elements until migration out of the magnetic trap was possible.

Ion bombardment at the substrate. (D): In relation to the above gas-phase electron/ion

interactions, the means by which negative ion creation and bombardment of the substrate

is substantially eliminated may be explained in a relatively straightforward manner.

Negative ions in sputtering processes have been observed to form largely at the target

surface in sputtering processes. Hence, if the electronegative oxygen flux can be

essentially eliminated from the target surface – a very "metallic-mode" process – then

negative ion production will cease, and a fundamentally different process will then exist.

In the "oxygen-starved" environment of this UBM reactive sputtering method, the

physical means by which bombarding negative ions may be produced have been

essentially eliminated – the only oxygen available is at the substrate, where the flux of

electrons renders its effective sticking coefficient much closer to unity. With the dynamic

equilibrium achieved through tailored transition gas flow, the substrate remains

insulating, while all other chamber surfaces remain reduced and metallic, as is seen in the

resultant deposition pattern. There is also a tendency for certain sputtered metals to form

negative ions, as has been discussed by Cuomo, *et al.* (Cuomo and al 1978). To the

degree that any negative ions do exist, their bombarding effect at the substrate would also

be negated by the presently hypothesized space-charge field, as is supported in Fig. 5.4.

Primary/secondary electron exchange processes and charge compensation at the

substrate. (B & E): While secondary electron emission ('B' in Figure 5.9) from the

floating substrate may be substantial in normal UBM, due to bombardment by electrons,

neutrals, ions, and vacuum ultraviolet radiation, the effect cannot explain the limiting of

substrate charging in the normal UBM mode. since secondary electron coefficients will be greatly enhanced in the EAD mode. The only possible cause of secondary electrons that is greater in the normal UBM mode is that of ion bombardment. Yet. the secondary electron coefficient for ion bombardment at these energies is relatively quite limited relative to that from electron bombardment (Cobine 1958).

In referring back to the secondary electron characteristic of Figure 5.8. one may note that. at primary electron energies lying between E_I and E_{II}. the secondary electron coefficient. δ. is greater than unity. In this latter condition. electron bombardment of the material surface can actually result in a net *decrease* in electronic surface charge. and a *positive* biasing of the bombarded surface. While this is a very different set of circumstances. partly in that the substrate. in the EAD-UBM mode. is biasing very negatively. it does strongly suggest that the secondary/primary electron exchange ratio at the substrate. especially at the sort of high negative biases witnessed here. may readily reach a state of unity.

The escape of electrons from the substrate fixture via field emission. thermionic emission (less favored). some combination of the two ('E' in figure 5.9). or even emission due to a parasitic discharge. are all also obviously far more enabled in the highly negative substrate potentials observed in the EAD mode. than in the normal UBM mode. Thus. it would be nonsensical to argue that the enhanced electron trapping of the EAD-UBM mode is due to a lower current of electrons escaping from the floating substrate. In fact. in the context of the EAD-UBM mode. the processes discussed here suggest strongly that the electron exchange mechanisms of 'B' and 'E' provide the

primary means. rather than positive ions. by which charge compensation is maintained at the floating substrate surface.

Electron conduction/surface migration at the substrate. (C): Another characteristic that appears to be necessary for establishing this EAD process is the interaction of the "Type II" UBM's magnetic field with a non-metallic terminating surface. i.e.. the depositing oxide film. In providing an insulating oxide surface as the termination of the UBM's magnetic field lines. it follows that the surface migration/bulk conduction of electronic charge ('C' in figure 5.9) at the substrate. in Figure 5.6. will be greatly reduced. Hence. the processes that allow absorption of electrons from the gas phase. and re-emission of electrons into different Larmor potentials of the UBM's magnetic trap. thus enabling escape from the magnetic trap. will also be greatly reduced. The prior art in "type II" UBM sputtering of oxides is actually quite limited. and offers little insight into this issue. In terms of fundamental principles. the complexity of UBM reactive sputtering has resulted in an even more limited understanding than in the case of balanced magnetron reactive sputtering. Probably the best review of the mechanics of magnetron sputtering to date. including UBM's. is offered by Penfold (Penfold 1995). Penfold notes that there are three possible variations encountered in the electron trapping regions of a magnetron sputtering environment:

(i)   The confinement region may be completely isolated from material surfaces. in which case the electron is completely trapped:

(ii)   The confinement region may be intersected at one or more places by material

surfaces capable of absorbing the electron. However. if the surface of intersection

is small enough. or located in a portion of the trap that is unlikely to be occupied.

then the electron will be "effectively" trapped:

(iii)   The confinement region may be intersected by a material surface of appreciable

area. which is readily accessible. In this case the electron is effectively

"channelled" toward this material surface where it will be absorbed.

To these three possibilities. in light of the above discussion of mechanisms 'B'. 'E'. and

'C'. it is suggested here that a fourth possibility be added. namely:

(iv)   The confinement region may be intersected by a material surface of appreciable

area. which is readily accessible. However. the material surface properties do not

readily allow absorption. so that re-emission of the electron. or a secondary

electron. back into the confinement region is probable. In this case the electron is

also "effectively" trapped.

As with any. essentially. cylindrical magnetic trap. the trap in the EAD environment must

be effectively closed at either end if electrons are to be efficiently contained. The fourth

possibility. above. is. therefore. also of fundamental importance in establishing the

efficient magnetic trapping of electrons that the EAD-UBM operational mode clearly

provides.

5.3.2 Gas-phase Diffusion And Mobility In The EAD Mode

We previously discussed interactions between the source and substrate fixture that allow the establishment of a closed magnetic trap in the EAD mode. We will presently discuss the changes that must take place in the gas (or plasma) phase for the EAD mode's electron trap and deposition environment to be provided. In discussing the trapping efficiency of the EAD mode due to electron loss mechanisms that do not concern the floating substrate assembly. we are solely concerned with the gas-phase migration of charge across the magnetic field lines. to ground. As such. we are primarily concerned with means by which the guiding center of electron gyration may be displaced. These mechanisms can be divided between collisional and noncollisional effects.

Because the environment in the previous studies of UBM sputtering. which involved the normal UBM mode. is shown to provide conditions consistent with normal plasma behavior. and because of the complexity of the environment. there was little motivation. in the previous work by other researchers. for attempting to differentiate diffusion mechanisms within the extended trap region of a UBM source. However. with the realization of the EAD mode. there arises both a motivation and something more of a means. The various mechanisms are consequently discussed by which plasma-generated species find grounded surfaces through transport across the magnetic field lines. which exist in the volume between the magnetron source and the substrate fixture. As discussed in Chapter 2. for the magnetron sputtering environments used here. diffusion of electrons

across magnetic field lines is of central importance in the effective magnetic trapping for either ambipolar plasma or an electron gas.

A primary question is whether or not diffusion. in the context of the EAD mode. may be characterized as ambipolar. However. having established the essentially "closed" nature of the trap in the EAD mode. we are allowed to simplify the situation with the same assumptions that were applied. in Chapter 2. to the diffusion of plasma from the closed magnetron field in the conventional magnetron trap region: namely. that only cross field diffusion is allowed. In this case. diffusion is again determined primarily by the perpendicular electron diffusion coefficient:

$$D_{\perp a} \cong D_{\perp e} (1 + T_i/T_e) \cong D_{\perp e}.$$

This result only suggests what we already know experimentally: that the diffusion coefficient of electrons across the field lines in the '$\underline{B}$' region of Figure 5.6 is quite low. and dominated by the limited mobility of the electrons.

However. we have used the growth behavior of SBT to determine the environment at the growth front of the film. and have determined that it is not plasma-like. This conclusion was supported by both the lack of positive ion bombardment of the growing film. as well as by the inability of the electrons to dissipate energy through gas phase collisions. As a result of these observations. we may justifiably conclude that the cross-field electron diffusion coefficient is not an ambipolar diffusion coefficient. but that of electron diffusion alone.

Positive ion currents and behavior in the EAD environment: With the absence of a

plasma region near the substrate, there is no basis by which to expect the field to become

increasingly negative toward the substrate. as it would now result only from the space-

charge of the expanding electron gas. Such a scenario underlines the earlier assertion that

the cathode region of the EAD-UBM source. during operation. should be viewed as the

combination of two functionally separate regions. A first region. `$\underline{A}$` in Figure 5.6.

comprises the normal magnetron trap region and its contained negative glow/sheath.

which provides the sputtered vapor and probably most of the secondary electrons. The

second region. `$\underline{B}$` in Figure 5.6. comprises the EAD magnetic trap region. which.

through the magnetic cusp regions. is not shielded from the cathode by the far more

positive potential of the negative glow. Electrons in the EAD trap. `$\underline{B}$`. may then be

accelerated directly from the cathode. quite independently of the field in the negative

glow. This independence from the negative glow is further insured by the very high flux

of electrons provided by the high-γ_{se} emission characteristics of the cathode. so that the

"congruence assumption" of equal electron and ion fluxes is no longer valid. and $n_e \neq n_i$.

In other words. the `$\underline{B}$` region of the EAD-UBM source performs more along the lines of

a magnetized electron diode. rather than as a discharge column. Positive ions can then be

expected to be accelerated in the opposite direction. toward the cusp regions. though not

as effectively guided by the EAD trap.

In observing that the environment at the substrate. in the EAD mode. lacks the

primary interactions of a plasma-like environment. and is instead performing as an

electron gas. we are able to account for the new behavior of the positive ions. Positive

ions are obviously still being produced in the negative glow region. It would also be

difficult to explain how the production of positive ion/electron pairs near the substrate

would not. if anything. be increased in the higher secondary electron flux of the EAD

mode. To be consistent with both these observations and the experimental results. it

would appear necessary that the space-charge of the EAD environment is no longer

providing any substantial acceleration potential at. or near. the substrate. This is

consistent with the observation that a plasma is no longer evident. $n_e >> n_i$. and the

environment is dominated by electron space-charge. similar to a vacuum diode.

This diode analogy does not. however. imply the normal validity of the previously

discussed Child's law. as in conventional vacuum diodes. The analogy with a normal

electron diode is actually very limited. since the electrons are essentially caught in a

magnetic trap. with the anode located outside of this trap. Additionally. emission of

electrons from the cathode is not determined primarily by electronic space-charge in the

aforementioned '$\underline{B}$' region. but rather by that in the cathode sheath in region '$\underline{A}$'. in

Figure 5.6. which further suggests our approach of treating this environment in terms of

two separate spatial regions. The primacy of the chemical state at the cathode surface. as

opposed to local space-charge. in determining both electron emission and global

operation of these magnetron sources also underlines the futility in applying Child's

sheath law in reactive plasma sputtering processes. in general.

Collisional ion/electron & nuetral/electron interactions: As a combination of stochastic

processes. magnetron sputtering may be viewed from the perspective of various sampling

rates in a random walk. The ability of this metallic-mode. reactive magnetron deposition system to remain highly non-equilibrium may be viewed. in a way that's useful. from the perspective that certain sampling rates are highly limited. The ability for an electron to "jump" magnetic field lines in a magnetron sputter source. and thus find a lower potential. has been attributed largely to collisions with atomic species (Penfold 1995). While these atomic species will consist primarily of neutrals at the higher pressures encountered in many plasma studies (>10mtorr). the same cannot be said of the nearly noncollisional environment in normal operating conditions of a UBM. If we eliminate most of the positive and negative ions from the volume that resides between the sputtering plasma and the substrate. as it appears we have in the EAD-UBM mode. then we may expect this effective sampling rate to be substantially lowered. and the electron population will be accordingly restricted from exiting the magnetic field. Thus. an absence of the gas-phase. ion-electron collisions. 'A' in Figure 5.9. in the EAD-UBM mode may contribute substantially to the increased electron confinement.

Collisionless mechanisms of electron diffusion: The lack of collisions to dissipate the average electron energy suggests that noncollisional processes are now the dominant diffusional mechanisms at work. While it is clear that the environment of the EAD mode is different from the magnetically trapped. weakly ionized plasma environment in the cathode trap. region 'A' in Figure 5.6 . of a conventional magnetron source. the dominance of electron diffusion. in either scenario. indicates that the same collisionless diffusion mechanisms should be relevant. though quite different in their importance.

Rossnagel has maintained in various publications that the near-collisionless nature

of electron diffusion in low-pressure magnetrons suggests that electron diffusion out of

the magnetron trap is dominated by Bohm diffusion (Rossnagel. 1987):

$$D_B = \frac{1}{16} \frac{T_e}{B}$$

The value of appealing to Bohm diffusion is limited. since it is not a first-principles

result. but is rather an empirically derived – under much different conditions – scaling

law for predicting collisionless diffusion effects of plasma turbulence in the electrical

field. Such turbulence would be brought on by large-scale disturbances. such as the

acoustic-scale ion plasma frequency and various plasma instabilities.

Sheridan performed studies in the negative glow region of magnetron plasma to

determine residence times of electrons in the trap region. which were correlated to an

argument that no evidence of Bohm diffusion existed (Sheridan. 1989)(Sheridan.

1990)(Sheridan. 1991). It should also be noted that Bohm diffusion was originally

modeled on the results of arc discharges in strong magnetic fields. which is a study of

"hot" (in thermal equilibrium) . collisional plasma. as opposed to the fundamentally

different "cold" (no local thermal equilibrium). nearly noncollisional. quasi-plasma

environment studied here. It is also relevant to note that confinement achieved by

tokamaks has been found to greatly exceed that allowed by Bohm diffusion. which

further underlines the empirical. rather than fundamental. basis for such diffusion.

It is clear, though, that the introduced EAD mode might provide for domination of such collisionless diffusion mechanisms in the absence of the normally dominant ambipolar effects in the normal UBM environment. and so Bohm diffusion would be more likely, in the context of the present EAD mode. However, while it seems clear that the electron-dominated space-charge in the EAD-UBM magnetic trap must mark a transition to a different set of dominant diffusion mechanisms that reflects a more collisionless scenario, it is thought here that Bohm diffusion is still an unlikely explanation, given the necessarily inhomogeneous electric and magnetic fields involved. In these conditions of steep field gradients and curvatures, diffusion would be expected to be dominated by the various drift currents, discussed in Table 2.1, themselves, as opposed to the secondary Bohm diffusion – also called anomalous transport – processes that might result from turbulence provided by instabilities in such drift currents. Many of these variously oriented drift currents will possess net velocity components toward a grounded surface. As such, the drift of guiding centers of electron motion, as discussed in Chapter 2, is suggested here to be the dominant limitation to trapping efficiency in the magnetically trapped EAD mode.

5.4 Conclusions for EAD Process

The transition of the normal UBM operating mode to that of the EAD mode is proposed to take place due to the complex relationships between several, inter-dependent mechanisms. Though seemingly conjectural, this synergistic quality is a common theme

for all glow discharges, where complete analytical descriptions are absent for even relatively simple systems.

The physics of gaseous conductors is very relevant here. It is possible that what plasma-like entity is found in the developed process could be more accurately viewed as a means for producing electrons and a metal vapor. rather than being viewed as the defining paradigm for describing charged-particle interactions at the film growth front. While the high magnitude of the self-bias voltages may appear inappropriate for many applications. it should be noted that the entire substrate is essentially at an isopotential.

In terms of thin film growth, the domination of surface chemistry in determining the growth mode in this EAD process further blurs any fundamental delineation between metallic-mode reactive sputtering processes and plasma-enhanced. low-pressure CVD. At the point that complexed precursor gases are used in such an EAD process. such delineation will be even less distinct. From a CVD point-of-view. the EAD process disclosed cannot be viewed in the traditional sense of either an "adsorption-limited" or a "diffusion-limited" process. as the limiting mechanism for film growth is actually the absence of electron bombardment. Therefore we have found. for the first time. the positive identification of an electron-assisted deposition process. That positive identification is found in the observation of an *activation-limited* growth mode. Bismuth and oxygen remain on the substrate only when activated by electron collisions (forming ions and radicals). so that the probability of forming the more stable bismuth-oxygen bonds of the desired compound is significantly increased.

6. CONCLUSION

While this dissertation work began as a study of RF sputtered SBT ferroelectrics from oxide targets. it eventually evolved to a successful means of implementing metallic mode reactive sputtering for such perovskite ferroelectrics. and. ultimately. to the development and study of a new mode of "Type II" UBM sputter deposition. Several general conclusions have developed out of this combination of approaches.

6.1 New Insights into Phase Formation in SBT Thin Film Deposition:

In terms of the specific ferroelectric material. SBT. treated in this work. the phase development exposed here is significant. While it is not yet incontrovertible. there is fairly conclusive evidence in this work to support the view that the frequently observed defective fluorite phase. rather than being a low-temperature intermediate phase. results from the initial competition between the high-temperature ferroelectric SBT phase and a high-temperature metastable fluorite (MF) phase. That development of the SBT super-lattice structure is favored in equilibrium growth. whereas the much smaller unit cell of the cubic MF phase is favored in highly non-equilibrium growth. indicates that the MF phase development might be due to the lower adatom mobility. or greater quenching. that can be expected with the combination of a lower-temperature substrate and a higher-energy vapor phase.

Given the reasoning above. a reasonable future course of action in SBT research would not be to implement yet higher effective temperatures – or. alternatively. more energetic environments – at the growth interface of the thin film. but to implement means for somehow suppressing nucleation of the fluorite phase. The more obvious route for accomplishing this would be to provide an appropriate seed layer. though it is not at all obvious which seed layer might work. Another option would be to introduce the long-term ordering of the SBT layered-perovskite through laminate growth of alternating Bi_2O_3 layers and SrO/Ta_2O_5 layers. though the resultant structure would correspond to the c-axis orientation. with its low P_r. and might be prohibitively complex in a production sputtering environment. A third option would be to find a means of converting the MF phase to the ferroelectric SBT phase in a low temperature environment. Such an approach might involve well-known methods. such as rapid thermal processing (RTP). or less explored options. such as the combination of ultraviolet irradiation with low temperature annealing.

That the fully crystallized metastable fluorite (MF) phase observed in this work has not been previously recognized as such is an indication that the MF phase development has not previously been observed in a vapor deposition process that provides the reproducibility of EAD. With respect to the limited published research which misidentifies the MF phase as that of the ferroelectric SBT phase. the present work also presents the lowest substrate temperatures at which the MF phase has been developed. This is not surprising. given the highly energetic process environment in the presently developed EAD process. It is surprising. though. that such an extremely non-

equilibrium method would seem to also provide high reproducibility relative to other non-equilibrium methods.

As has been found in the present work, the more energetic vapor deposition processes are capable of producing a wide variety of metastable phases. The complex phase development processes explored in the previous chapters indicates that many researchers who conduct energetic deposition processes in complex oxide systems should practice more caution when identifying x-ray diffraction peaks. For example, the small differences in peak positions found between ferroelectric SBT, the fully developed MF phase, and the various bismuth tantalate phases explored by Zhou would underline that little credence should be given to reported SBT phase development based solely on XRD data presented in a reduced format with no precise peak positions. It also indicates that the reader should be very skeptical when such x-ray or electron diffraction data provide the only means for establishing the existence of the phase of such complex materials.

6.2 First Development Of A Metallic Mode Reactive Deposition Process For Ferroelectrics, Or, Infact, Any Of The Perovskite Oxides:

DC sputtering of poisoned metal targets in deposition of perovskites, or indeed, any multicomponent oxide, is a limited and unstable process. The supposition, in past reports of d.c. sputtering of other perovskites, that d.c sputtering offers a high degree of process control because deposition rates can be changed independently, is untenable given the sputtering processes described in such studies; oxygen poisoning of the target causes instability in the deposition rate and makes run-to-run reproducibility impossible

to achieve. RF sputtering of the same poisoned metal targets may prevent arcing. and sputter oxidized portions of the metal target more efficiently. but the essential instability in sputtering conditions and yield remains the same.

The development. in this work. of the EAD process has enabled. for the first time. metallic mode sputtering of the important Bi- or Pb-containing perovskites. The establishment of a metallic mode sputtering process for perovskite compounds allows for true "dynamic equilibrium" to be established in the processing chamber. as metallic surfaces remain metallic. and insulating surfaces may remain a stoichiometric insulating oxide. Such equilibrium is viewed here as the first necessary step towards a reproducible sputtering process for these compounds.

This research also presents the first case in which the SBT ferroelectric has been deposited from an all-metal target configuration. which is understandable given the inherent difficulties that arose in earlier sputtering of such perovskites as PZT.

6.3 Unanticipated Reversal Of Established "Type II" UBM Behavior:

In the field of sputtering as a whole. more advanced thin film applications. which must take into account the magnetron design. have operated within the principle that the guiding surfaces of the magnetron's magnetic field serve to either promote or prevent plasma bombardment. Up until the present work. "Type II" UBM sputtering has been synonymous with highly energetic ion bombardment of the growing film. which incurs heavy resputtering of adatoms with lower bonding energy. As such. this method has not been utilized where volatile metals are a component of the deposited film.

In contrast. the UBM-EAD process developed here is ideally suited to the deposition of compounds that contain a highly volatile species. Rather than increase desorption of the volatile species. electron bombardment. as implemented in this UBM process. instead. *increases* adsorption of the volatile species through chemical activation. This development effectively reverses the established behavior of "Type II" unbalanced magnetrons in reactive environments. The process is enabled through high electron injection. and the implementation of highly non-equilibrium gas flows in the bottom-end of the transition flow region. such that negative ion generation at the cathode surface is substantially avoided. As a result of this process. the self-bias potentials recorded in the present are almost an order of magnitude higher than those previously associated with these sputtering sources. Also of fundamental importance to the field of oxide sputtering. the present work establishes that energetic negative ion bombardment can be eliminated in reactive sputtering processes by substantially eliminating the electronegative gas from the vicinity of the sputtering target surface.

6.4   Introduction of Electron-Assisted Deposition (EAD):

Accordingly. a new method of reactive sputtering has been developed. which warrants the new terminology. Electron Assisted Deposition (EAD). The term "electron assisted" is devised in direct counter-distinction to "ion-assisted" deposition techniques. The justification of this term. and the distinction. is based solidly on the novel and positive outcome of an electron-dominated – as opposed to ion-dominated – modification of the film growth process. The effects of electron bombardment are differentiated from

ion bombardment in the observation of an *activation-limited* growth process, analogous to that observed in ultraviolet-assisted CVD research.   As might be expected, the basic novelty of the EAD process developed has manifested in some other novel outcomes, as already discussed.

Such a basic-sounding process as "electron-assisted deposition" has not previously come into existence, for the reason that there are very limited means by which a growing non-conducting film can be irradiated with an abundance of low-to-medium energy electrons, such that the latter, and not ions, dominate the growth process. To do so without an equal number of positive ions, to maintain beam neutrality, would be difficult without the sort of magnetic trap provided in the present work, used in conjunction with a means of introducing an unusually large flux of electrons into the trap.

Future work: Future work might involve the implementation of a separate electron injection sources to accomplish the EAD mode of operation. While the latter implementation would be an unnecessary complication in many circumstances, the operation of such external electron sources would benefit from the absence of stray oxygen in the oxide growth processes developed herein.

REFERENCES

Adachi. H. (1990). "Basic thin film process for perovskite ferroelectric materials." Mat. Res. Soc. Symp. Proc. 200: 103-114.

Adachi. H.. et al (1985). Preparation and properties of (Pb,La)TiO$_3$ epitaxial thin films by multi-target sputtering. 5th Meeting on Ferroelectric materials and Their Applications. Kyoto. Jpn. J. Appl. Phys.

Aita. C. R. (1994). "Modelling the growth kinetics of sputter-deposited nanocrystalline zirconia films." Nanostructured Materials 4(3): 257-263.

Akinaga. M.. et al (1991). Fabrication of c-axis oriented PbTiO$_3$ transducer films for SAW in high-Tc superconducting films. 3rd international conference on properties and applications of dielectric materials. Tokyo. Japan.

Akjoscher (1983). Dielectric Relaxation in Solids. Chelsea Dielectrics Press.

Amanuma. K. and T. Kunio (1996). "Low-voltage switching characteristics of SrBi$_2$Ta$_2$O$_9$ capacitors." Jpn. J. Appl. Phys. 35: 5229-5231.

Amor. S. B. (1998). "Characterization of zirconia films deposited by r.f. magnetron sputtering." Mater. Sci. and Eng. B B57: 28-39.

Ayguavives. F. et al (1998). "Correlation between in situ optical emission spectroscopy in a reactive O$_2$/Ar r.f. magnetron sputtering discharge and PZT thin film composition." Mat. Res. Soc. Symp. Proc. 493: 333-338.

Banhart. F. (1997). "The transformation of graphite onions to diamond under electron radiation." J. Appl. Phys. 81(8): 3440-3445.

Bruchhaus. R. et al (1992). "Deposition of ferroelectric PZT thin films by planar multi-target sputtering." Ferroelectrics 127: 137-142.

Chapman. B. (1980). Glow Discharge Processes. New York. Wiley.

Chen. I.-S. S. and J. F. Roeder (1999). "Low temperature MOCVD of thin film PZT." Mat. Res. soc. Symp. Proc. 541: 375-380.

Cho. J. H.. S. H. Bang. et al. (1998). "Control of epitaxial growth for SrBi2Ta2O9 thin films." Applied Physics Letters 72(6): 665-667.

Cho. K.-J. et al (1998). "Microstructure-dependent ferroelectric properties of SrBiTaO thin films fabricated by radio frequency magnetron sputtering." J. Vac. Sci. Technol. A 16(3): 12581261.

Cobine. J. D. (1958). Gaseous Conductors. New York. Dover Publications.

Croteau. A. et al (1987). "Ferroelectric Pb(Zr.Ti)O$_3$ thin films prepared by metal target sputtering." Proceedings of the 6th Meeting on Ferroelectric Materials and Their Applications 26, suppl. 26-2: 18-21.

Croteau. A. and M. Sayer (1986). "Growth and characterization of PZT films deposited by reactive sputtering of metallic targets." IEEE: 606-609.

Cui. J. and R. Fang (1997). "Characterization of the diamond growth process using optical emission spectroscopy." J. Appl. Phys. 81(6): 2856-2861.

Cuomo. J. J. et al (1978). "Significance of negative ion formation in sputtering and SIMS analysis." J. Vac. Sci. Technol. 15(2): 281-287.

Dawley. J. T. (1999). Phase development. microstructure. and ferroelectric properties of sol-gel derived strontium bismuth tantalate thin films. Mater. Sci. & Eng. Tucson. U of A: 274.

Dhote. A. M. et al (1999). "Studies of metallic species incorporation during growth of SrBi$_2$Ta$_2$O$_9$ films on YBa$_2$Cu$_3$O$_{7-x}$ substrates using mass spectroscopy of recoiled atoms." Mat. Res. Soc. Symp. Proc. 541: 281-286.

Diaz. F. A. and L. E. Cross (1977). "Temperature dependence of second harmonic generation signal in SrBi$_2$Ta$_2$O$_9$ and BaBi$_4$Ti$_4$O$_{15}$." Ferroelectrics 17: 405-407.

Ding. Y. et al (2000). "Transmission electron microscopy study on ferroelectric domain structure in SrBi$_2$Ta$_2$O$_9$ ceramics." Applied Physics Letters 76(1): 103-105.

Dudney .

Fujisawa. A. et al (1993). "Effect of Zr/Ti ratio on crystal structure of thin lead zirconate-titanate films prepared by reactive sputtering." Jpn. J. Appl. Phys.: Part 1 32(9B): 4048-4051.

Fujisawa, A. et al (1994). "Ion-assisted deposition of lead titanate thin films by controlled-magnetic field sputtering." Jpn. J. Appl. Phys., p. 1 33(8): 4737-4741.

Fukami, T. (1983). "PZT films prepared by reactive sputtering." Elect. Eng. in Japan 103(3): 15-21.

Fukami, T. et al (1981). "Composition of reactively sputtered PLZT films." Jpn. J. Appl. Phys. 20(8): 1599-1600.

Fukami, T. et al (1983). Ferroelectric films deposited by reactive sputtering and their properties. 4th Meeting on Ferroelectric Materials and their Applications. Kyoto, Jpn. J. Appl. Phys.

Fukami, T. et al (1991). "Highly c-axis-oriented Pb(Zr, Ti)O_3 films prepared by sputtering." Jpn. J. Appl. Phys. 30(9B): 2155-2158.

Ganpule, C. S. et al (1999). "Scaling of ferroelectric and piezoelectric properties in Pt/SrBi$_2$Ta$_2$O$_9$/Pt thin films." Applied Physics Letters 75(24): 3874-3876.

Gopalakrishnan, J. et al (1984). "A homologous series of recurrent intergowth structures of the type Bi$_4$A$_{m+n-2}$B$_{m+n}$O$_{3m+3n+6}$ formed by oxides of the Aurivillius family." J. Solid State Chem. 55: 101-105.

Griswold, E. M. et al (1991). "The influence of niobium-doping on lead zirconate titanate ferroelectric thin films." Can. J. Phys. 69: 260-264.

Gutleben, C. D. (1996). "The evaluation of SrBi$_2$Ta$_2$O$_9$ for ferroelectric memories." Mat. Res. Soc. Symp. Proc. 433: 109-119.

Gutleben, C. D. et al (1995). . Metal-Organic Chemical Vapor Deposition of Electronic Ceramics II. S. B. Desu. Pittsburgh, PA.

Hartmann, A. J. et al (1998). "Electronic and microstructure characterization of strontium-bismuth tantalate (SBT) thin films." J. Korean Physical Soc. 32: S1329-S1331.

Hase, T. et al (1991). "Preparation and switching kinetics of Pb(Zr.Ti)O_3 thin films deposited by reactive sputtering." Jpn. J. Appl. Phys. 30: 2159-2162.

Hase, T. et al (1993). "Preparation of Pb(Zr, Ti)O_3 thin films by multi-target sputtering." Jpn. J. Appl. Phys.p. 1 32(9B): 4061-4064.

Hase. T. *et al* (1994). "Preparation of Pb(Zr. Ti)O$_3$ thin films by multitarget sputtering." Jpn. J. Appl. Phys., p. 1 33(9B): 5244-5248.

Hase. T. and T. Shiosaki (1991). "Preparation and switching kinetics of Pb(Zr. Ti)O$_3$ thin films deposited by reactive sputtering." Jpn. J. Appl. Phys. p. 1 30(9B): 2159-2162.

Hayashi. K. *et al* (1993). "Preparation and characterization of Pb(Zr$_x$i$_{1-x}$)O$_3$ thin films by reactive sputtering using an alloy target." Jpn. J. Appl. Phys. p. 1 32(9B): 4122-4125.

Hayashi. S. *et al* (1992). "Preparation of Pb-based ferroelectric thin films by ion- and photo-assisted deposition." Mat. Res. Soc. Symp. Proc. 243: 157-165.

Hendrix. B. C. *et al* (1999). "Correlations between composition. texture. and polarization in Sr$_x$Bi$_y$Ta$_2$O$_{5+x+3y/2}$ thin films deposited by MOCVD." Mat. Res. Soc. Symp. Proc. 541: 275-281.

Hoffman. D. W. (1994). "Perspective on stress in magnetron-sputtered thin films." J. Vac. Sci. Technol. A12(4): 953-961.

Howson. R. P. (1997). "Synthesis of sputtered thin films in low energy ion beams." Nucl. Instr. and Methods in Phys. Res. B 121: 65-72.

Howson. R. P. and H. A. J'Afer (1990). Substrate effects from an unbalanced magnetron. Thin Solid Films 17th International Conference on Metalurgical Coatings and 8th International Conference on Thin Solid Films. San Diego. CA. USA. AVS.

Hu. G. D. *et al* (1999). "Domain imaging and local piezoelectric properties of the (200)-predominant SrBi$_2$Ta$_2$O$_9$ thin films." Applied Physics Letters 75(11): 1610-1612.

Hu. G. D. *et al* (1999). "Effects of a Bi$_4$Ti$_3$O$_{12}$ buffer layer on SrBi$_2$Ta$_2$O$_9$ thin films prepared by the metalorganic decomposition." Applied Physics Letters 74(24): 3711-3713.

Hu. G. D. *et al* (1999). "Structure control and characterization of SBT thin films by a modified annealing method." Applied Physics Letters 74(9): 1221-1223.

Hubler. G. K. and J. A. Sprague (1995). Energetic particles in PVD technology: particle-surface interaction processes and energy-particle relationships in thin film deposition. 1st Australia-USA Workshop on Critical Issues in High Performance Wear Resistant films. Wollongong. Australia. Elsevier Science.

Ichinose. N. *et al* (1997). "Fatigue characteristics of $SrBi_2Ta_2O_9$ thin films by r.f. magnetron sputtering method." Jpn. J. Appl. Phys. **36**: 5893-5895.

Iijima. K. *et al* (1986). "Preparation of c-axis oriented $PbTiO_3$ thin films and their crystallographic. dielectric. and pyroelectric properties." J. Appl. Phys. **60**(1): 361-367.

Im. J. *et al* (1998). "Studies of metallic species and oxygen incorporation during sputter-deposition of SrBi2Ta2O9 films. using mass spectroscopy of recoiled ions." Applied Physics Letters **72**(20): 2529-2531.

Inoue. T. *et al* (1997). Mater. Res. Soc. Symp. Proc. **474**: 321.

Inoue. T. *et al* (1999). Thin Solid Films **343-344**: 594.

Inoue. T. *et al* (2000). "Surface morphology analysis in correlation with crystallinity of CeO_2(110) layers on Si(100) substrates." J. Vac. Sci. Technol. **18**(4): 1613-1618.

Inoue. T. *et al* (2001). "Electron-beam-assisted evaporation of epitaxial CeO2 thin films on Si substrates." J. Vac. Sci. Technol. A **19**(1): 275-279.

Isuji. H. *et al* (1996). "Negative-ion extraction of gaseous materials from a radio frequency plasma-sputter-type heavy negative-ion source." Review of Scientific Instruments **67**(3): 1012-14.

Isuji. H. *et al* (1997). Negative-ion production of reactive element from compound gases in the r.f. plasma-sputter-type heavy negative-ion source. Eleventh International Conference on Ion Implantation Technology. New York. N.Y... IEEE.

Ito. Y. *et al* (1997). "New low temperature processing of sol-gel $SrBi_2Ta_2O_9$ thin films." Integrated Ferroelectrics **14**: 123-131.

Ivanov. L. I. *et al* (1992). "Materials surface modification by reactive gas-ion bombardment: low-energy radiation." Vacuum **43**(10): 955-959.

Izumi. H. *et al* (1990). "Superconductivity and crystallinity of $Ba_2YCu_3O_{7-x}$ thin films prepared by pulsed laser deposition with substrate bias voltage." J. Appl. Phys. **68**(12): 6331-6335.

Ja'fer. H. A. and R. P. Howson (1992). Low-voltage, high-current, ion-bombardment source using magnetron principles. Conference of The Atomic collisions in Solids Group of the Institute of Physics.

Jiang. Q. D. *et al* (1998). "Nucleation and surface morphology evolution of ferroelectric $SrBi_2Ta_2O_9$ films studied by atomic force microscopy." Surface Science **405**: L554-L560.

Jiang. Q. D. *et al* (1998). "Surface microstucture of ferroelectric $SrBi_2Ta_2O_9$. $BaTiO_3$ and metallic $SrRuO_3$ epitaxial thin films." Mat. Res. Symp. Proc. **493**: 243-248.

Jones. F. (1988). "High-rate reactive sputter deposition of zirconium dioxide." J. Vac. Sci. Technol. A **6**(6): 3088-3097.

Kadlec. s. *et al* (1997). "Energy distribution of ions in an unbalanced magnetron plasma measured with energy-resolved mass spectroscopy." Surface & Coatings Technology **89**(1-2): 177-184.

Kato. K. (1998). "chemical routes for low-temperature processing of layer-structure perovskite thin films." Integrated Ferroelectrics **22**: 13-22.

Kato. K. *et al* (1999). "Low-temperature processing of ferroelectric layer-structured perovskite thin films by using an alkoxide complex." Key Engineering Materials **157-158**: 189-196.

Kim. J.-S. (1999). "The low temperature processing for removal of metallic bismuth in ferroelectric $SrBi_2Ta_2O_9$ thin films." Applied Surface Science **140**: 150-155.

Kim. K. Y. *et al* (1992). "Preparation and microstructural characterization of ferroelectric thin film $PbTiO_3$ on Si. MgO. and sapphire deposited by d.c. reactive multitarget co-sputtering." Mat. Res. Symp. Proc. **243**: 198-202.

Kim. S.-H. *et al* (2000). "Influence of Pt heterostructure bottom electrodes on $SrBi_2Ta_2O_9$ thin film properties." Applied Physics Letters **76**(4): 496-498.

Kim. S.-T. *et al* (1997). "Investigation of Pt/Ti bottom electrodes for Pb(Zr.Ti)O3 films." Jpn. J. Appl. Phys. **36**: 294-300.

Kim. Y. H. *et al* (2001). "Effects of electron-beam irradiation on the properties of CN thin films deposited by direct dual ion beams." JVST A **19**(1): 145-152.

Kingery. B.. and D. R. Uhlmann Introduction to Ceramics.

Kingon. A. (1999). Memories are made of... Nature. **401**: 658-659.

Koller (1965). Ultraviolet Radiation. Wiley & Sons.

Krishnan, A. *et al* (1999). "In-situ TEM study of domain propagation in ferroelectric barium titanate, and its role in fatigue." Mat. Res. Soc. Symp. Proc. **541**: 475480.

Kumar, C. V. R. V. *et al* (1992). "Crystallization of sputtered lead zirconate titanate films by rabid thermal processing." J. Appl. Phys. **71**(2): 864-874.

Kwok, H. S. (1992). "Formation of atomic beams and dynamics of in situ superconducting film growth by pulsed-laser deposition." Thin Solid Films **218**: 277-290.

Lee, J.-K. (1997). "Characteristics of $SrBi_2Ta_2O_9$ thin films fabricated by the r.f magnetron sputtering technique." Integrated Ferroelectrics **15**: 115-125.

Lee, J.-K. *et al* (1997). "Crystal orientation dependence on the ferroelectric properties of $SrBi_2Ta_2O_9$. $CaBi_2Ta_2O_9$ thin films fabricated by the r.f. magnetron sputtering technique." Integrated Ferroelectrics **18**: 369-376.

Lee, J.-K. *et al* (1998). "Ferroelectric characteristics of $SrBi_2Ta_2O_9$ thin films fabricated by the radio frequency magnetron sputtering deposition technique." Surface and Coatings Technology **98**: 908-911.

Lee, Y. S. *et al* (1999). "Structural characterization of the low-temperature phase in Sr-Bi-Ta-O films." Applied Physics Letters **74**(18): 2690-2692.

Lettieri, J. *et al* (1998). "Epitaxial growth of (001)-oriented and (110)-oriented $SrBi_2Ta_2O_9$ thin films." Applied Physics Letters **73**(20): 2923-2925.

Lettieri, J. *et al* (2000). "Optimization of the growth of epitaxial SrBi2Ta2O9 thin films by pulsed laser deposition." Thin Solid Films **379**: 64-71.

Lettieri, J., C. I. Weber. *et al*. (1998). "Comment on "Control of epitaxial growth for SrBi2Ta2O9 thin films"." Applied Physics Letters **73**(14): 2057-2058.

Li, T. *et al* (1996). "Metalorganic chemical vapor deposition of ferroelectric $SrBi_2Ta_2O_9$ thin films." Appl. Phys. Lett. **68**(5): 616-618.

Lieberman and Lichtenberg (1994). Principles of Plasma Discharges and Materials Processing. Wiley Interscience.

Lim, M. and T. S. Kalkur (1997). "Electrical characterizatics of Pt-bismuth strontium tantalate (BST)-p-Si with zirconium oxide buffer layer." Integrated Ferroelectrics **14**: 247-257.

Lim. M.-H. *et al* (1998). "Strontium bismuth tantalate based ferroelectric gate field effect transistor with yttrium oxide as buffer layer." Mat. Res. Soc. Symp. Proc. **493**: 465-470.

Lines. M. E. and A. M. Glass (1977). Principles and Applications of Ferroelectrics. New York. Oxford University Press.

Lowe. C. w. G. (1997). .

Macak. K. *et al* (2000). "Ionized sputter deposition using an extremely high plasma density pulsed magnetron discharge." J. Vac. Sci. Technol. **18A**(4): 1533-1537.

Maiwa. H. *et al* (1992). "Crystalline structure of $PbTiO_3$ thin films by multiple cathode sputtering." Jpn. J. Appl. Phys. **31**, Part 1(9B): 3029-3032.

Mansingh. A. (1990). "Fabrication and applications of piezo- and ferroelectric films." Ferroelectrics **102**: 69-84.

Matsuki. T. Crystalline-buffer-layer-aided (CBL) sputtering technique for mega-bit ferroelectric memory devices with $SrBi_2Ta_2O_9$ capacitors.

Mihara. T. *et al* (1992). "Relationship between crystal structure and chemical composition of $PbTiO_3$ thin films prepared by sputter-assisted plasma CVD." Jpn. J. Appl. Phys. **31**, Part 1(6A): 1872-1873.

Miyazaki. H. *et al* (1999). "Influence of unbalanced magnetron and Penning ionization for RF reactive magnetron sputtering." Jpn. J. Appl. Phys. **38**, Part 1(1A): 186-191.

Moon. S. E. *et al* (1999). "Controlled growth of a-/b- and c-axis oriented epitaxial $SrBi_2Ta_2O_9$ ferroelectric thin films." Applied Physics Letters **75**(18): 2827-2830.

Njoroge. W. *et al* (2000). "Defect formation upon reactive direct-current magnetron sputtering of GeO_2 films." J. Vac. Sci. Technol. A **18**(1): 42-47.

Ohashi. T. *et al* (1997). "Molecular dynamics simulations of low energy atomic collisions between an atom and a substrate: effect of incident angle and energy." Nucl. Instr. and Methods in Phys. Res. B **121**: 40-43.

Okamura. T. *et al* (1991). "Epitaxial growth and electrical properties of ferroelectric $Pb(Zr_{0.9}Ti_{0.1})O_3$ films by reactive sputtering." Jpn. J. Appl. Phys. p. 1 **30**(5): 1034-1037.

Park. S.-S. (1997). "Characterization of ferroelectric $SrBi_2Ta_2O_9$ thin films deposited by a radio frequency magnetron sputtering technique." J. Electrochemic. Soc. 144(8): 2855-2858.

Penfold. A. S. (1995). Glow Discharge Sputtering. Handbook of Thin Film Process Technology. D. A. Glocker. Bristol. Institute of Physics Pub.: A3.1.

Petrov. I. et al (1992). "Use of an externally applied axial magnetic field to control ion/nuetral flux ratios incident at the substrate during magnetron sputter deposition." J. Vac. Sci. Technol. A10(5): 3283-3287.

Rastogi. A. C. et al (1999). "Plasma-assisted pulsed laser deposition of $SrBi_2Ta_2O_9$ thin films of improved ferroelectric and crystalline properties." Applied Physics Letters 74(23): 3492-3495.

Rebholz. c. et al (1997). "Composite DLC-metal/metal-carbide coatings produced by electron enhanced unbalanced magnetron sputtering." Surface Engineering 13(5): 375-383.

Rodriguez. M. A. (1996). "Formation of $SrBi_2Ta_2O_9$: Part II. Evidence of a bismuth-deficient pyrochlore phase." J. Mat. Res. 11(9): 2282-7.

Rossnagel. S. M. (1987). "Charge transport in magnetrons." J. Vac. Sci. Technol. A5(4): 2276-2279.

Roy. R. A. et al (1990). "Lead Zirconate Titanate films produced by "facing targets" RF-sputtering." Mat. Res. Soc. Symp. Proc. 200: 77-82.

Sakamaki. K. et al (1999). "Characteristics of a metal/ferroelectric/insulator/semiconductor structure using an ultrathin nitrided oxide film as the buffer layer." Jpn. J. Appl. Phys. 38(4B): L451-L453.

Savvides. N. and A. Katsaros (1992). In-situ growth of epitaxial $YBa_2Cu_3O_7$ thin films by on-axis unbalanced d.c. magnetron sputtering. 12th International Vacuum Congress. Thin Solid Films.

Savvides. N. and A. Katsaros (1993). "In-situ growth of epitaxial $YBa_2Cu_3O_7$ thin films by on-axis unbalanced direct current magnetron sputtering." Applied Physics Letters 62(5): 528-530.

Savvides, N. and A. Katsaros (1994). "Growth and evolution of microstructure of epitaxial YBa$_2$Cu$_3$O$_{7-x}$ ultrathin and thin films on MgO." Physica C: Superconductivity 226(1-2): 23-26.

Savvides, N. and B. Window (1986). "Unbalanced magnetron ion-assisted deposition and property modification of thin films." J. Vac. Sci. Technol. A 4(3): 504-508.

Sawabe, A. and T. Inuzuka (1986). "Growth of diamond thin films by electron-assisted chemical vapor deposition and their characterization." Thin Solid Films 137: 89-99.

Sayer, M. (1986). "Fabrication and application of multi-component piezoelectric thin films." IEEE: 560-568.

Schofield, M. A. et al (1998). "Transmission electron microscopy of zirconia-alumina nanolaminates grown by reactive sputter deposition. Part I: zirconia nanocrystalline growth morphology." Thin Solid Films 326: 106-116.

Schofield, M. A. et al (1998). "Transmission electron microscopy of zirconia-alumina nanolaminates grown by reactive sputter deposition. Part II: behavior of tetragonal zirconia nanocrystallites." Thin Solid Films 326: 117-125.

Schrieter, M. et al (1998). "Sputtering of self-polarized PZT films for IR-detector arrays." IEEE: 181-185.

Scott, J. F. (1998). "The Physics of Ferroelectric Ceramic Thin Films for Memory Applications." Ferroelectrics Review 1(1).

Scott, J. F. et al (1996). "Some new results on strontium bismuth tantalate thin-film ferroelectric memory materials." Mat. Res. Soc. Symp. Proc. 433: 77-87.

Scott, J. F. and B. Pouligny (1988). J. Appl. Phys. 64: 1547.

Seong, N.-J. et al (1998). "Oxide interfacial phases and the electrical properties of SBT thin films prepared by plasma-enhanced metalorganic vapor deposition." Applied Physics Letters 72(11): 1374-1378.

Sheridan, T. E. et al (1990). "Electron and ion transport in magnetron plasmas." J. Vac. Sci. Technol. A8(3): 1623-1626.

Sheridan, T. E. et al (1990). "Model of electron transport in magnetron discharges." J. Vac. Sci. Technol. A8(1): 30-37.

Sheridan. T. E. *et al* (1991). "Observation of two-temperature electrons in a sputtering magnetron plasma." J. Vac. Sci. Technol. **A9**(3): 688-690.

Sheridan. T. E. and J. Goree (1989). "Low-frequency turbulent transport in magnetron plasmas." J. Vac. Sci. Technol. **A7**(3): 1014-1018.

Shimakawa. Y. *et al* (1999). "Crystal structures and ferroelectric properties of $SrBi_2Ta_2O_9$ and $Sr_{0.8}Bi_{2.2}Ta_2O_9$." Applied Physics Letters **74**(13): 1904-1906.

Shimakawa. Y. *et al* (1999). "Crystal structures of $SrBi_2Ta_2O_9$ and $SrBi_{0.8}Ta_{2.2}O_9$ ferroelectric materials." Mat. Res. Soc. Symp. Proc. **541**: 523-528.

Shiosaki. T. (1998). "Pb-based and Bi-based Ferroelectric Thin Films." J. Korean Physical Soc. **32**: S1316-S1320.

Song. T. K. (1996). "Structural and ferroelectric properties of the c-axis oriented $SrBi_2Ta_2O_9$ thin films deposited by the radio-frequency magnetron sputtering." Appl. Phys. Lett. **69**(25): 3839-3841.

Spatenka. P. *et al* (1997). "A comparison of internal plasma parameters in a conventional planar magnetron and a magnetron with additional plasma confinement." Plasma Sources Sci. Technol. **6**: 46-52.

Spatenka. P. *et al* (1999). "Langmuir probe measurements of plasma parameters in a planar magnetron with additional plasma confinement." Vacuum **55**: 165-170.

Sproul. W. D. (1993). "Ion-assisted deposition in unbalanced-magnetron sputtering systems." Materials Sci. and Eng. **A163**: 187-192.

Sreenivas. K. and M. Sayer (1988). "Characterization of $Pb(Zr.Ti)O_3$ thin films deposited from multi-element metal targets." J. Appl. Phys. **64**(3): 1484-1493.

Subbarao. E. C. (1962). "Crystal chemistry of mixed bismuth pxides with layer-type structure." J. Amer. Ceramic Soc. **45**(4): 166-169.

Suhail. M. H. *et al* (1991). "Studies on the properties of zirconia films prepared by direct current reactive magnetron sputtering." J. Vac. Sci. Technol. A **9**(5): 2675-2677.

Suhail. M. H. *et al* (1992). "Effect of substrate temperature on the properties of ZrO_2 films prepared by d.c. reactive magnetron sputtering." Mat. Sci. and Eng. B **B12**: 247-252.

Suhail, M. H. *et al* (1994). "Synthesis and properties of zirconia thin films." Bull. Mater. Sci. 17(6): 855-862.

Taylor, D. J. *et al* (1996). "Integration aspects and electrical properties of $SrBi_2Ta_2O_9$ for non-volatile memory applications." Mat. Res. Soc. Symp. Proc. 433: 97-107.

Telling, N. D. *et al* (1998). "Simple method for the control of substrate ion fluxes using an unbalanced magnetron." J. Vac. Sci Technol. A 16(1): 145-147.

Tsai, H.-M. *et al* (1998). "$Sr_{0.8}Bi_{2.5}Ta_{1.2}Nb_{0.9}O_{9+x}$ ferroelectric thin films prepared by two-target off-axis radio frequency magnetron sputtering." Appl. Phys. Lett. 72(14): 1787-1789.

Tsai, W.-C. *et al* (1997). "Off-axis unbalanced magnetron sputtering of $YBa_2Cu_3O_7$ thin films." Materials Chemistry and Physics 49(3): 229-233.

Tsai, W.-C. and T.-Y. Tseng (1997). "Off-axis unbalanced magnetron sputtering of $YBa_2Cu_3O_7$ thin films." Materials Chemistry and Physics 49: 229-233.

Voevodin, A. A. *et al* (1995). "Wear resistant composite coatings deposited by electron enhanced closed field unbalanced magnetron sputtering." Surface & Coatings Technology 73(3): 185-197.

Vossen, J. L., W. Kern, *et al.* (1978). Thin Film Processes. New York, Academic Press.

Wang, Y. H. (1994). "Phase structure characteristics of r.f. reactively sputtered zirconia thin film." Thin Solid Films 250: 132-134.

Wasa, K. *et al* (1991). "Thin film processing for High-Tc superconductors of the Bi-system." J. Mater. Res. 6(7): 1595-1604.

Westwood, W. D. (1976). "Glow Discharge Sputtering." Progress in Surface Science 7: 71-111.

Window, B. and N. Savvides (1986). "Charged particle fluxes from planar magnetron sputtering sources." J. Vac. Sci. Technol. A 4(2): 196-202.

Window, B. and N. Savvides (1986). "Unbalanced dc magnetrons as sources of high ion fluxes." J. Vac. Sci. Technol. A 4(3): 453-456.

Yan, F. *et al* (1999). "Mechanical relaxation in $SrBi_2Ta_2O_9$ ceramics." Applied Physics Letters 74(19): 2794-2796.

Yang. C.-H. *et al* (1997). "Electrical properties of SrBi$_2$Ta$_2$O$_9$ thin films deposited by r.f. magnetron sputtering." Integrated Ferroelectrics **18**: 377-387.

Yang. C.-H. *et al* (1998). "Effect of Bismuth on the ferroelectric properties of SrBi$_2$Ta$_2$O$_9$ thin films deposited on Pt/SiO$_2$/Si by a modified radio-frequency magnetron sputtering technique." J. Vac. Sci. Technol. A **16**(4): 2505-2509.

Yang. C.-H. *et al* (1998). "Low temperature preparation of ferroelectric SrBi$_2$Ta$_2$O$_9$ thin films by a modified r.f. magnetron sputtering technique." Integrated Ferroelectrics **21**: 475-483.

Yang. C.-H. *et al* (1999). "The correlation between composition and preferred orientation of ferroelectric SrBi$_2$Ta$_2$O$_9$ thin films." Electrochemical and Solid-State Letters **2**(1): 39-42.

Zhang. W. F. *et al* (1999). "Large third-order optical nonlinearity in SrBi$_2$Ta$_2$O$_9$ thin films by pulsed laser deposition." Applied Physics Letters **75**(7): 902-905.

Zhang. W.-X. *et al* (1995). "Low-temperature fabrication of Pb(Zr, Ti)O$_3$ films by reactive sputtering using Zr/Ti + PbO target." Jpn J. Appl. Phys., p. 1 **34**(9B): 5120-5123.

Zhang. W.-X. *et al* (1996). "Electrical properties of low-temperature (450C) Pb(Zr,Ti)O$_3$ films prepared in quasi-metallic mode r.f. reactive sputtering" Jpn. J. Appl. Phys. **35**: 5084-5088.

Zhou. W. (1992). "Structural chemistry and physical properties of some ternary oxides in the Bi2O3-Ta2O5 system." J. Solid State Chem. **101**: 1-17.

Zhou. W. (1992). "Structural chemistry and physical properties of some ternary oxides in the Bi$_2$O$_3$-Ta$_2$O$_5$ system." J. Solid State Chem. **101**: 1-17.

Zlatanovic. M. *et al* (1997). "Influence of magnetic field configuration on the deposition conditions in an unbalanced magnetron system." Surface and Coatings Technol. **90**: 143-149.